Engineering
Library

Journal of Research

of the

U.S. National Bureau of Standards

JANUARY 1948

VOLUME 40 NUMBER 1

PERIODICALS OF THE NATIONAL BUREAU OF STANDARDS

Journal of Research

The National Bureau of Standards is the principal agency of the Federal Government for fundamental research in physics, chemistry, and engineering. It has the custody of the national standards of physical measurement in terms of which all working standards in research laboratories and industry are calibrated, and carries on necessary research leading to improvement in such standards and methods of measurement. It also has a general responsibility for basic research in physics, chemistry, and engineering, and for development of improved methods for testing materials and equipment. It determines physical constants and properties of materials, tests and calibrates standard measuring apparatus and reference standards, and studies technical processes. The results of the Bureau's research and investigations are published in the JOURNAL OF RESEARCH.

Research Papers

Reprints of individual articles appearing in the JOURNAL OF RESEARCH. They are made available to serve the needs of research workers, technical groups, and others for the separate papers relating to the special subjects in which they are interested.

Technical News Bulletin

Contains short but complete summaries of research, development, and testing in progress at the Bureau, accounts of the Bureau's national and international activities, scientific and technical announcements of new plans and programs, and a list of publications by members of the staff. It is a prompt and reliable source of official information of value to those who desire to keep in touch with the general activities of the Bureau.

Basic Radio Propagation Predictions

The CRPL–D series, Basic Radio Propagation Predictions, is issued as a monthly publication for those concerned with radio communication in determining the best sky-wave frequencies over any path at any time of day for average conditions for the month of prediction, which is made 3 months in advance. Charts of extraordinary-wave critical frequency for the F2 layer, of maximum usable frequency for a transmission distance of 4,000 km, and of percentage of time occurrence for transmission by sporadic E in excess of 15 Mc, for a distance of 2,000 km, are included.

SUBSCRIPTION Send order, with remittance, to Superintendent of Documents, U. S. Government Printing Office, Washington 25, D. C.	United States, Canada, Cuba, Mexican, Spanish-Republic of Panama	Other countries
JOURNAL OF RESEARCH of the National Bureau of Standards:		
12 monthly issues (2 volumes), paper cover	$4.50	$5.50
Bound volume (½ year, 1 volume), blue buckram	3.00	3.50
RESEARCH PAPERS	(*)	(*)
TECHNICAL NEWS BULLETIN, 12 monthly issues	1.00	1.25
BASIC RADIO PROPAGATION PREDICTIONS, 12 monthly issues	1.00	1.25

*The prices of the separate Research Papers appearing in this JOURNAL are given in the Contents. If 100 or more copies of any separate are ordered, a discount of 25 percent is allowed. Those who desire occasional separate Research Papers should make deposit and maintain account without delay in the Superintendent of Documents, U. S. Government Printing Office, Washington 25, D. C. This will aid him to determine the number of copies to be printed for sale. Research Papers are not printed from electrotypes and usually no more copies can be had when the first and only printing is exhausted.

Published with approval of Bureau of the Budget

U. S. DEPARTMENT OF COMMERCE
W. Averell Harriman, Secretary
NATIONAL BUREAU OF STANDARDS
E. U. Condon, Director

JANUARY 1948
VOLUME • 40
NUMBER 1

JOURNAL OF RESEARCH

of the

NATIONAL BUREAU OF STANDARDS

Contents

RP		Page
1850.	Vulcanization of synthetic rubbers by the Peachey process. Norman Bekkedahl, Fred A. Quinn, Jr., and Elmer W. Zimmerman. (Price 10 cents)	1
1851.	Measurement of ozone over the Organ Mountains, New Mexico. Ralph Stair. (Price 10 cents)	9
1852.	Note on volume effect in coiling molecules. Robert Simha. (Price 5 cents)	21
1853.	Dissociation of SF_6, CF_4, and SiF_4 by electron impact. Vernon H. Dibeler and Fred L. Mohler. (Price 10 cents)	25
1854.	Physical properties of electrodeposited chromium. Abner Brenner, Polly Burkhead, and Charles W. Jennings. (Price 15 cents)	31
1855.	Surface tension of compositions in the systems PbO-B_2O_3 and PbO-SiO_2. Leo Shartsis, Sam Spinner, and Alden W. Smock. (Price 10 cents)	61
1856.	Expansion effects shown by some Pyrex glasses. Arthur Q. Tool and James B. Saunders. (Price 15 cents)	67
1857.	Cavity pressure method for measuring the gain of hearing aids. E. L. R. Corliss and G. S. Cook. (Price 10 cents)	85

For sale by the Superintendent of Documents, U. S. Government Printing Office, Washington 25, D. C. - Price 45 cents, $4.50 per year on subscription

UNITED STATES GOVERNMENT PRINTING OFFICE, WASHINGTON : 1948

Engineering Library
TA
1
.U58

U. S. Department of Commerce
National Bureau of Standards

Research Paper RP1850
Volume 40, January 1948

Part of the Journal of Research of the National Bureau of Standards

Vulcanization of Synthetic Rubbers by the Peachey Process[1]

By Norman Bekkedahl, Fred A. Quinn, Jr., and Elmer W. Zimmerman

The Peachey process, which vulcanizes natural rubber by subjecting it alternately to sulfur dioxide and hydrogen sulfide gases, has been found to vulcanize the more common synthetic rubbers. The polymers studied were natural rubber, GR–S, GR–M, GR–I, GR–A, Hycar OR–15, Hycar OR–25, Hycar OS–10, Hycar OS–20, and Hycar OS–30. Good cures were obtained with all of the polymers except GR–M. None of the synthetic rubbers cured any faster than natural rubber. The nitrile and the styrene copolymers of butadiene cured at about the same rate or somewhat slower. GR–I required roughly 50 times as long as natural rubber for an equivalent cure, and GR–M required even longer.

I. Introduction

The Peachey process, which has been used to vulcanize natural rubber by subjecting the rubber alternately to sulfur dioxide and hydrogen sulfide gases [1, 2, 4, 6, 7],[2] has now been applied to synthetic rubbers. This communication describes the results of an investigation initiated recently by McPherson [5]. The polymers studied include natural rubber, GR–S (butadiene-styrene copolymer), GR–M (polychloroprene rubber similar to Neoprene–GN), GR–I (isobutene-isoprene copolymer, or Butyl rubber), GR–A (butadiene-acrylonitrile copolymer, or nitrile rubber), Hycar OR–15 (similar to GR–A), Hycar OR–25 (lower acrylonitrile content than the OR–15), Hycar OS–10 (butadiene-styrene copolymer having a considerably higher styrene content than GR–S), Hycar OS–20 and Hycar OS–30 (both similar to GR–S with the exception that the OS–20 contains little or no fatty acid).

II. Experimental Procedure

The rubbers tested were sheeted as thinly as practicable, usually from 0.5 to 1 mm, by means of a laboratory rubber mill, and strips approximately 1.75 by 13 cm were cut from the sheets. These strips (usually four to six at a time) were placed on a long piece of heavy-gage galvanized wire screening that was inserted in a 25-mm diameter glass tube approximately 1 m in length, each end being equipped with a ground-glass joint. A triple inlet tube was connected to one end so that the gases, sulfur dioxide, air, and hydrogen sulfide, could be admitted separately. A single outlet tube at the opposite end led the unabsorbed gases first through a 20 percent solution of sodium hydroxide, then through a saturated solution of bromine in water, and finally through a dilute solution of sodium hydroxide in order to trap any of the remaining gases, including bromine vapors.

Except for the initial series of tests, which will be discussed later, all of the test strips were exposed to the vulcanizing gases for 5-minute cycles, the number of cycles being varied from one to as many as 128 in an effort to determine the conditions for optimum cure for each of the various synthetics tested. A single cycle consisted of a 5-minute exposure to sulfur dioxide, a brisk 10-second sweep of air to remove the sulfur dioxide gas not absorbed by the samples, and a 5-minute exposure to hydrogen sulfide, followed by another brisk sweep of air.

In all of the experiments a separate set of samples was used for each of the various numbers of cycles indicated, i. e., one set of samples was inserted into the tube, exposed for one cycle, and removed; a different set was exposed for two cycles

[1] This paper was presented at the 112th national meeting of the American Chemical Society held in New York City, September 15 to 19, 1947.
[2] Figures in brackets indicate the literature references at the end of this paper.

and removed, etc., until all of the desired number of cycles were completed. The samples were then placed in a vacuum oven at room temperature for 3 hours to remove all uncombined gases and also the water vapor that is formed in the vulcanizing reaction, and were then weighed to determine the weight increase, which was assumed to be caused by the added sulfur.

The extent of cure of each strip was qualitatively evaluated by hand-stretching. Some of the samples from each run were then quantitatively analyzed to determine how much sulfur had actually combined with the polymer. The difference between the percentage increase in weight and the combined sulfur was assumed to be free sulfur. Chemical analyses on a number of the samples for free sulfur indicated this assumption to be correct.

III. Results of Experiments

Before beginning the actual vulcanization studies, strips of each of the rubbers to be tested were submitted to a 16-hour exposure to sulfur dioxide gas; another set of samples was similarly exposed to hydrogen sulfide gas for the same length of time. The average increase in weight during this treatment was 0.2 percent, indicating that there was very little, if any, chemical addition of the gases to the rubber.

An initial series of tests was made to determine the most practical period of exposure of the rubber to each of the two gases. Natural rubber was used for this determination. In addition to the pure ribbed smoked sheet, three batches of smoked sheet containing various combinations of fillers and accelerators (see table 1) were exposed to determine whether or not these combinations would cause a change in the rate of vulcanization. Single cycles of 1.25, 2.5, 5, 10, and 20 minutes, respectively, were run. A study of the curve of the percent increase in weight plotted against the duration of the cycle (fig. 1) shows that the longer times of exposure to the gases in a given cycle vulcanize a sample of rubber in a smaller number of cycles, but that the sulfur can be added in less total time using shorter cycles. Extremely short cycles, however, waste vulcanizing gases and also do not give time for the gases to penetrate into the interior of the rubber samples. As a compromise it was decided to use 5-minute cycles for the experiments to be described here. The numerical

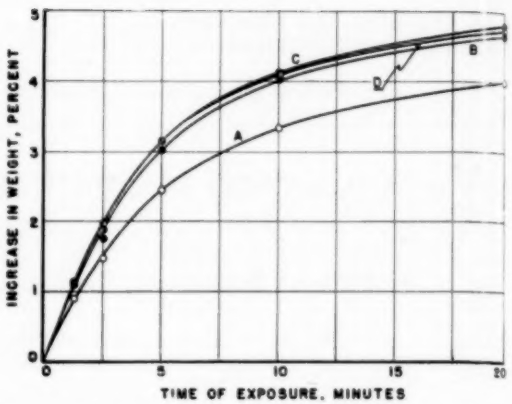

FIGURE 1. *Increase in weight of samples of compounded natural rubber plotted as a function of the time of exposure to sulfur dioxide and to hydrogen sulfide for one cycle of operation.*

The letters representing the curves refer to the compounding formulas given in table 1. Data from which these curves were prepared are given in table 2.

values for these tests are given in table 2. It will be noted that compounds *B*, *C*, and *D* effected a significantly greater absorption of sulfur than *A* (rubber alone), but that *C* and *D* produced no noticeable advantage over *B*. From the results of a repetition of this test, in which the samples were placed in reverse order in the tube, changing in effect the direction of flow of the gases with respect to the samples, it has been shown that the

TABLE 1. *Compounding formulas*

Ingredients	*A*	*B*	*C*	*D*
Ribbed smoked sheet	100.0	100.0	100.0	100.0
Zinc oxide		6.0	6.0	6.0
Stearic acid		0.5	0.5	0.5
Mercaptobenzothiazole			.5	.5
Zinc dimethyldithiocarbamate				.6

TABLE 2. *Vulcanization for one cycle*

Type of polymer	Duration of cycle	Weight increases			
		A[1]	*B*[1]	*C*[1]	*D*[1]
	min	*Percent*	*Percent*	*Percent*	*Percent*
Natural	1.25	0.90	1.10	1.10	1.10
	2.5	1.47	1.76	1.88	1.87
	5	2.44	3.02	3.14	3.10
	10	3.34	4.02	4.13	4.09
	20	3.99	4.66	4.82	4.75

[1] For compounding formulas, see table 1.

position of the sample in the reaction tube does not affect the percentage weight increase.

In table 3 are summarized the data obtained from all of the synthetic rubbers and natural rubber studied. The increase in weight is based on the weight of the original sample. The combined sulfur is also computed on this basis and therefore represents the parts of combined sulfur per hundred parts of original polymer. The extent of cure was estimated by hand-stretching the individual specimens and observing the rate and degree of recovery. It is believed that the optimum cure, as indicated for each type of rubber, represents the vulcanizate that has the highest tensile strength.

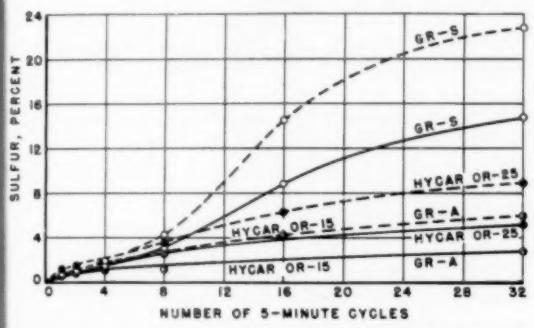

FIGURE 2. *Percentage of sulfur added to GR–S, GR–A, Hycar OR–15, and Hycar OR–25 rubber samples plotted as a function of the number of 5-minute cycles of exposure to the gases of the Peachey process.*

The solid lines indicate combined sulfur as determined by chemical analysis, and the broken lines indicate the total sulfur as determined by weight increase of the sample.

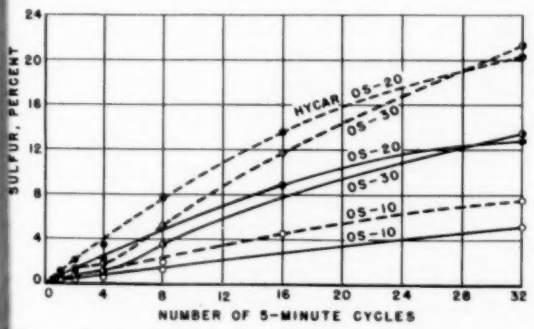

FIGURE 3. *Percentage of sulfur added to Hycar OS–10, Hycar OS–20, and Hycar OS–30 rubber samples plotted as a function of the number of 5-minute cycles of exposure to the gases of the Peachey process.*

The solid lines indicate combined sulfur as determined by chemical analysis, and the broken lines indicate the total sulfur as determined by weight increase of the sample.

Figures 2 and 3 show in graphical form the data obtained from the butadiene-type polymers. All of these rubbers were run simultaneously. The solid lines indicate the amount of combined sulfur, and the broken lines represent the total sulfur. Figure 4 shows similar results for GR–I and GR–M synthetic rubbers. These polymers were run separately from the others because of their extremely low rate of cure. The results obtained from vulcanizing natural rubber are shown on this same graph for comparison.

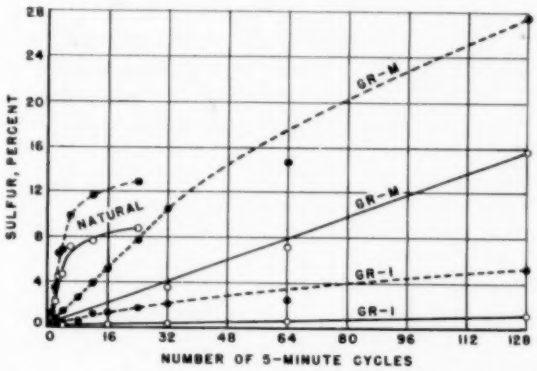

FIGURE 4. *Percentage of sulfur added to GR–M, GR–I, and natural rubber samples plotted as a function of the number of 5-minute cycles of exposure to the gases of the Peachey process.*

The solid lines indicate combined sulfur as determined by chemical analysis, and the broken lines indicate the total sulfur, as determined by weight increase of the sample.

A confirmatory experiment was performed in which natural rubber and all of the synthetic polymers, with the exception of GR–I and GR–M, were vulcanized simultaneously for 4, 8, 16, and 32 cycles, respectively. The increases in weight agreed so closely with those obtained in the previous runs that it was thought unnecessary to run chemical analyses for the amount of combined sulfur or to tabulate the additional data.

As a matter of interest, the vulcanized pure ribbed smoked sheet specimens described in table 2 were subjected to two physical tests, namely, stress at 15 kg/cm ^{2} (213 psi) and permanent set. Each group of similar degrees of vulcanization (1.25, 2.5, 5, 10, and 20 minutes) contained four strips, two of which had been cut longitudinal to the direction of passage of the rubber between the mixing rolls of the mill and two of which were cut

TABLE 3. *Vulcanizations for various numbers of cycles*

Type of polymer	Number of cycles	Weight increase	Combined sulfur [1]	Extent of cure [2]
		Percent		
GR–S	0	0	0.11	None.
	1	.56	.....	Extremely slight cure.
	2	1.43	.68	Slight cure.
	4	1.57	.99	Undercure.
	8	4.30	3.08	Good cure (optimum).
	16	14.47	8.83	Overcure.
	32	22.77	14.77	"Leathery" cure.
GR–A	0	0	0	None.
	1	.71	.....	Slight cure.
	2	.99	.79	Undercure.
	4	1.22	1.10	Fairly good cure.
	8	2.65	1.14	"Tight" cure (optimum).
	16	4.27	.....	Overcure.
	32	6.05	2.84	"Leathery" cure.
Hycar OR–15	0	0	0	None.
	4	1.30	.84	Fairly good cure.
	8	2.52	1.37	"Tight" cure (optimum).
	16	4.50	1.64	Overcure.
	32	6.03	2.05	"Leathery" cure.
Hycar OR–25	0	0	0	None.
	1	1.15	.....	Slight cure.
	2	1.48	.86	Undercure.
	4	1.90	1.28	Fairly good cure.
	8	3.58	2.55	"Tight" cure (optimum).
	16	6.39	.....	Overcure.
	32	8.98	5.34	"Leathery" cure.
Hycar OS–10	0	0	0.20	None.
	1	0.38	.26	Slight cure.
	2	.64	.54	Undercure.
	4	.96	1.24	Fairly good cure.
	8	1.93	.....	"Tight" cure (optimum).
	16	4.52	5.19	Overcure.
	32	7.55	.....	"Leathery" cure.
Hycar OS–20	0	0	0.30	None.
	1	1.09	.....	Slight cure.
	2	2.14	1.21	Good cure (optimum).
	4	3.49	2.29	Slightly overcured.
	8	7.73	5.32	Overcure.
	16	13.61	8.85	"Leathery" cure.
	32	20.32	12.81	Do.
Hycar OS–30	0	0	0.10	None.
	1	0.69	.....	Slight cure.
	2	1.29	0.66	Undercured.
	4	1.73	1.17	Good cure (optimum).
	8	5.21	3.58	Overcure.
	16	11.74	.....	"Leathery" cure.
	32	21.29	13.45	Do.
GR–M	0	0	0.46	None.
	1	0.31	.....	No noticeable cure.
	2	.75	.....	Do.
	4	1.41	.....	Do.
	8	2.65	.....	Do.
	12	3.97	.....	Do.
	16	5.17	0.12	Do.
	24	7.69	.....	Do.
	32	10.44	3.57	Do.
	64	14.63	7.18	Some cure noticeable.
	128	27.55	15.64	Slight undercure.

TABLE 3. *Vulcanizations for various numbers of cycles*—Continued

Type of polymer	Number of cycles	Weight increase	Combined sulfur [1]	Extent of cure [2]
		Percent		
GR–I	0	0	0	None.
	1	0.13	.....	No noticeable cure.
	2	.24	.....	Do.
	4	.39	0.10	Do.
	9	.55	.....	Do.
	12	1.19	.....	Slight cure.
	16	1.23	0.12	Do.
	24	1.77	.....	Undercure.
	32	2.13	0.22	Do.
	64	2.45	.51	Slight undercure.
	128	5.30	1.12	Good cure (optimum).
Natural	0	0	0	None.
	1	1.22	0.64	Appreciable cure.
	2	3.52	2.31	Good cure (optimum).
	3	6.60	4.55	Slight overcure.
	4	6.95	4.78	Overcure.
	6	9.98	7.20	Greatly overcured.
	12	11.79	7.76	"Leathery" cure.
	24	12.98	8.83	Do.

[1] Based on parts per hundred parts of polymer.
[2] Estimated by hand-stretching.

transverse to the direction of milling. After determining the cross-sectional area of each strip, the proper-sized dead weight was hung on the strip and the elongation between two gage marks was measured at the end of 1 minute. The weight was then allowed to continue hanging on the sample for an additional 4 minutes, after which time it was removed and the sample allowed to relax for 1 minute. The distance between the gage marks was again measured, and from this figure the permanent set was calculated. The results of these physical tests are summarized in table 5 and shown graphically in figure 5.

Another interesting conclusion may be drawn from the results. The amount of combined sulfur in the optimum cures for natural rubber and for all of the synthetics, with the exception of GR–M, is between 1 and 3 percent (see table 4). This agrees very well with Peachey's conclusion that an optimum cure is attained in natural rubber by his process when a coefficient of vulcanization of 2.0 to 2.5 is attained [6, 7]. The natural rubber and all of the synthetic rubbers investigated, with the exception of GR–I and GR–M, were also vulcanized to a "leathery" state, and to vulcanizing coefficients as high as 3 to 15. At these higher

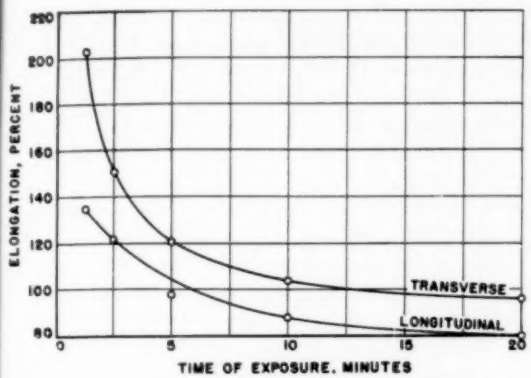

FIGURE 5. *Elongation at stress of 15 kg/cm² (213 psi) for natural rubber samples under different degrees of cure.*

For some of the samples the stresses were measured longitudinally and others transversely to the direction of passage between the mixing rolls.

degrees of vulcanization there was quite a large amount of free sulfur deposited on the surface of the rubber. No attempt was made to continue toward a higher degree of vulcanization. St. Reiner [8], however, did continue the reaction further and claims that hard rubber can be produced from natural rubber by this process.

TABLE 4. *Optimum cures from table 3*

Type of polymer	Cycles for optimum cure	Weight increase	Combined sulfur [1]
		Percent	*Percent*
Natural	2	3.52	2.31
GR-A	8	2.65	1.14
Hycar OR-15	8	2.52	1.37
Hycar OR-25	8	3.58	2.55
Hycar OS-10	8	1.93	1.24
Hycar OS-20	2	2.14	1.21
Hycar OS-30	4	1.73	1.17
GR-S	8	4.30	3.08
GR-I	128	5.30	1.12
GR-M	>128	>27.55	>15.64

[1] Based on parts per hundred parts of polymer.

IV. Discussion of Results

As only about 0.2 percent weight increase was effected by either of the Peachey process gases alone, it is clearly indicated that there are no appreciable side reactions whereby one gas might act independently of the other to cause any significant increase in weight in the rubber. Therefore it is reasonably certain that any appreciable increase in weight on the dry basis is caused by a combination of the nascent sulfur, which is released by the interaction of the two gases within the specimen, with the unsaturated bonds of the rubber, plus any free sulfur that the sample is able to hold in solution or as a deposit on the surface. This reaction of the gases within the rubber samples, in addition to forming nascent sulfur, also produces water. Although it is quite possible that the quantity of moisture present in the samples or in the gases may have an effect on the rate of the vulcanizing reaction [3] no attempt was made to measure this amount because all of the samples were subjected to the same general conditions that should produce comparative results.

It is interesting to note that in the initial series of tests on natural rubber, as can be seen in figure 1, a greater quantity of sulfur was taken up when the rubber had been compounded with zinc oxide and stearic acid, but that no further significant addition of sulfur was noted when an accelerator (mercaptobenzothiazole) and an ultra accelerator (zinc dimethyldithiocarbamate) were added. Several possible explanations may be suggested. The zinc oxide and the stearic acid may supply an accelerating effect that causes more sulfur to combine with the rubber in a given length of time, in effect speeding up the rate of cure. It may also be that the sulfur is merely displacing the oxygen of the zinc oxide to form zinc sulfide, which could readily account for the additional increase in weight. S. J. Peachey [6] believes that compounded rubber absorbs the gases more readily than pure rubber. As this phase was not of primary interest to this investigation, this problem was not probed deeply enough to ascertain the correct explanation. However, it is felt that these particular accelerators apparently had little or no influence on the amount of the sulfur added. St. Reiner [8], on the other hand, claims that certain organic accelerators speed up the reaction. Whether or not he too used a metallic oxide along with the accelerator, as is customary for hot curing, and mistakenly attributed the increase in

rate of the sulfur addition solely to the presence of the accelerator is not known.

In some of the preliminary runs, it was noticed that there were variations in the amounts of sulfur taken up by the same polymer for a similar number of cycles in different series of runs. In these early runs the polymers may not have been sheeted as uniformly in thickness as in the later runs. As has already been mentioned, the amount of moisture present in the polymer may also have affected the rate of cure. However, this phase of the problem was not studied further, as the sole purpose of this investigation was merely to learn whether or not synthetic rubbers could be vulcanized by this method.

It should be pointed out that Hycar OS–20 and Hycar OS–30 cured at approximately the same rate, showing that the presence or absence of fatty acids in the butadiene-styrene type polymers is immaterial as far as the vulcanizing process is concerned (see fig. 3). The Hycar OS–10, having a higher styrene content than the Hycar OS–20, Hycar OS–30, or the GR–S, must have fewer double bonds, and consequently vulcanizes at a slower rate. GR–A and Hycar OR–15 were so similar in their rates of cure that the data had to be plotted as one and the same curve (see fig. 2). Hycar OR–25 has a lower acrylonitrile content than the Hycar OR–15 and the GR–A, and therefore, because of the larger number of double bonds, vulcanizes at a greater rate.

After a large number of cycles GR–I had taken up very little combined sulfur, probably because of the presence of relatively few double bonds in this polymer. This may explain why so much time is required for a good cure. The vulcanization of GR–M, which normally is vulcanized by the use of metallic oxides rather than of sulfur, also behaves differently in the Peachey process. Much sulfur was taken up by the GR–M, and even combined chemically with it, but an undercure was still obtained when over 15 percent of sulfur had combined.

By vulcanizing strips of rubber by the Peachey process, it was possible to show a very striking illustration of the influence that the direction of milling has on certain physical properties of the vulcanizate. Table 5 and figure 5 show that all of the specimens cut transverse to the direction of passage of the rubber between the mill rolls have a substantially higher degree of elongation and permanent set than those cut longitudinal to the direction of milling when subjected to the same relative stress. The shearing action produced by the difference in speeds of the two rolls of the mill partially stretches and aligns the molecules of the rubber. The specimens that are cut and vulcanized in the same direction as the partially elongated chains naturally will not stretch as much as those cut at right angles to the already stretched configurations under the same force.

TABLE 5. *Effect of direction of milling on stress and set*

Type of polymer	Length of cycles	Weight increase	Elongation		Permanent set	
			Longitudinal	Transverse	Longitudinal	Transverse
	min.	*Percent*	*Percent*	*Percent*	*Percent*	*Percent*
Natural	1.25	1.16	135	203	4.8	8
	2.5	1.97	122	151	3.2	5
	5	3.18	98	121	1.6	4
	10	3.86	88	104	1.6	4
	20	4.29	80	93	1.6	4

These same conclusions are drawn from some unpublished experiments performed several years ago by W. H. Smith and F. L. Roth of the National Bureau of Standards. They stretched a wide flat strip of raw rubber and vulcanized it while in the elongated state by the sulfur chloride method. Dumbbell specimens were cut from this vulcanized strip both in the direction of stretch and also at right angles to it. The specimens that were cut transverse to the direction of original stretch were softer and showed considerably greater values of ultimate elongation and tensile strength.

The authors are indebted to Eleanor F. Pangborn for making the many sulfur determinations necessary for the preparation of the tables given in this paper. The investigation resulted from an original suggestion by Harry L. Fisher, Office of Rubber Reserve.

V. References

[1] Possibilities of the Peachey process, India Rubber World **62,** 787 (1920).

[2] The perfected Peachey process, Rubber Age **19,** 195 (1926).

[3] L. Hoch and H. Schmidt, The formation of sulfur from hydrogen sulfide and sulfur dioxide, Kautschuk **10,** 82 (1934).

[4] F. Jacobs, The Peachey process, Caoutchouc and Gutta-Percha **26,** 14506 (1929).

[5] A. T. McPherson, Vulcanization of GR-S by the Peachey process, Rubber Age **59,** 323 (1946).

[6] S. J. Peachey, Lecture on cold vulcanization, India Rubber J. **63,** 427 (1922).

[7] S. J. Peachey and A. Skipsey, New process for the vulcanization of rubber, J. Soc. Chem. Ind. Trans. **40,** 5 (1921).

[8] St. Reiner, Observations on the formation of sulfur from hydrogen sulfide and sulfur dioxide, Kautschuk **10,** 128 (1934).

WASHINGTON, September 5, 1947.

U. S. Department of Commerce
National Bureau of Standards

Research Paper RP1851
Volume 40, January 1948

Part of the Journal of Research of the National Bureau of Standards

Measurement of Ozone Over the Organ Mountains, New Mexico

By Ralph Stair

This paper gives data on the total amount of ozone above the Organ Mountains at White Sands Proving Grounds in New Mexico from June 29, to July 4, 1947, as determined from ultraviolet measurements by a phototube and filter method. The measurements indicate ozone in the stratosphere in amount equivalent to a layer of about 0.21 cm thickness at normal temperature and pressure, which is in good agreement with determinations by others for the same latitude and season of the year.

The total ozone value and the solar-energy curve in the region of short ultraviolet wavelengths outside the earth's atmosphere check closely with previous work with the same instruments at Mount Evans, Colo., in 1936 and 1938.

I. Introduction

The measurements recorded in this paper of the total amount of ozone in the stratosphere by a phototube and filter method developed at this Bureau were made at the request of and under the sponsorship of the Naval Research Laboratory as a check upon their methods employed in V–2 rocket experiments at White Sands Proving Ground, New Mex. They were planned as a check on a flight scheduled for July 3, 1947. Although the V–2 rocket misfired, the phototube measurements were carried through as planned from June 29 to July 4, inclusive, and the data reduced in a manner similar to that employed in the previous work at Mount Evans, Colo., in 1936 and 1938 [1].[1]

It is a well-known fact that the total amount of ozone varies from time to time, but at present little is known about any possible relationship between this variation and weather conditions, except in the instance of seasonal variations [2, 6] and that different types of air masses show variations that are associated with their origin or movement [3, 8]. Variations in short ultraviolet solar energy emission also produce changes in total ozone value that fluctuates from hour to hour or from day to day. Such fluctuations may account for or be associated with "ozone cloud" effects [4, 5] observed by other investigators.

The method employed in this work involves the use of titanium phototubes sensitive to radiation of about 3,400 A (angstroms) and shorter wavelengths and filters with transmittances beginning at 2,900 to 3,100 A and increasing with wavelength. Ozone is strongly absorbing below about 3,200 A. If one of the phototubes is exposed to radiation of a particular spectral distribution and intensity, it will give a measurable response. If one of the filters is now interposed, the response is reduced. The ratio of the response with the filter in place to that without it will be called the "transmittance", or "filter transmittance" and will be expressed in percentage.[2] The transmittance of the filter is independent of the radiant flux density but is dependent on its spectral distribution. The interposition of ozone in sunlight greatly changes its spectral distribution in the region to which the phototube is sensitive; hence, changes in the quantity of ozone traversed cause changes in the transmittance subject to observation. If we knew the

[1] Figures in brackets indicate the literature references at the end of this paper.

[2] It is hoped that the term "transmittance" of the filter as defined here, which is a function of the sensitivity of the phototube to each wavelength as well as the characteristics of the filter, will not be confused with "transmittance" also used in this paper in the ordinary sense, in which it is independent of the receiver beyond the filter. The term holotransmittance recently suggested by Van Lear [23] might be used. Certainly there is need for some prefix to properly signify this type of "transmittance."

spectral distribution of the solar radiation, the effect of a specified quantity of ozone on transmittance of a given filter in combination with a given phototube could be calculated or, in reverse, the quantity of ozone could be determined from a single observed transmittance of the filter.

The amount of ozone traversed by sunlight that reaches the earth's surface depends on the quantity of ozone in the atmosphere and on the direction of the light. The second effect will be referred to as that of the "air mass" and represented by M.[3] The air mass is nearly proportional to the secant of the angle the sun's rays make with the earth's surface.

As the sunlight unaffected by ozone is not available for direct observation, its spectral distribution must be deduced from observations made at the earth's surface. To explain in principle how this can be done, it should be pointed out first that from any spectral distribution that might be assumed for sunlight and the observed transmittance of a certain combination of filter and phototube, a quantity of ozone in the atmosphere may be calculated. If a simultaneous observation is made with another combination of instruments having different spectral absorptions and sensitivities, a quantity of ozone can likewise be calculated. If the instruments have been correctly calibrated and if the two values obtained for the ozone do not agree, something is wrong with the assumed spectral distribution of the sunlight. The correct distribution should give the same result for ozone with any combination of detecting equipment. Also, there is reason to believe that, on the average, there is little change in the ozone content of the atmosphere with time of day, but because of the change of air mass there is a large easily calculated change in mass of ozone traversed by the sunlight from morning to noon and from noon to evening. If, on the average, the changes in the effect attributed to ozone correspond to changes in air mass without change in the atmospheric content of ozone, there is evidence that the spectral distribution curve of the sunlight is correct. If, in general, the computed ozone content shifts with changing air mass, the spectral distribution curve of the sunlight may be assumed to be in error. By a process of trial and error, approximate spectral distribution curves initially assumed have been modified to make all observed data reasonably consistent. The unavoidably complicated processes employed in this derivation have been more fully explained in reference [1].

In either the method employed in this work, wherein comparisons are made between the relative intensities of different spectral regions, or with the photographic or photoelectric method wherein two single wavelengths in the solar spectrum are isolated and from their relative intensities the absorption by ozone and hence the total amount is calculated, it is impossible to separate changes in the spectral quality of solar radiation from true ozone changes. However, when the measurements are made at the earth's surface, radiated energy of wavelengths shorter than 3,000 A has little or no effect upon the calculated results when either method is employed, as it is almost completely absorbed even for low air masses on a mountain top. Hence it is believed that changes in solar emission may be neglected without making a serious error in the determination of the total amount of ozone.

In an earlier paper [9] it was first pointed out in 1937 by the author that it should be possible to follow the ozone cycle through the year and from year to year by means of phototube and filter measurements. At that time, suitable means and methods of accurately calibrating phototubes and filters for this purpose were not readily available. Nevertheless, with an improvised standard source of ultraviolet radiation in the form of a Mazda C lamp, a forward step was made in 1939 [1] in the evaluation of ultraviolet solar radiation data obtained at Mount Evans, Colorado, in the summers of 1936 and 1938. With the development of ultraviolet standards in the form of tungsten-quartz lamps [10, 11], the problem of accurately calibrating ultraviolet phototubes has been immeasurably simplified. Furthermore, the development of the Beckman [17, 18] and other ultraviolet spectrophotometers has made possible accurate determinations of filter transmittance within the Huggins ozone absorption region of 2,900 to 3,400 A.

Recently a preliminary survey was made of the possibility of using a recording infrared spectrometer to measure the total amount of ozone by the change in intensity of the absorption band

[3] Only relative values of M will be used. For sunlight outside the earth's atmosphere $M=0$. For vertical sunlight, never available outside the tropics, $M=1$. The reader must not confuse this use of the term "air mass" with the same term used to designate air of a particular origin, temperature, or other property.

0.7 microns. This method shows some promise, but because of temperature and pressure effects [12, 13] at this wavelength and because of interference of water vapor absorption on days of high humidity, it will probably not replace the use of the Huggins band in the ultraviolet. Furthermore, difficulties involved in keeping a proper image of the sun on the spectrometer-entrant slit rule in favor of the simple phototube and filter method employed in the present investigation.

II. Phototubes and Filters

In the work at San Augustine pass in the Organ Mountains, N. Mex., the same two titanium phototubes (Nos. 2 and 6) and the same filters (Corex D; Nillite; Barium Flint, 1 mm; and Barium Flint, 3 mm) were employed as at Mount Evans, Colorado [1] in 1936. The relative spectral responses of the phototubes and the transmittance of the filters are given in figure 1. It is to be noted that the relative spectral response of phototube Ti–2 has remained closely the same as it was in 1936. However, that for phototube Ti–6 has undergone a marked change during the years so that now it is more sensitive to longer wavelengths than is the case for Ti–2. A change of this type is unimportant so long as it does not occur between calibration and use of the phototube.

The original calibration of the relative spectral response of these phototubes is described in detail

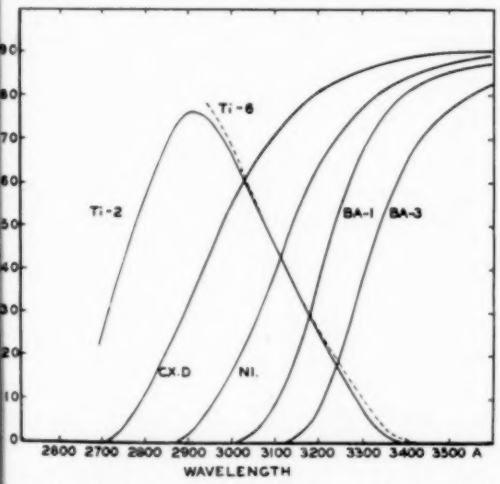

FIGURE 1. *Graphs showing the relative spectral response curves for the two titanium phototubes; also the spectral transmittances of the four filters.*

in the previous report [1]. Supplementary calibrations have been made by using the spectroradiometer and standards of continuous spectral ultraviolet radiation [10, 11] from time to time. A new spectral calibration was made for phototube Ti–6 following its use in this work.

III. Ultraviolet Meter

The phototube current was amplified by means of a portable balanced-tube direct current amplifier and read on a 0 to 15 microampere Weston Model 440 meter. This amplifier was battery-operated and of such dimensions that it was easily transported to the Organ Mountain station (elevation 5,640 ft) at the San Augustine pass. Figure 2 shows this amplifier, and figure 3 an

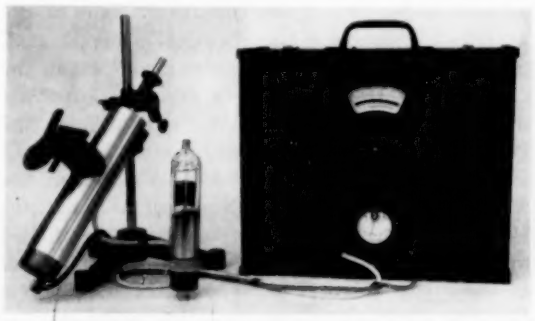

FIGURE 2. *Ultraviolet meter, titanium phototube, and phototube mounting.*

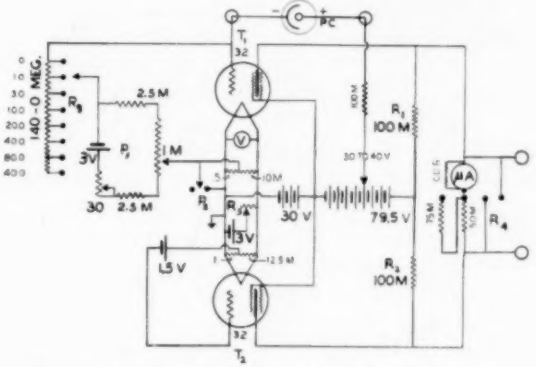

FIGURE 3. *Electrical circuit of the ultraviolet meter.*

electric circuit of the amplifier. Complete details covering the construction and operation of the amplifier are given in the previous publication [1]. Careful construction of this instrument through the use of high-grade parts and nonmicrophonic

balanced tubes enabled the operator to obtain measurements in strong winds wherein the instrument was jostled about on its table.

IV. Method for Evaluating the Amount of Ozone

Using the four filters whose transmittances are given in figure 1, measurements were alternately made with the two titanium phototubes. The total percentage transmittances of these filters for sunlight were calculated and plotted as a function of air mass (see figs. 5 and 6).

The determination of the solar air mass as a function of standard time at a station is a rather detailed operation that must be performed before it is possible to interpret the filter-transmittance data intelligently. From the yearly issue of the American Ephemeris and Nautical Almanac [19], the equation of time may be obtained. From the longitude of the observing station, a longitude time correction is calculated. For San Augustine Pass, this correction was about −6 min and 11 sec (pass longitude 109°32′45″ W). From the American Ephemeris and Nautical Almanac for 1947, the equation of time correction was found to be −3 min and 48 sec (for July 2). The sum of these two corrections is −9 min and 59 sec. For the other days the hour angle corrections ranged from −9 min and 23 sec to −10 min and 21 sec.

During the period of observations, June 29 to July 4, the solar declination ranged from 23°15′23″ to 22°54′59″. The latitude of the San Augustine Pass is approximately 32°27′35″ N (32.46° North). From Ball's altitude tables [20], in which true solar altitudes for even degree values of latitude are tabulated for hour angle intervals of 4 min, a new table for 32.46° was calculated by interpolation. These data were plotted using as ordinate and absissa, true solar altitude and solar declination, respectively. From this set of curves, true solar altitudes (for 4-min intervals throughout the day) were obtained for the solar declinations corresponding to the days on which observations were made. Finally, these true solar altitudes were translated into solar air masses (air mass equals approximately the secant of the sun's zenith distance) for 4-min intervals on the days on which observations were made, and plotted as a function of mountain standard time, hour angle correction being made for longitude and equation of time.

In order to obtain a measure of the amount of ozone at the time of the observations, a solar energy curve outside the earth's atmosphere is assumed. For this, the curve obtained in the Mount Evans work [1] (S. and H. 1936–38) was employed as an approximation for preliminary calculations. Starting with this spectral energy curve, and by a process of arithmetical integration (using 20 angstroms as a unit) a set of transmittance curves for the four filters and two phototubes, as a function of solar air mass was calculated. For these calculations, the Fabry and Buisson [15] transmittance coefficients for ozone and the Rayleigh scattering (atmospheric transmittance) coefficients as used by O'Brien [16] in the reduction of the stratosphere balloon data (*Explorer I* and *II*) have been used. Some of the ozone and scattering transmittance curves are reproduced in figure 4. Next, changes were made in the original solar curve and recalculations performed to give closer agreement between the slopes of the calculated curves and the observed data. Hence by trial and error the shape of the solar energy curve outside the earth's atmosphere is determined.

This method is illustrated by an example in table 1, which gives all the steps in the determination of one point (air mass=1.0) on each of the calculated (0.20 cm) ozone curves for phototube

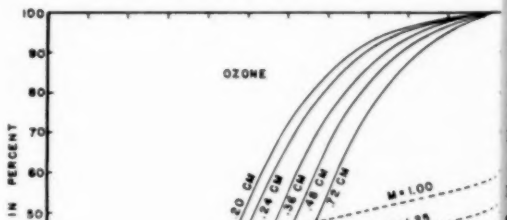

FIGURE 4. *Graphs showing the spectral transmittance of the atmosphere in terms of molecular (Rayleigh) scattering and ozone absorption.*

TABLE 1. *Method employed in the calculation of ozone values*

This example includes a single set of data for phototube Ti-2 for air mass $M=1.00$ and an ozone value of 0.20 cm ntp.

Center of wavelength interval	Relative spectral energy $M=0$	Scattering transmittance $M=1.00$	Transmittance 0.2 cm O_3	Column 2 x 3 x 4 relative energy $M=1.00$	Relative response phototube Ti-2	Column 5 x 6 integrated response	Transmittance Corex D	Column 7 x 8 integrated response	Transmittance Nillite	Column 7 x 10 integrated response	Transmittance Ba-1	Column 7 x 12 integrated response	Transmittance Ba-3	Column 7 x 14 integrated response
1	2	3	4	5	6	7	8	9	10	11	12	13	14	15
A														
2,900	15	0.350	0.0001	.....	0.76	.....	0.324	.....	0.014	.....	.....	.....	.....	.....
20	30	.360	.001	0.01	.76	0.01	.370	.....	.039	.....	.....	.....	.....	.....
40	47	.370	.006	.10	.75	.08	.420	0.03	.070	0.01	.....	.....	.....	.....
60	56.5	.379	.0195	.42	.73	.31	.468	.14	.100	.03	.....	.....	.....	.....
80	58	.388	.055	1.24	.70	.87	.514	.45	.132	.11	.....	.....	.....	.....
3,000	58.5	.397	.106	2.46	.66	1.62	.555	.90	.165	.27	.....	.....	.....	.....
20	55.5	.406	.170	3.83	.62	2.37	.595	1.41	.204	.48	0.003	0.01	.....	.....
40	52	.415	.247	5.33	.58	3.09	.630	1.95	.246	.76	.017	.05	.....	.....
60	50	.424	.340	7.21	.53	3.82	.660	2.52	.293	1.12	.035	.13	.....	.....
80	49.5	.433	.435	9.32	.49	4.57	.690	3.15	.343	1.57	.060	.27	.....	.....
3,100	49	.442	.526	11.39	.45	5.13	.717	3.68	.398	2.04	.090	.46	.....	.....
20	49.5	.451	.613	13.68	.405	5.54	.742	4.11	.457	2.53	.133	.74	0.001	0.01
40	52	.460	.684	16.36	.360	5.89	.763	4.49	.514	3.03	.180	1.06	.008	.05
60	56	.469	.747	19.62	.320	6.28	.779	4.89	.563	3.54	.237	1.49	.023	.14
80	59	.478	.800	22.56	.285	6.43	.793	5.10	.605	3.89	.310	1.99	.042	.27
3,200	64	.487	.848	26.43	.245	6.48	.807	5.23	.645	4.18	.380	2.46	.075	.49
20	74	.496	.884	32.45	.210	6.81	.818	5.57	.680	4.63	.455	3.10	.127	.86
40	88	.505	.914	40.62	.175	7.11	.830	5.90	.710	5.05	.526	3.74	.190	1.35
60	94	.514	.936	45.22	.140	6.33	.842	5.33	.737	4.67	.580	3.67	.250	1.58
80	96	.523	.951	47.75	.105	5.01	.850	4.26	.757	3.79	.630	3.16	.315	1.58
3,300	98	.532	.963	50.21	.075	3.77	.857	3.23	.775	2.92	.670	2.53	.380	1.43
20	99	.541	.973	52.11	.045	2.34	.865	2.02	.792	1.85	.703	1.65	.440	1.03
40	99	.550	.980	53.36	.023	1.23	.873	1.07	.805	0.99	.736	0.91	.505	0.62
60	99	.559	.987	54.62	.010	0.55	.878	0.48	.818	.45	.766	.42	.555	.31
80	99	.568	.995	55.95	.003	.17	.883	.15	.829	.14	.790	.13	.600	.10
Total.....	.....	.....	.....	.....	.....	85.81	.....	66.06	.....	48.05	.....	27.97	.....	9.82
Percentage transmittance	.....	.....	.....	.....	.....	.....	.....	77.0	.....	56.0	.....	32.6	.....	11.4

Ti-2. In this table, column 1 gives the center of each 20-A wavelength interval. Column 2 gives the relative spectral energy distribution assumed for $M=0$ that is, outside the earth's atmosphere. In column 3 are given transmittance values for air mass 1.0 when scattering only is taken into account. Similarly, transmittance values for 0.20 cm ozone (the ozone curve being calculated) are given in column 4.

The product of columns 2, 3, and 4 gives column 5 which represents, therefore, the relative spectral solar energy curve for air mass 1.00 and 0.20 cm ozone. In column 6, the relative spectral response values (for equal energy) for phototube Ti–2 are tabulated. The product (column 7) of columns 5 and 6 gives, consequently, the calculated integral response of the phototube for solar radiation, air mass 1.00, ozone value 0.20 cm. Columns 8, 10, 12, and 14 give the spectral transmittance of the four filters and columns 9, 11, 13, and 15 the integrated photoelectric responses through the four filters, respectively. From the sums of the integrated values for the phototube alone and through the several filters, the calculated filter percentage transmittances are obtained directly as ratios. In this case, the four values are 77.0, 56.0, 32.6, and 11.4, and are plotted as large circles in figure 5 at air mass 1.00. Other points on the same and on other curves for different assumed amounts of ozone are similarly calculated.

Although the preliminary calibrations and calculations for a particular phototube and set of filters are quite complicated, when they are once made it is simple from this set of curves to deter-

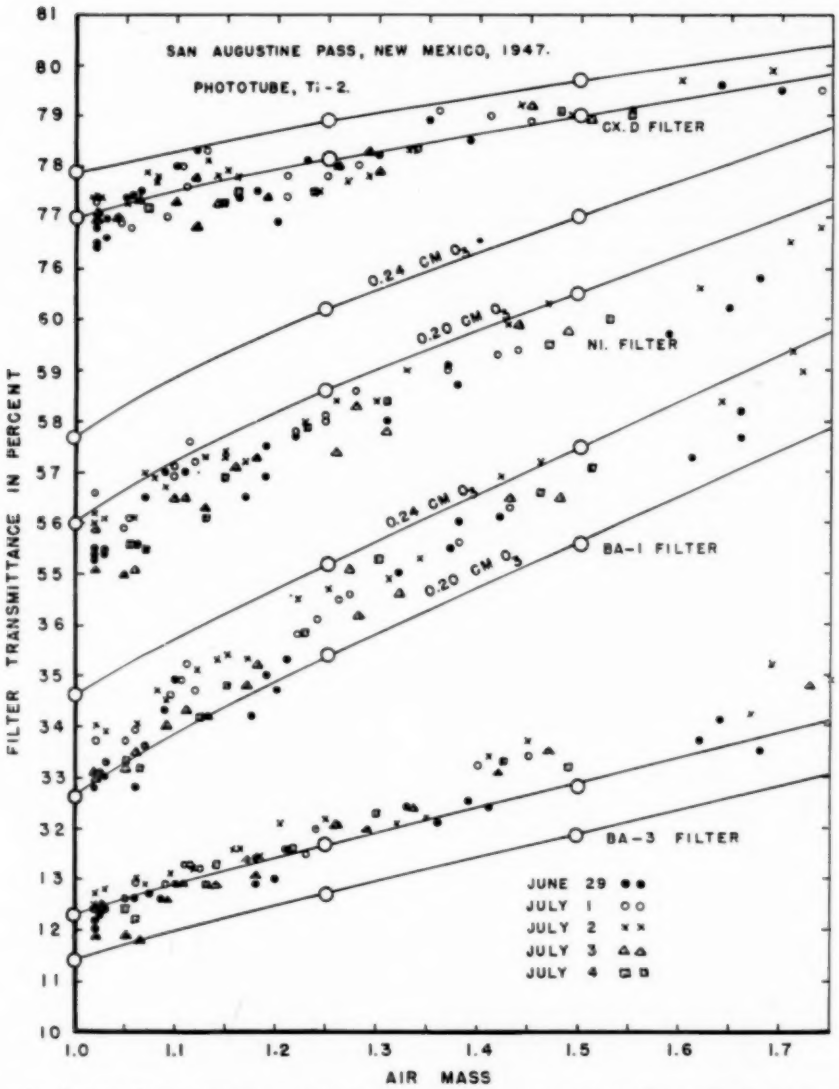

FIGURE 5. *Graphs showing the amount of ozone in the stratosphere, based on observations with titanium phototube N[illegible] calculations based on the 1947 Stair solar energy curve for air mass, m=0.*

mine the ozone value from measurements with a single filter within a few minutes time. This is a highly important factor should such measurements become useful for weather forecasting purposes.

V. Amount of Ozone Over the Organ Mountains on June 29 to July 4, 1947

In figures 5 and 6 are represented the observed data and the calculated effects of assumed amounts of ozone above the San Augustine Pass in t[illegible] Organ Mountains of New Mexico for the period June 29 to July 4, 1947. Although the data sh[illegible] some scatter, due principally to thin clouds a[illegible] haze which at times covered the area of the s[illegible] surrounding the sun, they show distinct chan[illegible] in the total ozone value from day to day. T[illegible] values for June 29 are near the mean value for the measurements, whereas those for July 1 a[illegible] 2 are higher and those for July 3 and 4 are lo[illegible]

than this mean value. These changes are no doubt associated with air mass changes for this area.

On June 29, according to the Weather Bureau reports, this area was covered by a layer of cold continental tropical air centered over the lower Rocky Mountain regions of New Mexico and Arizona. During most of the day a medium strong wind (probably 20 to 25 miles an hour) was blowing from the west. A quasi-stationary front existed in southern Colorado between a polar maritime air mass and a mass of cold continental polar air, which was moving into the northern part of the United States from Canada.

By the following day, June 30, a large mass of polar continental air had spread over the northern part of the country. There was practically no surface air movement (wind) at White Sands, and the sky was about one-half clouded over throughout the day, with clouds over the sun most of the

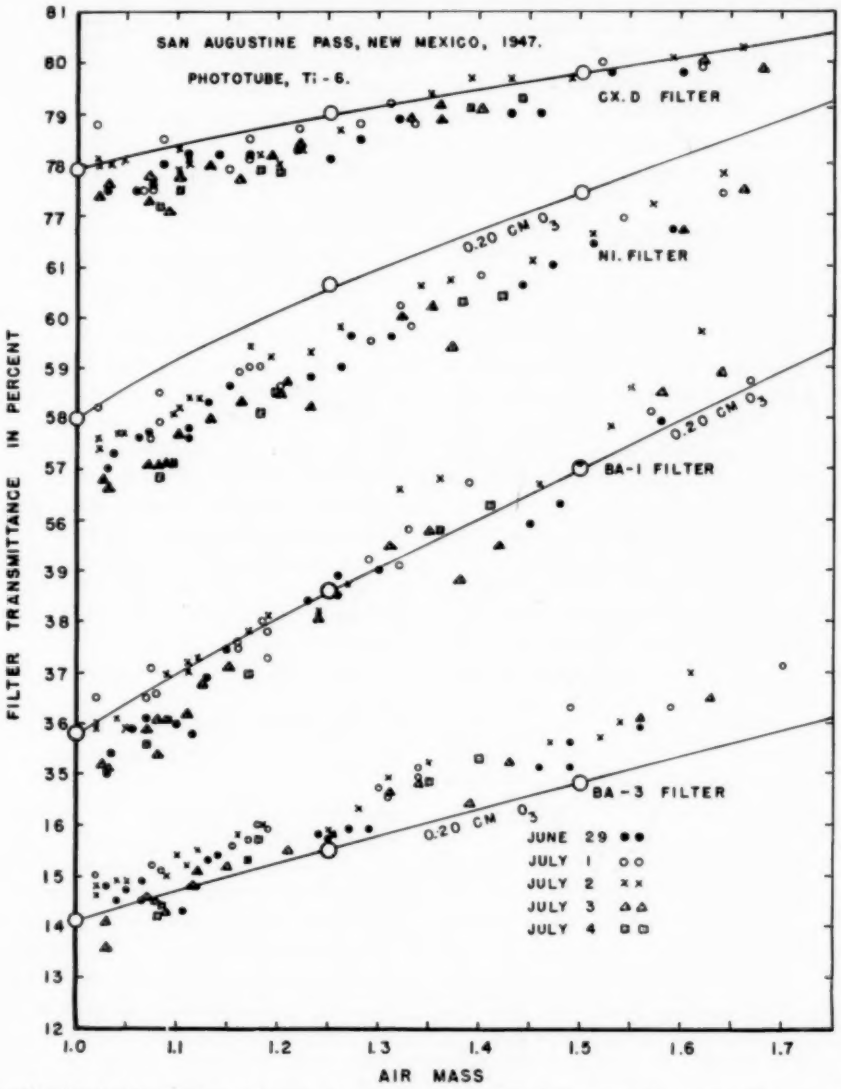

FIGURE 6. *Graphs showing the amount of ozone in the stratosphere, based on observations with titanium phototube No. 6; calculations based on the 1947 Stair solar energy curve for air mass, m=0*

768101—48——2

time as would be expected with the air mass front moving in from the north. Because of these clouds no ozone measurements could be made.

By the morning of July 1, the mass front had passed to the south of White Sands leaving the area blanketed with polar continental air at lower levels, with some tropical maritime above and continental tropical air at still higher levels. The higher ozone value observed is in agreement with other observations [2, 6, 7] showing greater amounts of ozone at higher latitudes or associated with polar air masses. A strong wind was blowing from the east throughout the day. Except for some haze and a few clouds, the sky remained relatively clear until late afternoon when it rapidly clouded up, giving rise to several thunder showers within the area. Early in the evening there was a light shower (less than $\frac{1}{10}$ in.) over the San Augustine Pass area.

On July 2, the atmospheric conditions remained about the same as on July 1, except there were but few clouds at any time. The wind continued from the east. By this time most of the continental United States was covered by the continental air mass that had moved in from Canada. However, the San Augustine Pass area was near a large mass of tropical maritime air, which was over the greater part of Texas and was moving to the north and west.

By July 3, the air mass over San Augustine Pass was probably tropical maritime, with tropical continental aloft. There was little wind at the ground level, and more clouds in the sky, especially of the fracto-cumulus type, as illustrated in the photograph (fig. 8), which was made on this day. During most of the day these clouds were continually forming over the Organ Mountain area. Although there was a light wind, the clouds remained relatively stationary through the process of breaking up and reforming. The lower ozone value observed on this day is in keeping with the probable air mass conditions.

By July 4, the air mass was no doubt a tropical maritime air mass or of similar constitution. The wind had practically ceased to blow, and the formation of fracto-cumulus clouds so nearly covered the mountain area that measurements were discontinued about noon of this day. Low values of ozone were to be expected and were observed on this day.

The mean value of ozone when all of these measurements are considered appears to be 0.20 and 0.21 cm ntp. The data obtained with phototube Ti–2 indicate the higher value. As the spectral response of this phototube has remained constant over the past 12 years following its original calibration, greater weight should probably be given to this higher value.

In obtaining the mean value of 0.21 cm ntp, greatest weight was given to the data for filter Ba–1 because its transmittance was within the range of greatest sensitivity to ozone changes. Furthermore, greater weight was given to the smaller air mass values, as the effects of haze, dust, and clouds were less near the noon hour on most of the days on which the observations were made.

The fact that there is not perfect agreement for the calculated amount of ozone between the measurements with the four filters for each of the two phototubes (eight independent determinations) is not disconcerting. The discrepancies are of the order of the errors in the measurements of the spectral transmittances of the filters or of the relative spectral responses of the phototubes. Filters having transmittances less than 30 percent or more than 70 percent (for sunlight) should not be used for the determination of total ozone. They are included in this case mainly for their value in establishing the spectral solar energy curve and are given but little weight in the ozone determinations. Furthermore, in this case it appears that the transmittance of the Ni filter is out of agreement with the mean of the other three filters, indicating that its spectral transmittance may be slightly in error.

VI. Solar Energy Curve Outside the Atmosphere

In this work it is necessary to know or else calculate the relative solar energy curve of the sun for a number of different air masses. In any case, one of these is either for air mass=0, or else that curve may be simply calculated. In the present work, the curve for the sun outside the atmosphere as previously published by Stair and Hand [1] was used for preliminary calculations. However, as data were needed for wavelengths extending up to 3,400 A, this curve was arbitrarily extended to that wavelength.

The preliminary calculations of filter transmi-

tance indicated that the arbitrary curve in the longer wavelengths was too high relative to the values at 3,000 to 3,200 A. Hence adjustments were made until there was reasonable agreement between observed and calculated transmittance values for different air masses for the four filters with the two phototubes. Calculations made using a solar energy curve obtained by Hulburt [22] at an altitude of 55 km (above more than 99 percent of the atmospheric ozone) give an ozone value about 0.015 cm greater than the values indicated by the calculations illustrated in figures 5 and 6. However, the filter transmittance indicated poorer agreement for the shape of this solar energy curve than for the one defined by the data of column 2 of table 1.

Up to this point only the relative shape of the solar energy curve has been considered. Nothing has been considered that would give it magnitude in terms of microwatts per square centimeter per unit of wavelength. That step is next. As the shape of the curve is defined by the relative values of column 2 of table 1, the magnitude of these values will now be discussed in terms of a wavelength unit of 10 A.

First, the calibration of the ultraviolet meter for total response to a standard of ultraviolet radiation will be considered [9, 14, 21]. Two calibration constants designated P and G for the standard lamp and for the sun respectively are required. The method of determination of factor P is given best by the presentation of the actual data of table 2. From this table, factor P is found to be 5.40 for Ti-2 and 6.73 for Ti-6.

Next, from the relative solar data for some observed air mass, factor G is obtained. In the present work the air masses 1.00 and 1.25 were employed, as curves are already calculated for these values (see table 1).

To obtain factor G for Ti-2 and air mass 1.00, the procedure is as follows: First take an arbitrary wavelength interval, for example all wavelengths shorter than 3,210 A (see table 1). This sum is 139.96 and is found by adding all the values in column 5 for the wavelength intervals shorter than 3,220 A. Next take the sum of all values in column 7. This is found to be 85.81. Finally, take the ratio of 139.96 to 85.81, which is 1.63—designated factor G. The factor G for $M=1.25$ was obtained in a similar manner and found to be 1.58. For phototube Ti-6, the corresponding values were 1.45 and 1.39.

TABLE 2. *Calibration of phototubes, using standard ultraviolet lamp with a Corex D filter; calculation of factor P*

Factor $P=38.48\div7.12=5.40$ for Ti-2.
Factor $P=39.86\div5.92=6.73$ for Ti-6.
(7.12 and 5.92 were the observed ultraviolet meter deflections when the standard lamp was used as the source of radiation).

Wavelength	Standard lamp energy through Cx. D filter	Relative response, Ti-2	Relative response, Ti-6	Energy times response, Ti-2	Energy times response, Ti-6
A	$\mu w/cm^2$				
3,340	6.6	0.023	0.047	0.15	0.46
3,132	53.3	.380	.385	20.25	20.52
3,024	18.5	.615	.627	11.38	11.60
2,967	7.0	.723	.76	5.06	5.32
2,890	1.8	.75	.85	1.35	1.53
2,804	0.5	.57	.85	0.29	0.43
Total				38.48	39.86

In order to arrive at a value of total response, all the observational data obtained for air masses 1.02 to 1.30 were plotted and the values read from a smooth curve at $M=1.00$ and $M=1.25$. The mean values thus obtained were 16.0 and 12.1 microamperes for phototube Ti-2, and 14.3 and and 11.0 for phototube Ti-6 for air masses $M=1.00$ and $M=1.25$, respectively.

From the above information, the total energy may be calculated for the two phototubes for the two air masses $M=1.00$ and $M=1.25$. These were as follows: (The factor 2 entering into each equation is an instrument scale factor, U. V. Q. is used as a symbol to denote the total radiant flux density within the selected spectral region.)

For Ti-2

U. V. Q. ($M=1.00$) $=16.0\times2\times5.40\times1.63=282\mu w/cm^2$.

U. V. Q. ($M=1.25$) $=12.1\times2\times5.40\times1.55=206\mu w/cm^2$.

For Ti-6

U. V. Q. ($M=1.00$) $=14.60\times2\times6.73\times1.45=285\mu w/cm^2$.

U. V. Q. ($M=1.25$) $=11.30\times2\times6.73\times1.39=211\mu w/cm^2$.

From these the mean values of the total solar energy for the two air masses, $M=1.00$ and $M=1.25$, becomes 283 and 209 $\mu w/cm^2$ for wavelengths shorter than 3,210 A.

If now the above information is applied to the data of table 1, an intensity factor may be found which, when multiplied by the relative values of solar energy in column 2, will give the absolute spectral solar energy outside the earth's atmosphere. This factor is found as follows (see table 1). Again take the sum of all values in column 5 for the same wavelength interval as used before, namely shorter than 3,210 A. This value was found to be 139.96. For phototube Ti-2 we have $282 \div 139.96 = 2.01$ for $M=1.00$, and similarly, $206 \div 101.59 = 2.03$ for $M=1.25$. For phototube Ti-6 the corresponding data are $285 \div 139.96 = 2.04$ for $M=1.00$, and similarly, $211 \div 101.59 = 2.08$ for $M=1.25$. The mean of these four values (2.04) is the intensity factor. However, as the data are to be evaluated in terms of a wavelength interval of 10 A (20 A have been used in the table), this factor becomes 1.02 as a multiplying factor to be applied to the data of column 2 of table 1 to give the solar energy curve outside the earth's atmosphere in microwatts per square centimeter per 10-A interval of wavelength. The values thus obtained are illustrated in figure 7.

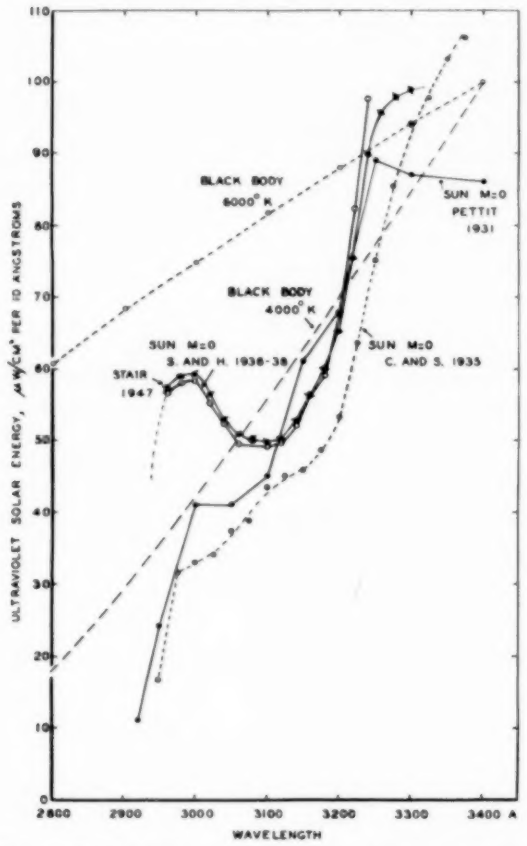

FIGURE 7. *Distribution of energy in the extreme ultraviolet of the solar spectrum.*

The Stair curve is the average of determinations with two phototubes at Organ Mountain. The S & H (Stair and Hand) curve is the average of determinations at Mount Evans, Colorado with four phototubes. Curves by other observers and for a black body (on relative scales) are given for comparative purposes.

The very close agreement in absolute units between the solar curve obtained from this work and that obtained at Mount Evans is encouraging and is much better than was expected. The fact that the two phototubes gave values in close agreement, although one of them had changed in both total and spectral response since it was employed at Mount Evans, indicates that with careful calibration this method is both reliable and practical for the measurement of total ultraviolet solar radiation.

VII. Conclusions

The preliminary calibrations and calculations for a particular phototube and filters for a particular station are complicated, but when these are once made it is possible, from a set of curves, to determine the total ozone value from measurements with a single filter within a few minutes. It is more efficient and accurate to use a filter having a total integrated transmittance near 3 percent, as the transmittance of a filter in this range is most sensitive to ozone changes when used with a phototube of the type employed in this work. Should ozone measurements of this type become useful for weather forecasting purposes, this method appears practical for use at an extended group of stations, with calibrations performed at some central station.

The total amounts of ozone determined for the San Augustine pass in the Organ Mountains are in agreement with other determinations for the same latitude and season of the year. The relationship between the change in total ozone and air mass agrees with observations made by others within the past 10 years.

The author expresses appreciation to the Naval Research Laboratory, which sponsored and financed this work at White Sands Proving Ground, N. Mex.; and to R. Tousey, who made the arrangements for this trip, to F. S. Johnson, S. S. Houston, and D. C. Olsen, who assisted in the observational program; and to other members of the White Sands Proving Ground staff who helped to make this work possible.

FIGURE 8. *San Augustine Pass, New Mexico, elevation 5,640 feet, looking north; showing clouds, on afternoon of July 3.*

VIII. References

[1] R. Stair and I. F. Hand, Monthly Weather Rev., **67**, 331 (1939).
[2] G. M. B. Dobson, Proc. Roy. Soc. (London) [A] **129,** 411 (1930).
[3] A. Vassy and E. Vassy, Compt. rend **207,** 1232 (1938).
[4] D. Barbier and D. Chalonge, J. phys. radium, **10,** 113 (1939).
[5] F. W. P. Götz, Helv. Phys. Acta. **13,** p. 3 (1940).
[6] G. M. B. Dobson and A. R. Meetham, Quart. J. Roy. Meteorolog. Soc. (London) **60,** 265 (1934).
[7] F. W. P. Götz, Gerlands Beitr. Geophys. **31,** 119 (1931).
[8] G. M. B. Dobson, A. W. Brewer, and B. M. Cwilong, Proc. Roy. Soc. (London) [A] **185,** 144 (1946).
[9] R. Stair and W. W. Coblentz, J. Research NBS **20,** 185 (1938) RP1075.
[10] R. Stair and W. O. Smith, J. Research NBS **30,** 449 (1943) RP1543.
[11] R. Stair and W. W. Coblentz, Nat. Geog. Soc., Contr. Tech. Papers, Solar Eclipse Series No. 2, p. 48 (1942).
[12] John Strong, Phys. Rev. **55,** 1114 (1939); J. Franklin Inst. **231,** 121 (1941); J. Opt. Soc. Am. **29,** 520 (1939).
[13] K. Walanabe, J. Franklin Inst. **236,** 461 (1943).
[14] W. W. Coblentz and R. Stair, J. Research NBS **16,** 315 (1936) RP877.
[15] C. Fabry and H. Buisson, J. Phys. [5] **3,** 196 (1913); Astrophys. J. **54,** 297 (1921).
[16] B. O'Brien, Nat. Geog. Soc. Contrib. Tech. papers, Stratosphere Series, No. 2, p. 49 (1936).
[17] H. H. Cary and Arnold O. Beckman, J. Opt. Soc. Am. **31,** 682 (1941).
[18] Kasson S. Gibson and Margaret M. Balcom, J. Research NBS **38,** 601 (1947) RP1798.
[19] The American ephermeris and nautical almanac (Nautical Almanac Office, U. S. Navy Dept., Washington, D. C., 1947).
[20] F. Ball, Altitude tables, 30° to 60° (J. S. Potter, London, 1907).
[21] R. Stair and I. F. Hand, Bul. Am. Meteorolog. Soc. **22**, 259 (1941).
[22] E. O. Hulburt, The upper atmosphere of the earth, J. Opt. Soc. Am. **37,** 405 (1947).
[23] George A. Van Lear, J. Opt. Soc. Am. **37,** 525 (1947).

WASHINGTON, September 16, 1947.

U. S. Department of Commerce
National Bureau of Standards

Research Paper RP1852
Volume 40, January 1948

Part of the Journal of Research of the National Bureau of Standards

Note on Volume Effect in Coiling Molecules

By Robert Simha

An estimate of the magnitude of the interference effect in a coil-like molecule is made by calculating the nearest neighbor density w around a given link as a function of the total number of contributing chain units. It is shown for instance, that in a chain consisting of several hundred units, the first 15 contribute about 75 percent of the total nearest neighbor density at distances below the length of a link. The plots presented indicate that after about the first 20 links, the rate of increase of nearest neighbor density begins to flatten off. It is also possible to derive the modification of the distribution function of chain-ends in real chains for a given form of w.

The familiar model of a chain molecule currently used consists of an array of links of fixed length, making a fixed valence angle with each other, and able to rotate relatively to each other freely or in a manner restricted by potential barriers. This model is amenable to the treatment given by Rayleigh [1] [1] in his theory of random flight. For a linear chain of i links, it leads to the well-known result for the probability of finding a distance within an interval r, $r+dr$ between the two ends:

$$p_i\left(\frac{r}{l}\right)dr=\left(\frac{3}{2\pi l^2}\right)^{3/2}\frac{1}{i^{3/2}}exp\left(-\frac{3r^2}{2l^2i}\right)4\pi r^2dr \quad (1)$$

In dealing with the model of a chain molecule of fixed valence angle, l is equal to the length of a link corrected for the valence angle and for restricted rotation due to a potential barrier around each link,[2] [2, 3]. Equation 1 holds strictly only in the limit $i\rightarrow\infty$. Using exact equations for small values of i [1], one finds, e. g., for $i=6$, $p_6(1/4)=0.017$, according to eq 1, as compared with the exact value of 0.015. As the correction for restricted rotation amounts to changing the effective magnitude of l, it is possible to replace the actual chain by an effective one possessing free rotation but consisting of $i_{eff}<i$ "segments" of length $l_{eff}>l$ [4].

From eq 1 we can derive the aggregate probability $_{\nu}^{N}f_c(r)4\pi r^2dr$ of finding the endpoint of any link i, $\nu\leq i\leq N$, at distances between r and $r+dr$ from one end of the chain, vz.

$$_{\nu}^{N}f_c(r)4\pi r^2dr=\sum_{i=\nu}^{N}p_i\left(\frac{r}{l}\right)dr\doteq$$

$$6\frac{r}{l}\left[\Phi\left(\sqrt{\frac{3}{2\nu}}\frac{r}{l}\right)-\Phi\left(\sqrt{\frac{3}{2N}}\frac{r}{l}\right)\right]\frac{dr}{l}. \quad (2)$$

Here the sum has been replaced by an integral. The function Φ is the error integral:

$$\Phi(\xi)=\frac{2}{\sqrt{\pi}}\int_0^{\xi}e^{-x^2}dx$$

In these considerations, configurations that allow different parts of the chain to occupy the same volume element are not excluded; in other words, volume effects are not taken into account. It is the purpose of this note to present essentially on the basis of results in eq 1 and 2 that constitute a zero approximation in respect to the above effect, a rough estimate of the magnitudes of the effects involved and particularly to examine the extent of the relative contributions of the links farther apart from a reference link to the volume effect. Let us now consider the probability $w(r)4\pi r^2dr$ of finding a nearest neighbor within a spherical shell with its center at one end of the chain. For values of r smaller than l, this function will be considered as a relative measure for the occurrence of interference, although such distances can also be realized without interference. In the limit of $r\rightarrow 0$, the function w becomes, of course, identical with f. For finite distances, w can be obtained by a slight extension of an argument first given by Hertz [5]. Let $f(r)d\tau$ represent the number of points in a volume element $d\tau$, within a spherical shell between r_2 and r_1, such that

$$\int_{r_1}^{r_2}f(\rho)d\tau=N,$$

[1] Figures in brackets indicate the literature references at the end of this paper.

[2] P. Debye, lectures presented on various occasions.

where N is the total number of points. Then the following relation exists between w and f:

$$\left[1-\int_{r_1}^{r} w(\rho)4\pi\rho^2 d\rho\right]\cdot\frac{Nf(r)4\pi r^2 dr}{\int_{r}^{r_2} f(\rho)4\pi\rho^2 d\rho}=w(r)4\pi r^2 dr. \tag{3}$$

The validity of this equation can be seen readily. The probability of finding a nearest neighbor between r and $r+dr$ (the right-hand side of eq 3) equals the probability of finding no nearest neighbor at a distance smaller than r (the factor in the bracket) multiplied by the probability of one of the N points being confined to a shell between r and $r+dr$, if the space between r_1 and r is empty (the second factor). Taking into account the normalization condition, eq 3 can be transformed by suitable differentiation into:

$$\left[1-\frac{\int_{r_1}^{r} f(\rho)4\pi\rho^2 d\rho}{N}\right]\frac{d}{dr}\left(\frac{w}{f}\right)+4\pi r^2 f\left(1-\frac{1}{N}\right)\frac{w}{f}=0,$$

which has the solution:

$$W=f\left[1-\frac{\int_{r_1}^{r} 4\pi\rho^2 f(\rho)d\rho}{N}\right]^{N-1}\doteq f\exp\left[-\int_{r_1}^{r} f(\rho)4\pi\rho^2 d\rho\right]. \tag{4}$$

In interpreting this result one notes that the factor f on the left indicates the probability of finding a point in the volume element in question, and the quantity in the first bracket represents the probability of no point being in the volume between r_1 and r. This consideration could have been used directly to arrive at the expression for w. The second equation holds in the limit when r is close to r_1 and N is large.

In applying eq 4 to the problem under consideration, the distribution ${}^{N}_{\nu}|f_c$ is inserted for the function f. For values of ν larger than or equal to 6, eq 2 will be used. For values of ν between 2 and 6, Rayleigh's [1] exact polynomial expressions will be employed. For this purpose the function $p_5\left(\frac{r}{l}\right)$ not given in reference [1] was computed. The details of the calculation will be omitted. Setting $x=\frac{r}{l}$ and r_1 in lf 4 equal to zero one finds

$${}^{5}_{2}f_c(r)4\pi r^2 dr=\frac{x}{2}\left(1+\frac{21}{8}x-\frac{3}{8}x^2-\frac{1}{8}x^3\right)dx;\ x<1. \tag{2a}$$

The integrations required by eq 4, using eq 2 and 2a and setting r_1 equal to zero can be readily performed. Integration of eq 2, for instance, yields:

$${}^{N}_{\nu}\Big|\int_{1}^{r} f(\rho)4\pi\rho^2 d\rho=2\left\{\frac{3}{2}x^2\left[\Phi\left(\sqrt{\frac{3}{2\nu}}x\right)-\Phi\left(\sqrt{\frac{3}{2N}}x\right)\right]-\frac{\nu}{2}\Phi\left(\sqrt{\frac{3}{2\nu}}x\right)+\frac{N}{2}\Phi\left(\sqrt{\frac{3}{2N}}x\right)+\sqrt{\frac{3\nu}{2\pi}}xe^{-\frac{3x^2}{2\nu}}-\sqrt{\frac{3N}{2\pi}}xe^{-\frac{3x^2}{2N}}\right\}. \tag{5}$$

Figure 1 shows the contributions of links from the second to the Nth, inclusive, to the nearest neighbor probability $w(r)4\pi r^2 dr$ as function of N for values of $r/l=\frac{1}{4}$ and $\frac{1}{2}$, respectively, calculated from the pertinent equations. It can be seen for instance that the links from the fifteenth to the two hundredth relative to a reference link still make a contribution of the order of 25 percent to the total effect, although the larger part is of course due to the nearest links. Analogous conclusions may be drawn regarding interference around links in the interior of the chain or for shorter chains. In a chain with $N=50$, for instance, the first 15 members contribute 85 percent of the total nearest neighbor effect. As shown, the use of eq 1 for a short chain of six links is really not adequate. However, this equation makes the contribution for low N's larger and

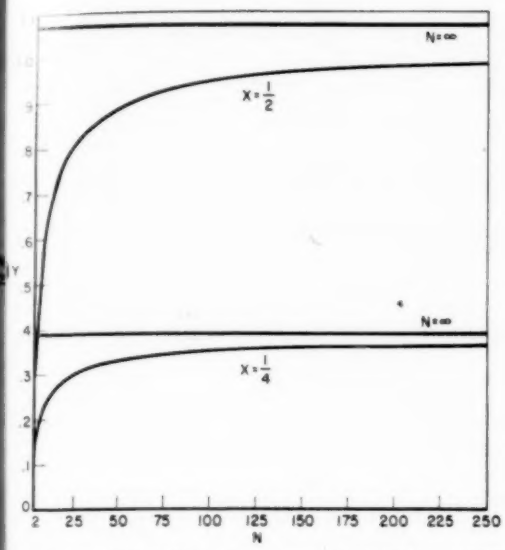

FIGURE 1. *Contribution to the nearest neighbor density* $\frac{N}{2}[w(r)4\pi r^2$, *designated by* $\frac{N}{2}]Y$, *around a reference point as function of the number of successive links for* $r=l/4$ *and* $r=l/2$.

therefore does not alter the conclusion that the volume effect does not entirely originate from a small number of neighboring units in the chain. The segment size in "effective" chains referred to above would have to be quite large. The correct form of $w(r)$ would tend rapidly to zero on approaching a critical distance r below l, and would assume the form used above for larger distances. Therefrom modified expressions for $\frac{N}{2}[f_c(r)$ and the distribution functions p_i can be derived by utilizing the method discussed.

Mary Budge aided in the numerical calculations.

[1] Lord Rayleigh, Sci. Papers **6** (Cambridge Univ. Press, Cambridge, 1920); S. Chandrasekhar, Rev. Mod. Phys. **15,** 1 (1943).
[2] C. Sadron, J. chim. phys. **43,** 12 (1946).
[3] W. J. Taylor, J. Chem. Phys. **15,** 412 (1947).
[4] W. Kuhn, Kolloid-Z. **68,** 1 (1934).
[5] P. Hertz, Math. Ann. **67,** 387 (1909); G. Jaffé, Phys. Rev. **58,** 968 (1940).

WASHINGTON, August 12, 1947.

U. S. Department of Commerce
National Bureau of Standards

Research Paper RP1853
Volume 40, January 1948

Part of the Journal of Research of the National Bureau of Standards

Dissociation of SF_6, CF_4, and SiF_4 by Electron Impact

By Vernon H. Dibeler and Fred L. Mohler

The dissociation by electron impact of SF_6, CF_4, and SiF_4 has been studied with a consolidated mass spectrometer. Data are also given on the appearance potentials of various ions in the mass spectra and measurements on the isotope abundance of sulfur, carbon, and silicon. The observed appearance potentials of the F^+ ion in SF_6 and CF_4, and the C^+ ion in CF_4 were found to be lower than the calculated value assuming formation of a positive atom ion and a free electron, but nearly equal to the calculated value assuming the formation of a positive atom ion and a negative fluorine ion. The large relative abundance of the SF_4^{++} ion in SF_6 and the CF_2^{++} ion in CF_4 is taken to indicate the formation of these ions by removal of two F^- ions in the former and possibly an F^- ion and a free electron in the latter case.

I. Introduction

The results reported in this paper are a part of a general study of the dissociation of volatile fluoro compounds by electron impact. Many of these compounds have been useful in isotope abundance studies of a number of the elements because of their relatively high vapor pressure and the monoisotopic character of fluorine. Apparently very little has been published, however, concerning the dissociation of such molecules by electron impact except to note in the isotope studies that dissociation, rather than formation of the molecular ion, is the more probable process. Kusch, Hustrulid, and Tate, [1],[1] and Baker and Tate [2] have shown that this is a property shared with the chlorides of phosphorous, arsenic, and antimony, as well as some halogen derivatives of methane namely, CCl_4, $CHBrF_2$, and CCl_2F_2. More recently, White and Cameron [3] have reported the critical potentials of various ions in the mass spectrum of UF_6. No value was listed for the UF_6^+ ion, presumably because of its very low intensity. No information was given as to the relative abundance of the various dissociated ions. In view of considerable interest in these compounds, therefore, we wish to report in detail the dissociation patterns for several fluorocompounds as well as the appearance potentials of various ions in the mass spectra. Data are also given on the isotope abundance of sulfur, carbon, and silicon for purposes of comparison with value previously obtained for these elements using other types of mass spectrometers and other compounds.

[1] Figures in brackets indicate the literature references at the end of this paper.

II. Experimental Procedure

Pertinent details of the Consolidated mass spectrometer and the methods used to obtain the reported data have been described in detail in previous reports [4, 5]. The voltage scale of the appearance potential measurements was corrected using the observed value of the argon A^+ ion compared to the spectroscopic value [6]. The mass spectra were obtained at ionizing electron energies of 50, 70, and 100 volts. The most abundant ion in each 50-volt spectrum is assigned a value of 100 percent. The other ions are evaluated according to their abundance relative to the most abundant ion. The isotope abundance measurements were made at several different values of ion accelerating voltage and of electron energy and current. Whenever possible, the ratios were checked using different ions in the same mass spectrum. The fact that no significant variation in the isotope abundance ratios was observed under these conditions was assumed to indicate minimum discrimination in the ion source.

The SF_6 was obtained from the high voltage laboratory of the Massachusetts Institute of Technology and was a portion of a sample submitted to the Temperature Measurements Section of the Bureau for test purposes. Mass spectro-

metric analysis indicated an approximate purity of 99 percent with small amounts of fluorocarbons as impurities. It was used without further purification. The CF_4 was obtained from the Jackson laboratory, E. I. du Pont de Nemours Co., and used without further purification. Mass spectrometric analysis showed a total impurity of about 2 percent, principally $CClF_3$, N_2, and CO_2. Several samples of SiF_4 were prepared by Howard W. Bond [2] by reacting H_2SO_4 and CaF_2 in the presence of SiO_2 from various sources. These samples were also used without further purification. The mass spectrometer indicated a purity >99 percent. The principal impurity was CO_2.

III. Results and Discussion

Sulfur hexafluoride.—Table 1 shows the mass spectrum of SF_6 at three different ionizing voltages. No correction has been made in this or following mass spectrum tables for the contribution of the ion accelerating field to the electron energy. No SF_6^+ ion was observed. Its abundance is estimated to be less than 2/10,000 of the abundance of the SF_5^+ ion. The most probable dissociation process is loss of one fluorine atom from the molecular ion. In the formation of ions requiring further dissociation, however, the subsequent loss of three fluorine atoms from the molecular ion is more probable than the loss of 2 atoms. For example, the abundance of the SF_3^+ ion is greater than that of the SF_4^+ ion, and the SF^+ ion is more abundant than the SF_2^+ ion. The doubly charged ions S^{++}, SF^{++}, SF_2^{++}, SF_3^{++}, and SF_4^{++} were observed. The ions F^{++}, SF_5^{++}, and SF_6^{++} were not found and are estimated to be less than 0.02 percent of the SF_5^+ peak. It is of interest that for 100-volt electrons, the abundance of the SF_2^{++} ion and SF_4^{++} ion is greater than the abundance of the corresponding singly charged ions. The peak at $m/e=91.8$ is a metastable ion that has undergone dissociation after traversing the ion accelerating field [7]. It can be ascribed to the transition

$$SF_5^+ \rightarrow SF_4^+ + F.$$

If m_a is the apparent mass, m_i and m_f, the initial and final masses, respectively, $m_a=(m_f)^2/m_i=(108)^2/127=91.8$.

[2] Now at the National Institute of Health, Bethesda, Maryland.

TABLE 1. *Mass spectrum of SF_6 for 50, 70, and 100-volt electrons*

m/e	Ion	Relative intensities		
		50 volts	70 volts	100 volts
16	S^{++}	0.03	0.06	0.09
19	F^+	3.37	5.63	9.11
25.5	SF^{++}	.....	0.76	1.97
32	S^+	5.60	9.96	13.5
33	S^+	0.06	0.09	0.11
34	S^+	.27	.47	.60
35	SF_2^{++}	1.36	6.80	13.3
35.5	SF_2^{++}	.....	0.10	0.10
36	SF_2^{++}	0.07	.33	.62
44.5	SF_3^{++}	0.38	1.26	2.17
45.5	SF_3^{++}	.....	0.07	0.11
51	SF^+	8.66	11.0	11.6
52	SF^+	0.07	0.09	0.11
53	SF^+	.90	.51	.64
54	SF_4^{++}	4.05	11.0	17.6
54.5	SF_4^{++}	.....	0.09	0.11
55	SF_4^{++}	0.23	.54	.78
70	SF_2^+	5.74	6.39	6.46
71	SF_2^+	0.04	0.07	0.09
72	SF_2^+	.27	.30	.27
89	SF_3^+	27.6	33.5	35.7
90	SF_3^+	0.20	0.26	0.24
91	SF_3^+	1.22	1.48	1.36
91.8	$SF_3^+ \rightarrow SF_4^+ + F$	0.21	0.26	0.24
108	SF_4^+	8.98	10.8	11.5
109	SF_4^+	0.07	0.11	0.10
110	SF_4^+	.41	.47	.51
127	SF_5^+	100	113	117
128	SF_5^+	0.92	1.14	1.15
129	SF_5^+	4.30	4.89	4.87
131	SF_5^+	0.04	0.04	0.04

Table 2 lists the appearance potentials of various ions in the mass spectrum of SF_6. A complete analysis of the appearance potential data is not possible because of the lack of necessary spectroscopic or thermochemical data. However, from the relation

$$D(SF_6)=Q(SF_6)+3D(F_2)+L(S),$$

where $Q(SF_6)$ is the energy of formation of SF_6, $D(F_2)$ is the dissociation energy of molecular fluorine, $L(S)$ is the heat of sublimation of sulfur, and the thermochemical data of Bichowsky and Rossini [8] the energy of dissociation of the process $SF_6 \rightarrow S+6F$, is calculated to be 516 kcal/mole or 22.4 electron volts. It follows that the minimum energy required to produce an S^+ ion and a free electron will be $D(SF_6)$ plus the ionization poten-

tial (10.3 volts) [6] of sulfur (22.4+10.3=32.7 volts). The observed appearance potential of the S^+ ion is 37.3 volts. This is 4.6 volts in excess of the calculated minimum energy required to produce an S^+ ion and a free electron. It is concluded that the production of S^+ gives considerable kinetic energy to the seven dissociation fragments; namely 4.6 volts if a free electron is removed. If it is assumed that one of the fluorine atoms combines with the electron to form an F^- ion in the ionization process, the excess energy is increased to 8.6 volts by the value of the electron affinity (4.0 volts) [9] of fluorine. One could also assume that one or two pairs of fluorine atoms combined in the ionization process to form molecular fluorine with an energy of 2.7 volts per molecule of F_2, but this seems to be an improbable process in spontaneous dissociation.

TABLE 2. *Appearance potentials of various ions in the mass spectrum of* SF_6

m/e	Ion	Appearance potential
		v
19	F^+	35.8±1
32	S^+	37.3±1
35	SF_2^{++}	46.5±0.5
51	SF^+	31.3± .3
54	SF_4^{++}	40.6± .5
70	SF_2^+	26.8± .3
89	SF_3^+	20.1± .3
91, 8	SF_3^+ SF_4^{++}+F	20 ±1
108	SF_4^+	18.9±0.2
127	SF_5^+	15.9± .2

An F^+ ion could conceivably be found in any process in which SF_6 is dissociated. However the appearance potential of F^+ (35.8 volts) is higher than the appearance potential of any of the polyatomic singly charged ions. This suggests that F^+ occurs from complete dissociation like the S^+ ion. From the same dissociation process, the minimum energy required to produce an F^+ ion and a free electron is 22.4+18.6[6]=41.0 volts. The observed appearance potential of F^+ (35.8 volts) is insufficient to produce F^+ and a free electron. The minimum energy required to produce an F^+ and an F^- from SF_6, however, is 37.0 volts. The observed value (35.8 volts) is close enough to leave little doubt that this is the actual process involved.

Table 3 gives the observed isotope abundance of sulfur. Also given in table 3 are the results reported by Nier [10] from a study of SO_2 using a specially designed mass spectrometer. The disagreement of the S^{36} abundance is greater than the estimated experimental error whether calculated from the SF_5^+ ion, the SF_4^+ ion or the SF_2^+ ion. Other ions were not usable because of low intensity or interference by the metastable ion or doubly charged ions. From the isotopic masses listed by Pollard [11] (assuming same packing fraction for S^{34} and S^{36}) and the conversion factor 1.000275, the authors' values give a chemical weight of 32.065. The accepted value by chemical methods is 32.066 [12].

Carbon Tetrafluoride.—Table 4 shows the mass spectrum of CF_4 at several energy values of the ionizing electrons. The most probable dissociation process is again the loss of one fluorine atom to produce the CF_3^+ ion. The abundance of the CF_4^+ ion is estimated to be less than 1/1,000 relative to the CF_3^+ ion. The relatively large abundance of the CF_2^+ ion is unusual by analogy with other halogenated molecules (see, for example, [1] and [2], and tables 1 and 7). Doubly charged

TABLE 3. *Isotope abundance of sulfur*

	m/e			
	32	33	34	36
Mean	95.03	0.76	4.17	0.035
Average deviation	±0.02	±.01	±0.01	±.003
Nier [10]	95.1	.74	4.2	.016

TABLE 4. *Mass spectra of* CF_4 *for 50, 70 and 100-volt electrons and* CH_4 *for 50-volt electrons*

Carbon tetrafluoride					Methane	
m/e	Ion	Relative intensities at—			Ion	Relative intensities at 50 volts
		50 volts	70 volts	100 volts		
12	C^+	6.72	10.1	11.0	C^+	2.40
13	C^+	0.08	0.11	0.12		
15.5	CF^{++}	.....	.06	.15		
19	F^+	3.09	5.95	8.14	H^+	3.21
25	CF_2^{++}	1.51	5.93	11.0		
25.5	CF_2^{++}	.....	0.06	0.13		
31	CF^+	3.67	4.85	6.17	CH^+	7.91
34.5	CF_3^{++}	.....	2.04	3.92		
50	CF_2^+	12.4	15.4	15.6	CH_2^+	15.9
51	CF_2^+	0.13	0.17	0.17		
69	CF_3^+	100	120	133	CH_3^+	84.6
70	CF_3^+	1.16	1.31	1.46	CH_4^+	100

ions CF^{++}, CF_2^{++}, and CF_3^{++} were observed. No metastable ions were observed. The mass spectrum of methane is also included in table 4 for comparison. No doubly charged or metastable ions are observed in methane.

Table 5 lists the appearance potentials of various ions in the mass spectrum of CF_4. A complete analysis of the appearance potential data is impossible due to the lack of sufficient thermochemical or spectroscopic data. From Bichowsky and Rossini [8] the energy of dissociation into atoms $CF_4 \rightarrow C+4F$ is calculated to be 458 kcal/mole, or 19.9 electron volts. The minimum energy required to produce a C^+ ion and a free electron is $19.9+11.2^6=31.1$ volts. The minimum energy to give F^+ and a free electron with complete dissociation is $19.9+18.6^6=38.5$ volts. The observed appearance potentials of both ions are less than these values, and it must be assumed that in both cases F^- ions are formed in the ionization process and not free electrons. The process $CF_4 \rightarrow C^+ + F^- + 3F$ requires $31.1-4.0=27.1$ volts compared to the observed appearance potential of 27.5 ± 1 volts. The process $CF_4 \rightarrow C+F^++F^-+2F$ requires $38.5-4.0=34.5$ volts compared to the observed appearance potential of 35.5 ± 1 volts.

TABLE 5. *Appearance potentials of various ions in the mass spectrum of* CF_4

m/e	Ion	Appearance potential
		e
12	C^+	27.5±1.
19	F^+	35.5±1.
25	CF_2^{++}	44.3±0.5
31	CF^+	29.8± .3
34.5	CF_2^{++}	43.8± .5
50	CF_2^+	21.8± .3
69	CF_3^+	15.9± .2

The C^{12}/C^{13} ratio as measured from the CF_3^+ and the CF_2^+ ions was 89.9 ± 1.7, compared with the value of 90 ± 2 reported by Nier and Gulbranson [13], using carbon dioxide from the air.

Silicon Tetrafluoride.—Table 6 shows the mass spectrum of SiF_4 for 50, 70, and 100-volt electrons. The removal of one fluorine atom to form the SiF_3^+ ion is again the most probable process. In contrast to SF_6 and CF_4, however, the molecular ion has an appreciable abundance. Further dissociation to SiF_2^+, SiF^+, and Si^+ follows the general pattern of halogenated molecules, i. e., the abundance of ions with an odd number of halogen atoms is greater than the abundance of those with an even number. The doubly charged ions SiF^{++}, SiF_2^{++}, and SiF_3^{++} were observed. The SiF_2^{++} ion becomes more abundant than the singly charged ion above 50 volts. No metastable ions are observed.

TABLE 6. *Mass spectrum of* SiF_4 *for 50, 70 and 100-volt electrons*

m/e	Ion	Relative intensities at—		
		50 volts	70 volts	100 volts
19	F^+	1.18	2.26	3.10
23.5	SiF^{++}	0.10	0.87	1.82
24	SiF^{++}		.05	0.09
24.5	SiF^{++}		.02	.05
28	Si^+	2.89	4.99	6.27
29	Si^+	0.18	0.28	0.38
30	Si^+	.11	.18	.21
33	SiF_2^{++}	1.35	4.56	7.48
33.5	SiF_2^{++}	0.08	0.23	0.38
34	SiF_2^{++}	.06	.16	.25
42.5	SiF_3^{++}	.46	1.37	2.13
43	SiF_3^{++}	.06	0.10	0.16
43.5	SiF_3^{++}		.04	.05
47	SiF^+	3.57	4.67	4.22
48	SiF^+	0.20	0.24	0.23
49	SiF^+	.15	.17	.17
66	SiF_2^+	.66	.79	.66
67	SiF_2^+	.06	.07	.07
68	SiF_2^+	.03	.04	.03
85	SiF_3^+	100.	122.	133
86	SiF_3^+	5.01	6.10	5.86
87	SiF_3^+	3.34	4.08	4.53
104	SiF_4^+	1.79	2.14	2.39
105	SiF_4^+	0.10	0.12	0.12
106	SiF_4^+	.06	.07	.08

The appearance potentials of several ions in the mass spectrum of SiF_4 are given in table 7.

The relative abundance of the isotopes of silicon have recently been measured by several investigators. The results of Ney and McQueen [14], Inghram [15], and Williams and Yuster [16], together with the authors' values are given in table 8. The agreement between the present work and the previously reported values is within the experimental uncertainty. The chemical weight calculated from the isotopic masses listed by Pollard [11] is 28.09 compared to the accepted chemical value of 28.06 [12].

TABLE 7. *Appearance potentials of several ions in the mass spectrum of SiF_4*

m/e	Ion	Appearance potential
		e
66	SiF_2^+	27.5±0.5
85	SiF_3^+	16.1±.2
104	SiF_4^+	16.9±.5

TABLE 8. *Isotope abundance of silicon*

	m/e		
	28	29	30
Mean	92.32	4.58	3.10
Average deviation	±0.03	±0.03	±0.02
Ney and McQueen [14]	92.24	4.69	3.07
Inghram [15]	92.28±0.08	4.67±0.05	3.05±0.03
Williams and Yuster [16]	92.27	4.68	3.05

IV. Conclusions

In a few cases in which appearance potentials could be computed from thermochemical and spectroscopic data, it was found that the observed appearance potential was considerably less than the computed potential required to give an atom ion and a free electron, but nearly equal to the calculated potential required to give a positive atom ion and a negative fluorine ion. This was observed for F^+ ion from SF_6 and CF_4, and for the C^+ ion from CF_4. The mass spectra support the hypothesis that for these molecules, removal of a F^- ion rather than an electron is the most probable process in production of the positive ions. This would also explain the absence of the parent ions SF_6^+ and CF_4^+. In the case of SF_6, the heaviest doubly charged ion is SF_4^{++}, which indicates that two F^- ions are removed to form the double positive charge. The fact that SF_4^{++} is more abundant than SF_4^+ at 100 volts is not surprising if this is the mechanism of ionization. In the case of CF_4, a CF_3^{++} ion is observed although the CF_2^{++} ion is more abundant. This indicates that it is possible to ionize CF_4 by removing either two F^+ ions or one F^- ion and a free electron. The appearance potentials for these two processes are nearly the same.

In the case of SiF_4, the molecular ion is observed although its abundance is less than 2 percent of the SiF_3^+ ion. The appearance potential of the former is actually somewhat greater than the latter, which again indicates that the SiF_3^+ ion is formed by removal of an F^- ion from SiF_4. Consider the other possibility; i. e., the SiF_3^+ ion arises from the removal of a free electron and a fluorine atom. This is the same as removing a fluorine atom from the SiF_4^+ ion, and consequently must require work. Therefore, the appearance potential of SiF_3^+ must be higher than SiF_4^+ by that amount of work unless a negative ion is formed in the process.

V. References

[1] P. Kusch, A. Hustrulid, and J. T. Tate, Phys. Rev. **52,** 840 (1937).

[2] R. F. Baker and J. T. Tate, Phys. Rev. **53,** 683 (1938); **55,** 236 (1939).

[3] J. R. White and A. E. Cameron, Phys. Rev. **71,** 907 (1947).

[4] V. H. Dibeler, J. Research NBS **38,** 329 (1947) RP1775.

[5] V. H. Dibeler, F. L. Mohler, and R. M. Reese, J. Research NBS **38,** 617 (1947) RP1799.

[6] R. F. Bacher and S. Goudsmit, Atomic energy states (I $(A+)=15.76$ electron volts) (McGraw-Hill Book Co., New York, N. Y., 1932).

[7] J. A. Hipple, R. E. Fox, and E. U. Condon, Phys. Rev. **69,** 347 (1946.)

[8] F. R. Bichowsky and F. D. Rossini, Thermochemistry of chemical substances (Reinhold Publishing Co., New York, N. Y., 1936).

[9] H. S. W. Massey, Negative ions (Cambridge Univ. Press, London, 1938).

[10] A. O. C. Nier, Phys. Rev. **53,** 282 (1938).

[11] E. Pollard, Phys. Rev. **57,** 1186 (1940).

[12] International atomic weights (Published by the J. Am. Chem. Soc., 1947).

[13] A. O. C. Nier and E. A. Gulbranson, J. Am. Chem. Soc. **61,** 697 (1939).

[14] E. P. Ney and J. H. McQueen, Phys. Rev. **69,** 41 (1946).

[15] M. G. Inghram, Phys. Rev. **70,** 653 (1946).

[16] D. Williams and P. Yuster, Phys. Rev. **69,** 556 (1946).

WASHINGTON, September 25, 1947.

U. S. Department of Commerce
National Bureau of Standards

Research Paper RP1854
Volume 40, January 1948

Part of the Journal of Research of the National Bureau of Standards

Physical Properties of Electrodeposited Chromium

By Abner Brenner, Polly Burkhead, and Charles Jennings

The following properties of chromium, deposited under a wide variety of plating conditions, have been measured; density, hardness, tensile strength, Young's modulus of elasticity, ductility, electrical resistivity, and stress in the deposit. The oxygen and hydrogen content were determined. The effect of heat treatments up to 1,200° C on certain of these properties has been determined, and some work has been done on the properties of chromium-iron alloys deposited from modified chromic acid solutions. A relation between the hydrogen and oxygen content of the deposits has been shown to exist, and the effect of the oxygen content on the physical properties has been studied.

I. Introduction

One of the advantages of electrodeposited metals is the possibility of producing deposits of a given metal with widely different properties by varying the conditions of deposition. This feature is even more important in engineering applications of electrodeposits than for their ornamental use. The increased use of plated metal coatings and of electroformed articles during the war led to a demand for a more exact knowledge of the physical properties of deposited metals, as a guide in the selection of metals to meet specified types of service.

The original impetus for this study came from an attempt to electrodeposit either chromium or one of its alloys in a form that would have some ductility. Although this aim was not achieved, this work led to the study and measurement of these properties of chromium on which little data were available.

The great hardness of electrodeposited chromium has been of considerable practical and theoretical interest, and consequently most study has been devoted to this property in the past. Few broad investigations of the other properties of chromium deposits have been made, and the trend has been to study minutely a few types of deposits with respect to a given property. In this investigation no exhaustive study of any single physical property was made, but several properties of deposits, which were produced under widely different conditions, were determined in order to correlate the physical properties and the conditions of depositions; and to establish the range of each property. Reference to table 11 will give an idea of the great range attainable in the properties of chromium deposits.

In this study the following measurements were made on the deposits: Oxygen and hydrogen content, hardness, density, tensile strength, Young's modulus, ductility, and electrical resistivity. The effect of heat treatment up to 1,200° C on some of these properties was determined. In addition, observations were made on the cathode current efficiency and on the stress in the deposits as plated. Certain factors, such as the crystal structure, were not investigated, because that subject has been adequately treated by others.[1] No previous data on either the tensile strength or Young's modulus were found in the literature.

One result of this study has shown that deposits obtained at 85° C and above are much sounder than the bright deposits at about 50° C.

II. Plating Solutions and Conditions of Deposition

The specimens employed in these studies were deposited from solutions, containing chromic acid in concentrations from 50 to 500 g/liter together with either (a) sulfate with a weight ratio of

[1] After this paper was written, a paper was received from Cloyd A. Snavely on the theory of chromium plating. He discusses the mechanism of chromium plating on the basis of X-ray data and attributes the differences in properties of chromium to the formation of hydrides.

768161—48——3

TABLE 1. *Conditions used in chromium deposition*

Deposit No.	Bath	CrO_3	SO_4	Fluoride	Temperature		Current density		Cathode Efficiency	Appearance
		g/liter	*g/liter*	*g/liter*	*°C*	*°F*	*amp/dm²*	*amp/ft²*	*Percent*	
1	Standard	250	2.5		30	86	5	47	9	Bright.
2	do	250	2.5		30	86	10	95	17	Frosty.
3	do	250	2.5		40	104	15	140	17	Bright.
4	do	250	2.5		45	113	20	186	15	Do.
5	do	250	2.5		45	113	25	237	17	Do.
6	do	250	2.5		50	122	5	47	7	Milky.
7	do	250	2.5		50	122	10	93	11	Bright.
8	do	250	2.5		50	122	20	186	15	Do.
9	do	250	2.5		50	122	30	280	18	Frosty.
10	do	250	2.5		50	122	40	370	19	Bright.
11	do	250	2.5		50	122	60	560	20	Do.
12	do	250	2.5		50	122	80	745	22	Do.
13	do	250	2.5		50	122	100	930	22	Do.
14	do	250	2.5		50	122	200	1,860		Matte.
15	do	250	2.5		60	140	40	370	16	Bright.
16	do	250	2.5		65	149	10	93	7	Matte.
17	do	250	2.5		65	149	20	186	10	Do.
18	do	250	2.5		65	149	30	280	13	Bright.
19	do	250	2.5		65	149	40	370	14	Milky.
20	do	250	2.5		65	149	80	745		Do.
21	do	250	2.5		65	149	100	930	16	Frosty.
22	do	250	2.5		70	158	40	370	12	Matte.
23	do	250	2.5		70	158	80	740	14	Bright.
24	do	250	2.5		70	158	100	930	15	Do.
25	do	250	2.5		75	167	50	465	13	Matte.
26	do	250	2.5		75	167	60	560	13	Milky.
27	do	250	2.5		75	167	80	740		Do.
28	do	250	2.5		75	167	100	930	14	Do.
29	do	250	2.5		85	185	20	186	5	Matte, spalled.
30	do	250	2.5		85	185	40	370	7	Matte.
31	do	250	2.5		85	185	60	560	10	Do.
32	do	250	2.5		85	185	80	740	11	Do.
33	do	250	2.5		85	185	120	1,110	12	Do.
34	do	250	2.5		85	185	160			
35	do	250	2.5		90	194	80	740	8	Satin.
36	do	250	2.5		95	203	80	740	4	Matte, spalled.
37	do	250	2.5		100	212	80	740	4	Do.
38	do	250	2.5		100	212	300	2,790		Spalled.
39	High SO_4	250	5		85	185	80	740	10	Matte.
40	Dilute	50	0.5		50	122	10	93	13	Bright.
41	do	50	0.5		50	122	20	186	20	Do.
42	do	50	0.5		85	185	20	186	15	Matte.
43	do	50	0.5		85	185	80	740	18	Do.
44	do	50	0.5		90	194	80	740		Satin.
45	do	50	0.5		100	212	80	740	8	Do.
46	do	50	0.5		100	212	100	930	6	Do.
47	Concentrated	500	5		50	122	10	93		Matte.
48	do	500	5		50	122	20	186		Do.
49	do	500	5		85	185	80	740		Do.
50A	Fluoride	250		10	85	185	60	560	16	
50	Fluoride-1	250		6	50	122	20	186		Milky.
51	do	250		6	50	122	30	280	25	Bright.
52	do	250		6	50	122	40	370	15	Do.

TABLE 1. *Conditions used in chromium deposition*—Continued

Deposit No.	Bath	CrO_3	SO_4	Fluoride	Temperature		Current density		Cathode Efficiency	Appearance
		g/liter	*g/liter*	*g/liter*	*°C*	*°F*	*amp/dm²*	*amp/ft²*	*Percent*	
53	Fluoride-1	250		6	85	185	20	186	15	Matte.
54	do	250		6	85	185	40			
55	do	250		6	85	185	80	740	27	Matte.
56	Fluoride-2	250		2.4	85	185	80	740	15	Do.
56A	do	250		2.4	85	185	40	372	18	
57	Fluoride-3	250		1.2	85	185	20	186	20	Matte.
58	Fluoride-4	50		2.4	85	185	20	186		
59	do	50		2.4	85	185	80	740	16	
60	Fluoride-5	50		1.6	50	122	10	93		Satin.
61	do	50		1.6	50	122	30	280		Do.
62	do	50		1.6	50	122	60	560	24	
63	do	50		1.6	85	185	60	560	30	Matte.
64	Fluoride-6	50		1.2	85	185	80	740		
65	Reduced	[a] 250	2.5		16		11		22	Dark, smooth.
66	Trivalent [b]									Matte.

[a] Solution and plating conditions according to Wright, Hirst, and Riley [39]. A solution containing CrO_3, 250 g/liter, was reduced with oxalic acid to contain 25 percent of the chromium in the trivalent condition.

[b] Specimen of chromium received from the U. S. Bureau of Mines. Deposited from a trivalent solution [22].

CrO_3/SO_4 from 50 to 100; or (b) fluoride with a weight ratio of CrO_3/F of from 20 to 200. The range of plating conditions was as follows: Temperature, from 16° to 100° C; current density, from 5 to 300 amp/dm². The principal baths and conditions of operation are listed in table 1.

The baths were made from a pure grade of commercial CrO_3, the sulfate content of which was determined. Required additions of sulfate were added as sulfuric acid. The sulfate content was checked by analysis and the CrO_3 content with a hydrometer. Fluoride was added as hydrofluoric acid of a known strength, or as potassium fluoride. Some exploratory studies were made on trivalent chromium baths of the type developed by the United States Bureau of Mines [22]* for the electrowinning of chromium, and a few analyses and measurements were made on samples received from the Bureau of Mines.

The baths were contained in 6-liter glass cylinders. The anode was a cylinder of chemical lead, which lined the inside of the container. The cathode tube was supported vertically in the center of the jar. The desired temperature was thermostatically controlled to ±1°C, and the solution level was maintained constant. The current density was controlled to ±5 percent. The solutions containing fluorides were also contained in glass vessels, as it was found that for the concentrations employed no appreciable attack of the glass occurred. Because both lead and graphite anodes were rapidly attacked in baths containing fluoride, platinum anodes were used.

The cathode efficiencies reported in table 1 were determined by depositing chromium on gold rods under the same conditions as were used for deposition of test specimens. The literature [9] contains data on the cathode current efficiencies of chromium plating solutions for temperatures up to 65° C. However, the data for solutions operated at 85° C are not very extensive. For this reason data are given in figure 1 for solutions operated at 85° C and containing either sulfate or fluoride. The current efficiency of the dilute sulfate solution, containing CrO_3, 50 g/liter and SO_4, 0.5 g/liter, is about double that of the standard solution. The curves for the fluoride solutions are unusual in that they show maxima at a moderate current density. The maxima occur only for a limited range of fluoride concentration (from 0.8 to 2.0 g/liter). Outside of this range the curves resemble those for the sulfate solutions, which

* Figures in brackets indicate the literature references at the end of this paper.

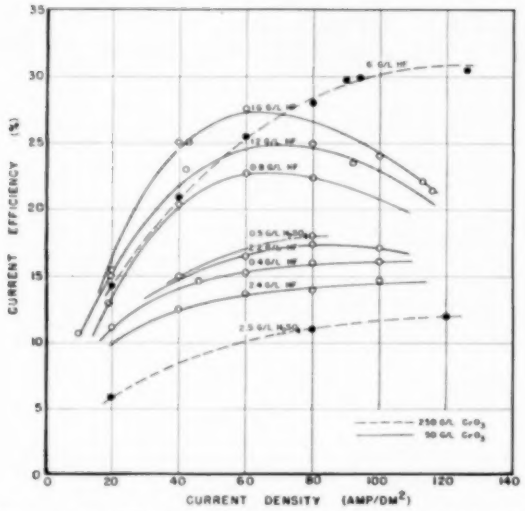

FIGURE 1. *Effect of current density on the cathode efficiencies of chromium deposition at 85° C.*

Standard, ●; dilute, ○.

normally show a continuous increase of current efficiency with current density. Wick [36] however, reports that at 85° C a maximum efficiency is also found for sulfate solutions at a very high current density. (It may be noted that a strike was necessary to obtain initial plating from certain of the flouride solutions when a low current density was used.)

III. Deposition of Specimens

For most of the measurements, the chromium was deposited on a copper tube, which was then dissolved out to leave a tube of chromium. The use of a tube has some advantages over a flat specimen: (1) A more uniform current density can be obtained on a tube, (2) the tubular specimen does not distort, when the base metal is dissolved away, because the stresses are evenly distributed, whereas a thin, flat deposit might curl or warp, (3) a thin walled tube can be handled more safely than a flat specimen, because it has a shorter length of edge. Thin sheets of chromium are quite fragile.

The copper tube used as a base for the chromium deposit had an outside diameter of about 5 mm ($\frac{3}{16}$ in.) and a wall thickness of 0.25 mm (0.01 in.). The outside of the copper tube was buffed to a bright smooth finish with Vienna lime. A suitable length, e.g. 20 to 40 cm (8 to 16 in.) was flattened at each end and sealed. Stop-off lacquer was applied to the lower end for a distance of about 1 cm and to the top for a distance of about 1 cm both above and below the solution level.

The deposits of chromium varied in thickness from 0.05 to 0.25 mm (0.002 to 0.01 in.), depending on the properties to be measured. As the current density was slightly higher at each end of the tube than over the remainder of the surface, about 1 cm of the deposit from each end was discarded in preparing the specimens for test. The copper was dissolved from the inside of each tube by immersion in dilute nitric acid, or in a solution containing CrO_3, 500 g/liter and sulfuric acid, 30 g/liter.

Spectrochemical analyses showed that the chromium deposits contained no more than a few hundredths of a percent of foreign metals.

IV. Appearance and Structure of Chromium Deposits

Inasmuch as the surface appearance and microstructure of chromium have been extensively studied by previous investigators, and numerous photomicrographs are in the literature, no specific work on this phase of the subject was attempted, and our observations on the structure were incidental. However, a summary of the available information on the structure of chromium is given here as a basis for discussions of its relation to other properties.

1. Macrostructure

It is difficult to define the appearance of the deposits in words. The terms used in table 1 have the following meanings: A bright deposit is one that is both bright and smooth; a milky deposit is semibright and smooth; a frosty deposit appears bright but slightly rough or coarse; a satin deposit is semibright and rough; a matte deposit is dull and rough; a spalled deposit is one from which, on standing, small particles are spontaneously detached, often audibly (fig. 2).

Bright chromium deposits have been of the most commercial value. The conditions for their production cannot be closely defined, because they involve both temperature and current density. It is customary to specify the conditions in terms of "a bright plating range" that shows the limits

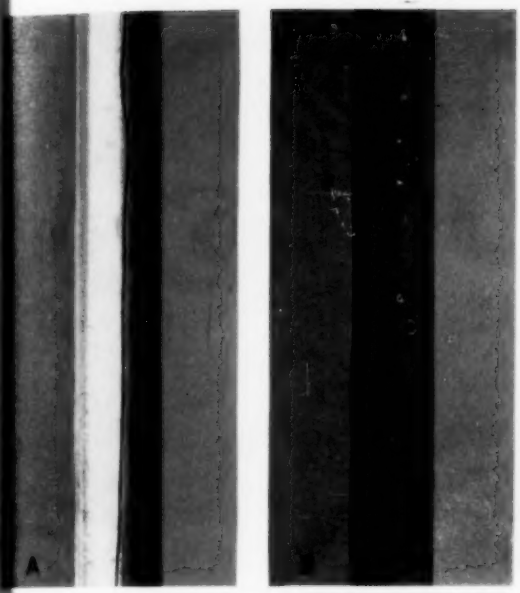

FIGURE 2. *A, Chromium deposit, showing crack formed after dissolving away the copper tube upon which it had been plated; deposit obtained from the standard bath at 85° C and 80 amp/dm². B. spalled deposit obtained from a standard bath at 100° C and 80 amp/dm².*

of current density and temperature. In the standard chromium plating solution, containing CrO_3, 250 g/liter, and sulfate 2.5 g/liter, bright deposits are usually obtained at cathode efficiencies between 8 and 16 percent. At temperatures above 75° C, it is doubtful if bright deposits can be obtained, even at high current densities. Milky deposits are obtained at cathode efficiencies below 8 percent, and frosty or matte deposits above 16 percent. The data in table 1 show that, if the observations are not restricted to the standard solution, there is no close correlation between the appearance of the deposits and the conditions of deposition.

Bright chromium contains a network of hairline cracks and/or inclusions that are visible with low magnification or occasionally even to the unaided eye (fig. 3). As the temperature of deposition is raised above 55° C, the deposits contain fewer cracks, and the matte deposits obtained at higher temperature may be entirely free from cracks (fig. 4). Some of the matte deposits, however, occasionally develop a few very large coarse cracks when the base metal is stripped from them (fig. 2). The deposits obtained at the higher temperatures

FIGURE 3. *Inclusions in bright chromium, deposited at 50° C, and 20 amp/dm² from a standard bath, ×500.*
Etched with hydrochloric acid.

afford better protection to steel in salt spray tests than the bright deposits because of the absence of cracks.

The spalled deposits described above (see fig. 2) do not appear to have been mentioned in the literature previously. They are produced at relatively low current densities and at temperatures of 85° C or above, under which conditions the current efficiencies are less than 6 percent. (Table 1; deposits 29, 36, 37, 38).

FIGURE 4. *Structure of chromium, deposited from the dilute bath at 100° C and 80 amp/dm², ×500.*
Etched with hydrochloric acid.

2. Microstructure

Chromium deposits are very fine grained. On the basis of X-ray data, the bright deposits have been estimated to have grains as small as 10^{-7} cm in diameter. It is generally held that the grain size of chromium is too small to be resolved under the microscope. Cymboliste [7] showed photomicrographs that he believed to show the presence of grains. The authors do not concur with his interpretation. In common with others, the authors have been unable to detect microscopically any grain structure in chromium as deposited, but have obtained well defined grains in chromium annealed in vacuum at 1,400° C. (fig 5). A similar result was obtained by Adcock [2]. In this photomicrograph, it will be noticed that the inclusions shown in figure 3 have coalesced into granular particles (probably of Cr_2O_3) situated mainly at the grain boundaries. In a preliminary examination of a chromium deposit with the electron microscope, at a magnification of 50,000, a photomicrograph was obtained showing light and dark areas, the meaning of which was not interpreted. Figure 6 shows the result obtained by transmitting the electron beam through a film of chromium about one-millionth inch (0.000025 mm) thick.

Ordinary electrodeposited chromium has a body-centered cubic cell. Several different investigators have measured the lattice parameter and obtained closely agreeing values of about 2.878 A. Under certain conditions of deposition, chromium can be obtained as a hexagonal close-packed modification [31]. Wood [38] has shown that the lattice of electrodeposited chromium is 0.3 percent larger than that of annealed chromium. The interpretation of this expansion is not clear, as it may result from strains in the lattice or from the presence of dissolved hydrogen or oxygen. The bright deposits have a preferred crystal orientation so that one set of the 111 planes are parallel to the plane of the deposit [3, 40]. The condition of dull deposits may range from partially oriented to completely random. Hume-Rothery [40] correlated the crystal orientation of the deposits with their brightness, hardness, and stress, but did not discuss the reason for the relationships. We do not believe that crystal orientation is primarily responsible for the hardness or stress in deposited metals, but that it is merely an attendant circumstance. The oxide content of deposits, which Hume-Rothery does not discuss, has a far greater influence on physical properties than crystal orientation.

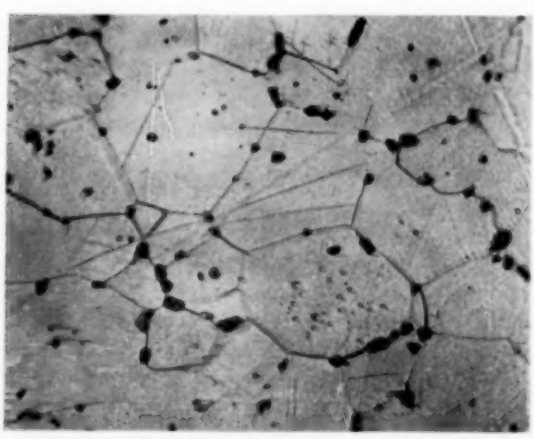

FIGURE 5. *Grain structure in the deposit of figure 2, after annealing at 1,400° C, ×500.*

Etched with hydrochloric acid. Note particles of chromic oxide at grain boundaries.

FIGURE 6. *Photomicrograph by the electromicroscope, ×50,000.*

Electron beam transmitted through a film of bright chromium one millionth of an inch thick.

V. Hydrogen and Oxygen Content of Chromium Deposits

Electrodeposited chromium contains appreciable amounts of hydrogen and oxygen. The

earlier investigators were interested in determining the amount of hydrogen in chromium because of the theory, once prevalent, that the hardness was caused by hydrogen. They did very little work on the determination of the oxygen content of the deposits, although at the present time this impurity is considered to have a larger effect on the physical properties of electrodeposits.

1. Methods of Determining Hydrogen and Oxygen

Previous investigators determined the hydrogen in chromium by heating the deposit to different temperatures in a vacuum and noting the increase in pressure. Adcock [2] determined the oxide content of chromium by heating it to 800° C in a vacuum, and then dissolving the metal in hydrochloric acid. A residue of Cr_2O_3 was left that contained the oxygen originally present in the sample. Prior to the heat treatment the chromium dissolved completely in acid.

Most of the data given in table 2 on the hydrogen and oxygen content of chromium were obtained by the vacuum-fusion method, which has the advantage that the determination of both hydrogen and oxygen can be made on a single sample. For these measurements the authors are indebted to H. E. Cleaves of the Metallurgy Division of this Bureau. Some oxide determinations were made also by Adcock's method, and the results were found to agree well with those of the vacuum-fusion method.

The vacuum-fusion method [33] consists in heating a sample of chromium, about 0.5 g, in molten iron at 1,600° C. The iron is contained in a graphite crucible and, hence, is saturated with carbon. The apparatus is highly evacuated. The hydrogen is given off uncombined and the oxygen as carbon monoxide. The quantity of these gases is determined by noting the decrease in the pressure of the system when they are consecutively removed through oxidation and absorption. This method is not suitable for measuring the amount of hydrogen existing in a deposit immediately after it is withdrawn from the bath, because about 3 hours of pumping at room temperature is required to get the system outgassed before the analysis begins, and during this time some hydrogen may escape from the specimen. There is evidence, however, to show that chromium does not rapidly lose its hydrogen at room temperature, and that there is no necessity for immediate analysis of the sample. Makariewa and Birühoff [26] found that a specimen of chromium that had stood 1½ years had virtually the same content of hydrogen as one that was analyzed immediately. The data in table 3 show that specimens *B* and *C*, which were analyzed immediately after deposition, had about the same hydrogen content as specimens *D* and *E*, which had been allowed to age a few months.

TABLE 2. *Hydrogen and oxygen content of electrodeposited chromium*

Deposit No.	Bath	Temperature	Current density	Cathode efficiency	Oxygen	Hydrogen	Weight ratio oxygen to hydrogen	Volume hydrogen (per volume Cr.)	
								Total	Free [a]
		°C	amp/dm²	Percent	wt %	wt %			
1	Standard	30	5	9	0.87	0.029	30	23	0
3	do	40	15	17	.57	.065	9	52	24
5	do	45	25	17	.44				
8	do	50	20	15	.40	.046	9	37	17
12	do	50	80	22	.35	.056	6	45	27
14	do	50	200		.42	.062	7	50	29
18	do	65	30	13	.22				
19	do	65	40	14	.22	.033	7	26	15
21	do	65	100	16	.22				
22	do	70	40	12	.095				
26	do	75	60	13	.117	.020	6	16	10
30	do	85	40	7	.082				
31	do	85	60	10	.053				
32	do	85	80	11	.052	.014	4	11	9
33	do	85	120	12	.031				
38	do	100	300	<4	.024	.130	0.2	128	102
39	High SO_4	85	80	10	.050	.014	4	11	9
41	Dilute	50	20	20	.40	.035	11	28	8
42	do	85	20	15	.044	.012	4	10	7
43	do	85	80	18	.113	.017	7	14	8
45	do	100	80	8	.076	.011	7	9	5
48	Concentrated	50	20		.49	.042	12	34	9
51	Fluoride-1	50	30	25	.51	.035	15	28	2
55	do	85	80	27	.24	.034	7	27	15
65	Reduced	16	11	22	.82	.066	12	53	12
66	Trivalent				.54	.034	16	27	0
	Avg [b]						8		

[a] Calculated on basis of oxygen combining with hydrogen in weight ratio of 16, i. e., as OH.

[b] Experiments 1 and 38 excluded from average.

TABLE 3.—*Effects of standing or heating upon the oxygen and hydrogen content of electrodeposited chromium*

[All deposits produced in the standard bath at 50° C and 20 amp/dm.²]

Experiment	Treatment	Oxygen	Hydrogen	
		Weight, %	Weight, %	Volume [a]
A	Copper stripped from chromium	0.42	0.028	22
B	As deposited, on copper	.36	.048	38
C	As deposited, on steel		.044	35
D	Stood 2 months	.43	.044	35
E	Stood 3 months	.39	.046	37
F	Heated at 200° C for 1 hour		.024	19
G	Heated at 300° C for 1 hour	.47	.018	14
H	Heated at 350° C for 1 hour		.008	6
I	Heated at 400° C for 1 hour	.46	.005	4
J	Heated at 450° C for 1 hour		.001	1
K	Heated at 800° C for 1 hour		.002	2
L	Heated at 1,200° C for 1 hour		.002	2

[a] Volume of hydrogen per volume of chromium.

In some analyses the chromium deposits were allowed to remain on the copper tube upon which they had been plated; in others the copper was dissolved away with nitric or chromic acid. According to Gernet's data [13] no hydrogen escapes from chromium during solution of the copper. The single experiment (A) recorded in table 3 indicates some loss of hydrogen during this removal of copper.

2. Effect of Temperature and Current Density on Hydrogen and Oxygen Content

The temperature of deposition of chromium has the most important effect upon the content of oxygen in the deposit, as shown in table 2 and in figure 7. As the temperature of deposition is increased, the percentage of oxygen diminishes from 0.87 percent for deposits plated at 30° C to about 0.03 percent for deposits at 100° C. The hydrogen content of the deposits show less regularity, but in general it parallels the oxygen content and decreases as the temperature of the plating solution is raised. The hydrogen contents of the deposits, with one exception, range from about 0.06 percent (50 volumes) for specimens plated at 50° C to about 0.01 percent (9 volumes) for deposits at 100° C. This general trend with temperature agrees with the findings of Gernet [13], but not with those of Makariewa and Birükoff [26] who found an increase in hydrogen for deposits plated between 30° and 60° C at 13

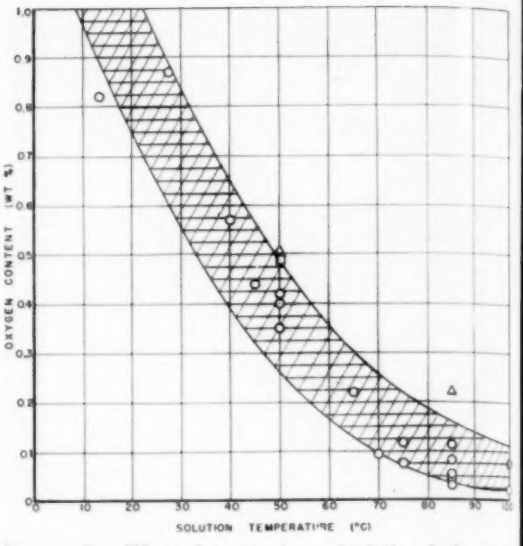

FIGURE 7. *Effect of temperature of plating bath on the oxygen content of chromium deposits.*

Standard, ○; dilute, ●; concentrated, □; fluoride, △.

amp/dm.² The effect of current density on the oxygen content of the deposits is surprisingly slight, inasmuch as one would expect more basic material to be included in the deposits at higher current densities. The deposits obtained at 50° C, (table 2, deposits 8, 12, and 14) and at 65° C (deposits 18, 19, and 21) show virtually no increase in oxide content as the current density is raised from 20 to 200 amp/dm.² At 85° C over the range of current density from 40 to 120 amp/dm² (deposits 31 to 33), the oxygen content decreases.

The hydrogen content of the deposits increases moderately with current density, as indicated by deposits 8, 12, and 14 prepared at 50° C, and 42 and 43 prepared at 85° C. This is in general agreement with the results of Makariewa and Birükoff, who analyzed deposits plated at 45° C and found that the hydrogen increased from 30 volumes to 48 volumes as the current density increased from 3 to 120 amp/dm²; but the change was slightly between 25 and 120 amp/dm². The general conclusion from this work, and that of Gernet [13] is that the hydrogen content, like the oxygen content of chromium changes only slightly with a several-fold change in current density.

The data in table 2 as a whole show no relation between cathode current efficiency and oxygen or

hydrogen content. For example, at a current efficiency of 15 to 17 percent, deposits can be obtained ranging in hydrogen content from 0.01 to 0.06 percent and in oxygen content from 0.04 to 0.6 percent. However, if the variables of plating are more restricted, the content of hydrogen and oxygen in the deposit is found to increase with current efficiency. This is illustrated by deposits 32, 39, 43, and 55 all plated at a current density of 80 amp/dm^2 and a temperature of 85° C but from solutions of different compositions. As the cathode current efficiency rises from 10 to 27 percent, the hydrogen content increases from 0.014 percent (11 volumes) to 0.034 percent (27 volumes) and the oxygen content from 0.05 to 0.24 percent. One might have expected a higher hydrogen content at low current efficiencies, because a larger excess of hydrogen is produced.

The content of hydrogen in deposit 38, table 2, is abnormally high. This deposit was one of those that spalled. It seems likely that the spalling is the result of a high internal pressure generated by the large excess of hydrogen. The phenomenon is similar to the blistering of nickel foil that occurs when hydrogen is cathodically discharged upon it [28].

3. Removal of Hydrogen from Chromium by Heating

The evidence cited above, in connection with the discussion of analytical methods, shows that at room temperature hydrogen does not readily leave the deposit, but that it readily leaves when the deposit is heated. The determination of the quantity of hydrogen expelled from chromium at various temperatures has been the subject of investigations by Guichard [16], Makariewa and Birukoff [26], and Gernet [13], all of whom were interested in the relation between hydrogen content and hardness of the deposit. In our study of the hydrogen content, specimens of chromium were sealed in evacuated tubes and heated, and the residual hydrogen in the deposit was determined by the vacuum fusion method. This latter procedure has the disadvantage, as compared to the vacuum extraction method of the other investigators, that a separate specimen must be used for each temperature investigated.

The data obtained by the vacuum fusion method are shown in table 3, and are plotted in figure 8, along with data from the work of Guichard [16] and Makariewa [26]. The main features of the expulsion of hydrogen from chromium are that the hydrogen escapes gradually as the temperature is raised, until at about 400° C virtually all of the hydrogen has been removed. It is to be noted that only a certain proportion of the hydrogen escapes at a given temperature. Holding the chromium at a given temperature for an indefinite period apparently will not cause a further appreciable loss of hydrogen. Guichard heated his specimens for as long as 3 days to obtain the maximum removal of hydrogen, but his curve is not far different from that of Makariewa and our own curve where the heating was only of 1 hour's duration.

Hydrogen is expelled from chromium as the free element and not as water. This has been shown by analyses of the evolved gas by Makariewa and Guichard [26, 16] and by the fact that the oxide content of chromium does not change as a result of heating. Evidence for the latter is that the method of Adcock, which involves heating the specimen to a high temperature before analyses, gives the same oxide content as the vacuum fusion method. The data given in table 3 for specimens

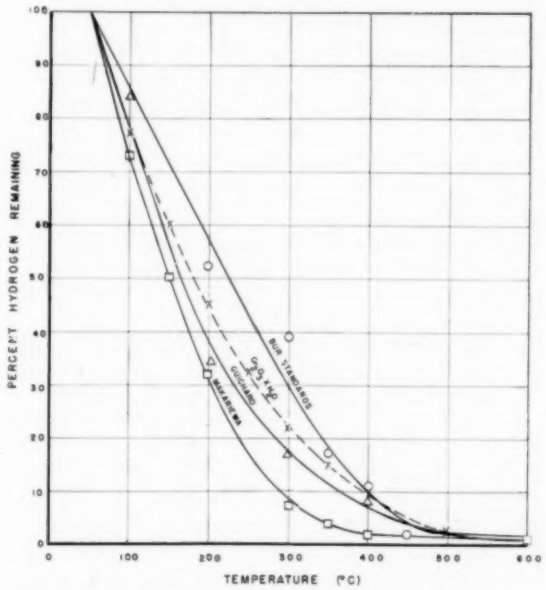

FIGURE 8. *Percentage of the initial amount of hydrogen, remaining in chromium after annealing at various temperatures.*

The curve marked "Cr_2O_3" represents the percentage of water remaining in hydrous chromic oxide, which initially contained 3 to 5 molecules of water.

heated to different temperatures show the same oxygen content.

TABLE 4. *Hydrogen and oxygen content of electrodeposited metals* [a]

Deposit	Bath type	Temperature	Current density	Oxygen	Hydrogen	Weight ratio oxygen to hydrogen	Volume hydrogen (per vol. metal)	
							Total	Free [b]
		°C	amp/dm²	wt, %	wt, %			
Nickel	Watts' pH 5.2	30	2	0.004	0.0017	2	1.7	1
Do	Watts' pH 5.8	30	2	.021	.0060	4	6	5
Do	High sulfate, pH 6.6	30	2	.014	.0053	3	5	4
Nickel-tungsten (5% W)	Ammoniacal	90	2	.006	.004	2	4	4
Nickel-tungsten	do	30	2	.360	.042	9	42	20
Cobalt	Chloride, pH 4	30	2	.049	.004	12	4	1
Cobalt-tungsten (14% W)	Ammoniacal tartrate	90	2	.084	.011	8	11	6
Cobalt-tungsten (22% W)	do	25	2	1.14	.064	18	64	6
Cobalt-tungsten (18% W)	do	90	5	0.165	.014	12	14	4
Cobalt-tungsten (25% W)	do	90	2	.087	.008	11	8	3
Cobalt-tungsten (23% W)	do	90	2	064	.009	7	9	5
Cobalt-tungsten (42% W)	Ammoniacal citrate	90	2	.430	.027	16	27	0
Cobalt-tungsten (29% W)	do	90	2	.177	.012	15	12	1
Iron	Ferrous chloride	95	10	.020	.001	20	1	0
Iron-tungsten (50% W)	Ammoniacal citrate	90	3	.043	.002	22	2	0
Avg						10.5		

[a] Data in this table taken from a paper on the electrodeposition of tungsten alloys now in course of publication.

[b] Calculated on basis of oxygen combining with hydrogen in weight ratio of 16, i. e., as OH.

4. Form and Distribution of Hydrogen and Oxygen in Electrodeposits

The form and distribution of the hydrogen and oxygen in chromium are subjects for speculation, as neither metallographic nor X-ray studies have thrown much light on this point. Because the role played by these elements is so important in determining the properties, not only of chromium, but also of other electrodeposits, the subject will be discussed in some detail and pertinent data concerning other electrodeposits will be introduced.

The most plausible explanation for the inclusion of oxygen in electrodeposits is the formation of basic compounds in the cathode layer, the pH of which is always higher than that of the body of solution. These basic compounds may be adsorbed or deposited as charged colloidal particles, on the cathode where they interfere with grain growth in the same manner as addition agents, and thus cause the formation of small crystals, which are characteristic of chromium deposits. From its interference with grain growth, it seems likely that the basic impurity would be concentrated on the surface of the grains in a finely dispersed form.

There is not much evidence on the nature of the basic compound present in electrolytic chromium. The suggestion that the oxygen content of chromium comes from plating solution that is trapped in cracks is untenable. Adcock found no traces of chromates on extracting a deposit with water. Furthermore, the high-temperature deposits have no cracks with which to trap solution, and yet they contain oxide. The best evidence on the nature of the oxygen compound in chromium comes from the work of Cohen [6], who isolated films of a basic material, from chromium deposits by a process of electrolytic etching. This material came mainly from the cracks and inclusions, but accounted for less than a tenth of the oxygen that was probably present in the deposit. The bulk of the basic compound, therefore, must be very finely dispersed, but there is no reason to expect that it would differ in composition from the material isolated by Cohen, which was found by analyses and X-ray examination to be chromic oxide. It is very likely a hydrous chromic oxide, $Cr_2O_3.nH_2O$, as anhydrous chromic oxide is not soluble in acids, and it is known that chromium deposits dissolve completely in dilute hydrochloric acid. It may be noted that chromic hydroxide, $Cr(OH)_3$, does not exist [35].

To determine the state in which hydrogen exists in chromium requires a more extensive examination of the evidence than was necessary for oxygen. As hydrogen is given off as the free element when chromium is heated, most of the investigators of the hydrogen content of chromium have tacitly assumed that all of the hydrogen was present as the uncombined element. This conclusion is contradictory to the idea, just outlined, that the basic materials that are adsorbed on the cathode are either hydroxides or hydrous oxides. It is unlikely that oxides can separate

from a water solution without carrying along basic OH groups or adsorbed water. The evidence to be cited here indicates that part of the hydrogen is combined with oxygen in basic compounds, and that the remainder exists as the free element.

The reasons against the belief that all of the hydrogen is present as the free element will be considered first. Martin [25] has shown that the equilibrium solubility of hydrogen in chromium is very small, probably about 0.00001 percent. Therefore, the gas cannot be in true solution in the chromium. It might be assumed that all of the hydrogen is present in chromium in the same condition that it is present in cathodically treated iron or nickel (for example between slip planes). However, if this were the case, most of the hydrogen would gradually escape on standing or gentle warming, as it does from iron and nickel, whereas it is still present in chromium after many months.

The best evidence that the oxygen is combined with part of the hydrogen comes from chemical analyses, which show that a simple relation exists between the amount of hydrogen and oxygen in most electrodeposits. Previously, sufficient data on the content of hydrogen and oxygen in electrodeposits have not been available in the literature to permit drawing conclusions. In addition to the data for chromium in table 2, data are given for a variety of electrodeposits in table 4.

The data in tables 2 and 4 as a whole show that the weight ratio of oxygen to hydrogen varies from 2 to 22, with an average of 10. The average ratio is 8 for the chromium deposits and 11 for the others. The majority of deposits have a ratio between 8 and 12. It is surprising that the ratio should be so similar for solutions differing as widely in type as hexavalent and trivalent chromium solutions; moderately acid nickel, cobalt, and iron solutions; and ammoniacal alloy solutions. The range of oxygen content for all of these deposits is from 0.004 to 0.8 percent, a 200-fold variation. The range of hydrogen content is from 0.001 to 0.06 percent, which is a 60-fold variation. If the oxygen and hydrogen contents were entirely unrelated, their ratios might vary several thousand-fold. The relatively small variation of the ratio is strong evidence that the oxygen is combined with the hydrogen in electrodeposits.

It would be of interest to determine the proportion of free and combined hydrogen in electrodeposits, but in general we do not know the composition of the basic inclusions. The ratio of oxygen to hydrogen could vary from 8 for water, 16 for OH groups, to 32 for materials such as basic chromium chromate. To estimate the upper limit of the content of free hydrogen in electrodeposits, it will be assumed that the oxygen is combined with hydrogen in the weight ratio of 16, and that the remainder of the hydrogen is free. On this assumption, it is found that the content of free hydrogen in electrodeposits other than chromium is less than 6 volumes (0.006%) and is usually less than half of the total hydrogen present. The excess of hydrogen in most chromium deposits is less than 15 volumes.

One difficulty yet to be explained is why, on heating, all of the hydrogen is expelled from chromium in the free state, instead of partly as water produced by the decomposition of basic material. Thermodynamic calculations (made by D. D. Wagman of this Bureau) show that water vapor will react with chromium or iron at 100° C to yield hydrogen, and hence no evolution of water should be expected. The ratio of the partial pressures of hydrogen to water at 100° C in the presence of chromium is 10^{15}, and in the presence of iron, 10^{2}, which indicates that the formation of hydrogen from water by chromium is very greatly favored. In this connection, the curve marked "Cr_2O_3" in figure 8, representing the loss of water from hydrous chromic oxide (containing 3 to 5 molecules of water), is of interest. Not only is the curve similar in shape to that for the removal of hydrogen from chromium, but the temperature at which all the water is driven off is the same as that at which all the hydrogen is expelled from chromium (about 400° C). This may be only a double coincidence, but it suggests that the expulsion of hydrogen from chromium on heating involves first a liberation of water vapor from the inclusions of hydrous chromic oxide.

VI. Density of Chromium

The density of electrodeposited chromium has been determined previously by a number of investigators, but no systematic study has been made of the effect of the conditions of deposition on the density. The density of chromium is not of interest in itself, but if it can be correlated with other properties, it may throw light on the struc-

ture of the deposit. The increase in density of chromium on heating is of particular interest.

The density of chromium was measured at 28° C by the method of loss in weight, using tetrabromoethane (density 2.96). The density of chromium, calculated from the value of its cell parameter, 2.878 A, for a body-centered cube, is 7.20 g/cm³. The data in table 5 indicate that the density of electrodeposited chromium is, with a few exceptions, less than that of pure annealed chromium, and varies with the conditions of deposition, from 6.90 to 7.20 g/cm³, a range of about 4 percent.

TABLE 5. *Density of electrodeposited chromium*

Deposit No.	Bath	Temperature	Current density	Density			
				As deposited	Heated 1 hour		[a] Corrected for oxide content
					450° C	1,200° C	
		°C	amp/dm²	g/cm³	g/cm³	g/cm³	g/cm³
1	Standard	30	5	6.90	7.08	7.12	7.19
2	do	30	10	6.92			
3	do	40	15	6.94	7.10	7.13	7.18
6	do	50	5	7.06	7.12	7.17	
7	do	50	10	7.06		7.17	
8	do	50	20	7.05	7.11	7.15	7.18
9	do	50	30	7.01	7.10	7.14	
10	do	50	40	7.01	7.11	7.14	
11	do	50	60	6.98			
12	do	50		6.99	7.10	7.13	7.16
14	do	50	200	6.99			
19	do	65	40	7.11	7.14	7.17	7.19
26	do	75	60	7.17	7.15	7.19	7.20
32	do	85	80	7.17	7.20	7.19	7.20
35	do	90	80	7.10		7.18	
36	do	95	80	7.03		7.19	
37	do	100	80	7.04		7.16	
40	Dilute	50	10	7.02			
41	do	50	20	7.01			
42	do	85	20	7.18		7.18	7.19
43	do	85	80	7.16		7.19	7.20
45	do	100	80	7.20		7.19	7.20
46	do	100	100	7.21		7.22	
48	Concentrated	50	20	7.07			
51	Flouride-1	50	30	6.98		7.09	7.14
52	do	50	40	7.05			
53	do	85	20	7.18			
55	do	85	80	7.14		7.18	7.20
57	Flouride-3	85	20	7.18		7.21	
58	Flouride-4	85	20	7.17			
63	Flouride-5	85	60	7.18			
64	Flouride-6	85	80	7.15			
66	Trivalent			6.97		7.14	7.19

[a] Density of deposits heated to 1,200° C, corrected for oxide content, assuming the oxide to be Cr_2O_3.

1. Factors Affecting Density

The density of a deposit is lowered by a number of factors, such as content of oxygen and hydrogen, cracks and inclusions, and strains. The curve in figure 9 illustrates the increase in density of chromium as the oxygen content decreases. Figure 18, b, shows that the density decreases as the current density is raised. As the deposits obtained at the lower temperatures have cracks and/or inclusions, they have a lower density than those deposited at elevated temperatures, which are relatively free from these defects. Exceptions to this statement are the spalled deposits, such as 36 and 37 (table 5), which had an abnormally low density, as might have been expected from their lack of soundness.

Cold-worked metals have a lower density than annealed metals because of internal strain represented by a distortion of the space lattice. Because electrodeposited metals are, effectively, in a more severely cold-worked state than an ordinary cold-worked metal, it might be assumed that their density would be affected. However, the effect of cold work on the density of metals is quite small [10, p. 137], usually less than 0.1 percent. If the lattice expansion of 0.3 percent (as compared with chromium annealed at 1,500° C observed by Woods [38] for bright chromium

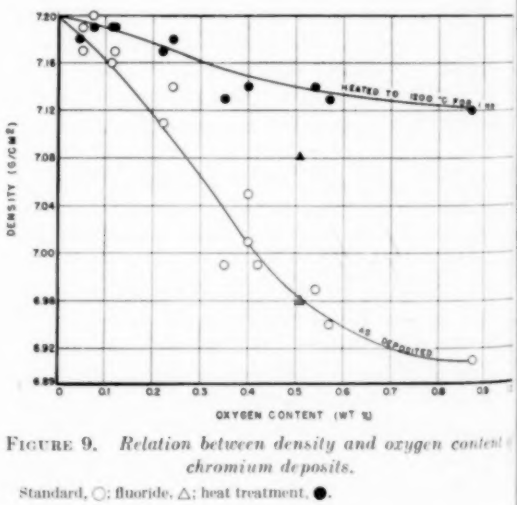

FIGURE 9. *Relation between density and oxygen content of chromium deposits.*

Standard, ○; fluoride, △; heat treatment, ●.

were all attributed to internal strain, this would correspond to a lowering of the density of chromium by only 0.02 g/cm^3.

2. Effect of Annealing on Density

The density of chromium increases on annealing, as shown in table 5. This change in density was first observed by Hidnert [15] and Jenicek [17] in the form of a contraction of a chromium tube on heating. Jenicek showed, and we have confirmed his observation, that the contraction of chromium occurs uniformly in all directions. Because the dimensional changes are isotropic, it was found simpler to follow them by measuring the change in density instead of the contraction.

The change in density on heating is gradual. For those deposits that undergo a large change in density on heating, most of the change occurs below 450° C. This indicates that the expulsion of the hydrogen must be responsible for a large part, but not necessarily all, of the increase in density. The density of most deposits after annealing at 1,200° C is still below 7.20 g/cm^3, the value for pure chromium. However, if a correction is made for the presence of Cr_2O_3 (last column of table 5) the density of chromium is found to be between 7.18 and 7.20 g/cm^3. Apparently at 1,200° C most of the cracks and defects in chromium are eliminated by sintering.

VII. Hardness of Chromium Deposits

Hardness is the physical property of chromium of most practical importance. It has, therefore, been the subject of considerable study, not only because of this, but also because of the theoretical interest in the great difference in hardness between electrolytic and cast chromium. If the hardness of chromium is correlated with other properties, it may serve to define the general character of a deposit.

The hardness of chromium was measured on a polished cross section of a deposit plated on a copper tube. The thickness of the deposit varied from 0.075 to 0.25 mm (0.003 to 0.01 in.). A few check measurements showed that the same hardness was obtained on the cross section as on the surface parallel to the cathode. The hardness was measured with a Knoop diamond indenter, using loads up to 500 g. Most of these measurements were made by Irene C. Minor of the Metallurgy Division of this Bureau.

The data in table 6 show that the hardness of chromium may vary from 300 Knoop to 1,000 Knoop, depending on the conditions of deposition. In comparison, the hardness of cast chromium has been given as ranging from 70 Brinell to 130 Brinell.

TABLE 6. *Hardness of electrodeposited chromium*

Deposit No.	Bath	Temperature	Current density	Hardness
		° C.	amp/dm^2	Knoop
1	Standard	30	5	985
2	do	30	10	960
3	do	40	15	905
5	do	45	25	900
6	do	50	5	920
7	do	50	10	960
8	do	50	20	920
9	do	50	30	946
10	do	50	40	880
11	do	50	60	880
12	do	50	80	875
14	do	50	200	750
15	do	60	40	745
16	do	65	10	600
17	do	65	20	625
18	do	65	30	800
19	do	65	40	975
20	do	65	80	825
21	do	65	100	925
22	do	70	40	600
23	do	70	80	875
24	do	70	100	870
25	do	75	50	580
26	do	75	60	685
27	do	75	80	885
28	do	75	100	650
29	do	85	20	325
30	do	85	40	425
31	do	85	60	475
32	do	85	80	550
33	do	85	120	550
35	do	90	80	575
36	do	95	80	525
37	do	100	80	670
39	High SO_4	85	80	625
41	Dilute	50	20	900
42	do	85	20	325
43	do	85	80	500
45	do	100	80	310
48	Concentrated	50	20	675
50a	Fluoride	85	60	885

TABLE 6. *Hardness of electrodeposited chromium*—Con.

Deposit No.	Bath	Temperature	Current density	Hardness
		° C.	amp/dm²	Knoop
51	Fluoride-1	50	30	900
53	do	85	20	470
54	do	85	40	836
55	do	85	80	800
63	Fluoride-5	85	60	445
66	Trivalent			710

1. Effect of Temperature and Current Density

In general softer deposits are obtained at low current densities and at elevated temperatures: This simple statement will require considerable modification and restriction in the light of the following discussion.

At a given temperature, deposits of a considerable range of hardness can be obtained by a suitable choice of both composition and plating conditions. Thus at 65° C, the hardness may vary from 600 to 825 Knoop. (Table 6, deposits 16 and 20). However, if the optimum conditions for producing soft deposits are selected for each temperature, a softer deposit can be obtained at an elevated temperature than at a lower temperature. As shown in figure 10, there is a fairly well defined lower limit to the hardness at each temperatur but not an upper limit. Almost as hard a deposi can be obtained at 70° C as at 50° C, but such har deposits are not obtainable at still more elevate temperatures.

If the deposits obtained from the "standard" plating solution are considered, more specifi effects of temperature and current density on hard ness are apparent. This is shown by the curves i figure 10, b. Cymboliste [7], and Hume-Rothery and Wylie [40] have also studied the effect of tem perature and current density on the hardness o deposits from the standard solution. Curve from their papers are shown in figures 11 and 1 and they show that at a given current density th hardness of the deposit reaches a maximum at a certain temperature. If the conditions of platin were to the left of the maximum, then an increas of temperature would result in a harder deposit and an increase of current density in a softe deposit. These effects are opposite to the genera trends mentioned at the start of this discussion Cymboliste and Hume-Rothery differ as to th temperature at which the maximum hardnes occurs. Cymboliste's curves show the maximum to be at 50° C for all current densities, whereas Hume-Rothery's reports show that the maximum is at a different temperature for each current density. Our data in figure 10, b, confirm the ob servations of Cymboliste, i. e., the curve represent

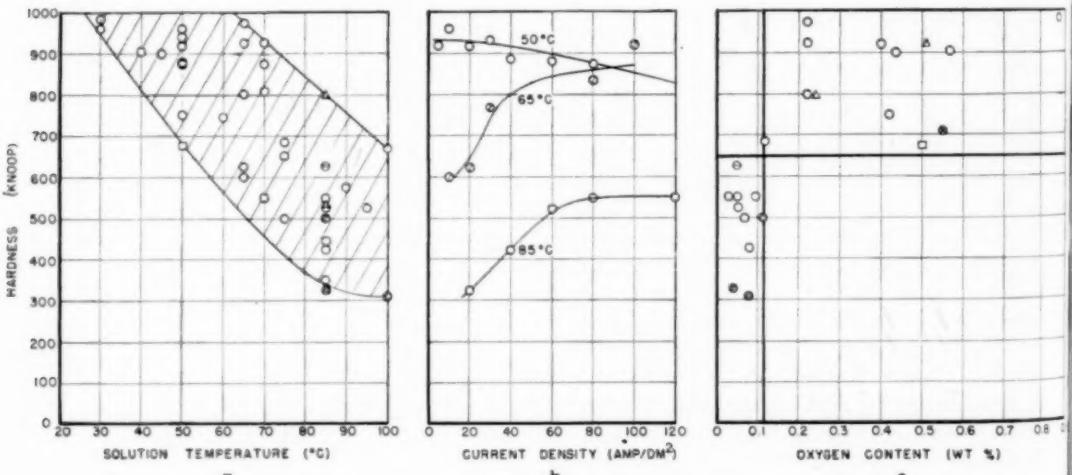

FIGURE 10. *Hardness of electrodeposited chromium.*

a, Effect of temperature of deposition on hardness of chromium; *b*, effect of current density on the hardness of chromium, deposited from the standard ba *c*, relation between hardness and oxygen content of chromium deposits—standard, ○; dilute, ●; fluoride, △.

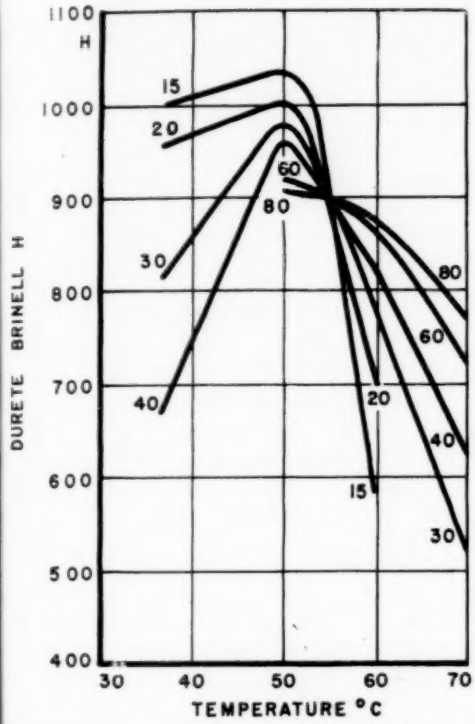

FIGURE 11. *Cymboliste's data* [7], *showing the effect of temperature of deposition on the hardness of chromium deposits.*

Values on the curves are in amp/dm².

ing the hardness of the 50° C deposits, is above the curves for the deposits plated at other temperatures.

It will be noted from figure 10, b, that the curves of hardness plotted against current density do not show the maxima characteristic of figures 11 and 12 in which hardness is plotted against temperature. The trend of hardness with current density is downward at 50° C and upward at more elevated temperatures. It is likely that all the curves would show the downward trend if the observations were extended to very high current densities.

2. Effect of Composition of Bath

As compared with temperature and current density, the composition of the plating solution has only a minor effect of the hardness of deposits. Cymboliste found that softer deposits are obtained from solutions high in chromic acid. Our data do

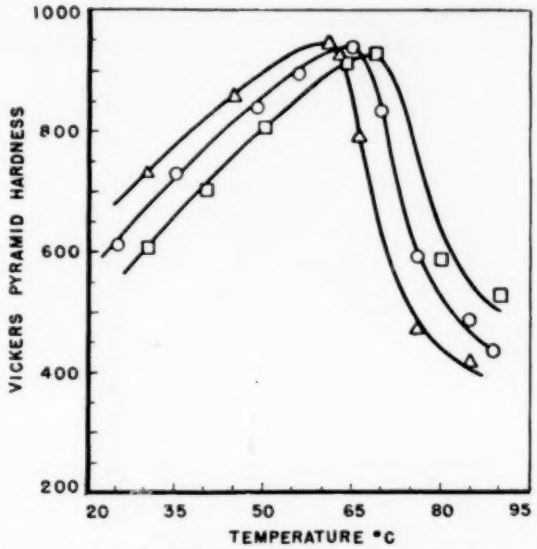

FIGURE 12. *Hume-Rothery's data, showing the effect of temperature of deposition on the hardness of chromium deposits.*

□, 1,750 amp/ft²; ○, 1,000 amp/ft²; △, 500 amp/ft².

not indicate any such definite trend. In deposits 8 and 48 (table 6), the deposits from the stronger solution is softer, but a comparison of 29, 32, and 37, respectively, with 42, 43, and 45 shows that the change is either slight or in the opposite direction. The data on deposits from solutions containing fluorides indicate that these deposits may be harder than those from the sulfate solutions. (Compare deposits 29, 30, 31, and 32 with 53, 54, 50a, and 55, respectively).

3. Effect of Heat Treatment of Chromium

Chromium softens on annealing at high temperatures. Several investigators have shown that chromium does not begin to soften until the temperature of annealing is carried above 400° C. The curves in figure 13 show that the hardness of all types of deposits drops to 200 to 250 Knoop after annealing at 1,200° C for 1 hour.

4. Relation Between Hardness and Oxygen Content

The oxygen content of chromium is one of the most important factors affecting its hardness. The data illustrated in figure 10, c, (for all types of deposits) show a definite trend of hardness with oxygen content, but no very precise relationship,

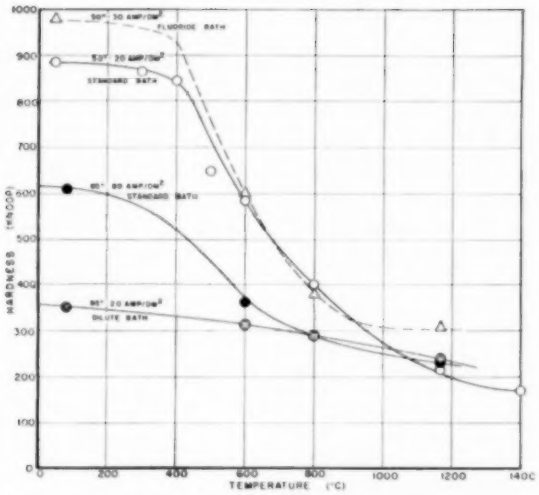

FIGURE 13. *Effect of the temperature of annealing on the hardness of chromium deposits.*

as other factors besides oxygen content influence the hardness. According to figure 10, *c*, if the oxygen content of the deposit is above 0.12 percent, the deposits have a hardness ranging from 650 to 1,000 Knoop, and if below 0.12 percent the hardness ranges from 625 down to 325 Knoop. It is to be noted that deposits having about the same oxygen content may vary 200 points or more in hardness.

5. Cause of the Hardness of Chromium

The cause of the great hardness of electrodeposited chromium, as compared with cast chromium, has been the subject of considerable speculation and study. At one time it was believed that the hardness of chromium was caused by the presence of hydrogen, but this explanation is no longer tenable for several reasons. The work of Guichard and of Makariewa is perhaps the most conclusive, as they showed that virtually all of the hydrogen can be removed from chromium at a temperature of 400° C without the chromium showing any appreciable softening (see fig. 13). Furthermore, no relation was found between the hydrogen content of a chromium deposit and its hardness. An attempt has been made recently to revive the hydrogen theory in another form. It is suggested that during deposition, hydrogen enters the chromium lattice and then escapes, leaving the latter in a state of strain that results in increased hardness. On this basis, the hardness of chromium is to be attributed, not to the hydrogen that is present but to the hydrogen that has escaped. There is no direct evidence to support this view. Chaudron and Moreau [5] found a relatively slight hardening of iron on cathodically charging it with hydrogen; hence, it is not likely that the strain produced in this way could explain the great hardness of chromium.

Hume-Rothery found a correlation between the hardness of chromium deposits and their degree of crystal orientation. According to him, the brightest deposits are also the hardest and have a preferred crystal orientation, whereas the matte deposits have a random orientation and are softer. However, as he does not show why a preferred orientation should cause a high hardness, it is difficult to explain the hardness of chromium on this basis.

The hardness of chromium is probably the result of three factors: oxide inclusions, small grain size, and internal stress, of which the first two factors are probably the most important. The effect of small grain size and internal stress in increasing the hardness of a metal is well known in general metallurgical practice, but not completely understood. Chromium deposits have been shown by X-ray studies to have a small grain size and a high internal stress. The fact that chromium does not soften appreciably unless annealed at relatively high temperatures indicates that the internal stress is not an important factor in its hardness, because the effects of an internal strain, such as are produced by cold-work, are usually removed by annealing at a relatively low temperature.

The idea that oxide inclusions were responsible for the hardness of electrodeposits was first brought out by MacNaughton [23], but, the manner in which the inclusions produce hardening was not discussed. Nonmetallic inclusions in a metal do not necessarily cause hardening. Desch [8] has made the suggestion, without any further elaboration, that the oxide inclusions in electrodeposits produce hardening in the same manner as the precipitated material does in an age-hardened alloy. In precipitation-hardening, a second phase consisting of microscopic or even submicroscopic particles, precipitates at the grain boundaries and between the slip planes and causes hardening by

interfering in some manner with the motion of the slip planes. The precipitated material must be present in sufficient quantity and be of a certain critical size; if too coarse or too fine, an increased hardness does not develop. The phenomena of precipitation-hardening may explain how the oxide content of chromium affects its hardness. If the oxide is in a suitably fine degree of dispersion, as must be the case in the bright deposits, it interferes with the movement of slip planes and produces a high hardness. If the oxide is in a coarse dispersion, as in a burnt deposit, the hardness will be low, even though the oxide content may be high. Hence, a simple precise relation between oxide content and hardness does not exist. As an example, the chromium-iron alloy deposits in table 10 have a very high oxygen content but are relatively soft.

The effects of heat treatment on the hardness of chromium can also be explained on the basis of precipitation-hardening. To the extent that the precipitated material is resistant to agglomeration, age-hardened alloys maintain better their hardness at elevated temperatures and show a higher recrystallization temperature [30]. The oxide dispersion in chromium seems to be stable, as it is only in specimens that have been heated to 1,200 or 1,400° C that the oxide can be seen under the microscope. The softness of chromium that has been heated to 1,200° C is explained by the agglomeration of the oxide into coarse particles [fig. 5], in which condition they no longer interfere with slip planes.

6. Machinable Chromium

The production of a machinable chromium plate may be of interest for special commercial applications. Gardam [12] described a plating solution that would yield a soft chromium of this type having a hardness of about 350 Vickers. It consisted of a standard type chromium plating solution to which iron, aluminum, or chromium had been added, as oxides, to the extent of about 25 g/liter, for the purpose of improving the cathode current efficiency. The deposit was plated at 55° C and 20 amp/dm.^{2} We have found that an equally soft deposit may be obtained from a simpler plating solution, containing only CrO_3, 250 g/liter; and SO_4, 0.5 g/liter (table 1; deposit 12). Furthermore, the cathode current efficiency of this solution, at 85° C and 20 amp/dm^2 is 15 percent, as compared with 8 percent for Gardam's solution.

A drill rod was plated with chromium from the dilute solution, and the coating was machined with an ordinary high-speed tool. It machined readily, although some dulling of the tool took place, and there was a tendency for the chromium to chip. The same chromium deposit, when annealed at 600° C for an hour, machined more easily, but the deposit was cracked as a result of the heat treatment.

VIII. Tensile Strength, and Young's Modulus of Elasticity

1. General

A knowledge of the mechanical properties of chromium might enable one to decide upon the applicability of chromium for a given engineering use. For example, information on the tensile strength and Young's modulus of elasticity would enable one to calculate the extent to which a plated article could be bent or flexed without cracking the coating. As will be shown, measurement of the mechanical properties of the as-deposited metal does not yield the true physical constants, but values that are dependent on the soundness of the material. Such measurements may give an indication of the relative soundness of different types of deposits.

A survey of the literature showed no previous measurements of the tensile strength or modulus of chromium. The measurement of these properties is difficult, as chromium is very brittle and cannot be gripped readily in a testing machine without cracking. The preparation of test specimens with standard dimensions would involve the plating of very thick deposits, which would require an inordinate period of time. Subsequent machining would be required, which is quite difficult to perform because of the hardness and brittleness of chromium. To expedite the preparation and testing of chromium deposits, test samples were therefore made from tubes, prepared in the manner described above.

2. Test Specimens and Methods of Measurement

(a) Tensile Strength

Because of their brittleness, the chromium tubes could not be directly gripped in the jaws of a testing machine. Grips were provided by attaching a

708101—48——4

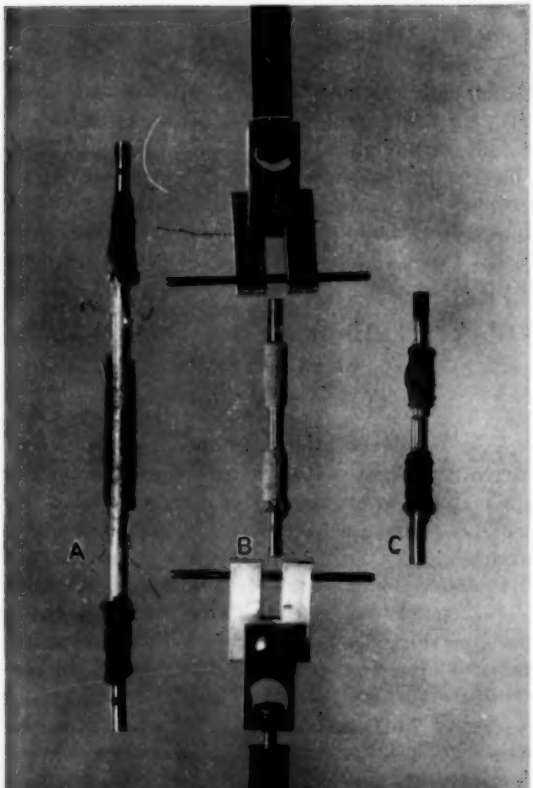

FIGURE 14. *A, Chromium tube provided with wire strain gages for determination of Young's modulus of elasticity. B, Chromium tube prepared for tensile test, and adapters used for mounting specimen in tensile machine; C, specimen broken in tensile test.*

steel rod to each end of the tube. This was accomplished by inserting a closely fitting steel rod for a short distance into the end of the chromium tube and then "cold-welding" the rod to the chromium by electro depositing copper over the juncture of the rod and the chromium. The mid-section of the test specimen was protected with "stop-off" lacquer during the plating procedure. The plating procedure included use of a nickel strike (Wood's nickel strike: $NiCl_2.6H_2O$, 240 g/liter; HCl, (conc.) 120 ml/liter; current density = 5 amp/dm^2) to produce an adherent nickel coating on chromium, followed by deposition of a thick deposit of copper in an acid bath. Guards were used to produce a tapered copper deposit. A thick nickel deposit could not be used for "cold-welding", because the stress in it broke the ends of the chromium tube.

The specimen was held in an adaptor by means of a pin that passed through a hole near the end of the inserted steel rod. To promote proper alinement of the specimen for uniform distribution of force, the adapter was jointed so as to turn readily in any direction. The adapter was held by the grips of a 600-lb Amsler testing machine. The length of tube subjected to tensile stress was about 1.5 to 2 cm (0.5 to 0.8 in.), or about 3 to 4 times the diameter of the tube. A test specimen and the adaptor are shown in figure 14.

In some preliminary experiments, an attempt was made to determine the mechanical properties of chromium by plating it on a standard steel tensile specimen and observing it while stress was applied. This method was unsatisfactory because the moment at which the chromium cracked could not be ascertained even though the method of detecting cracks by means of copper deposition was used.

(b) Modulus

In engineering and metallurgical practice, Young's modulus of elasticity is conveniently determined by measuring the extension of a specimen while tension is applied. Some machines have a mechanical device for directly measuring the extension, but usually some form of strain gage that may be mechanical, electrical or optical, is attached to the sample. This procedure could not be applied readily to the tensile test specimen described in the previous section, because the chromium tube was not strong enough to support the weight of most types of strain gages. An optical method [11] that involved the observation of a pair of extensometers with a microscope (in the manner used for measuring creep of metals) was tried, but was not sensitive enough. A few tests were made with an electric strain gage, as described below, but this method was somewhat cumbersome and required the use of highly specialized equipment.

The method that was most satisfactory for a tubular specimen, involved the measurement of the deflection of the midpoint of a tube that was supported horizontally at the two ends and was loaded at the center. The only special equipment required was a low power microscope (a Brinell microscope was used) to measure the de-

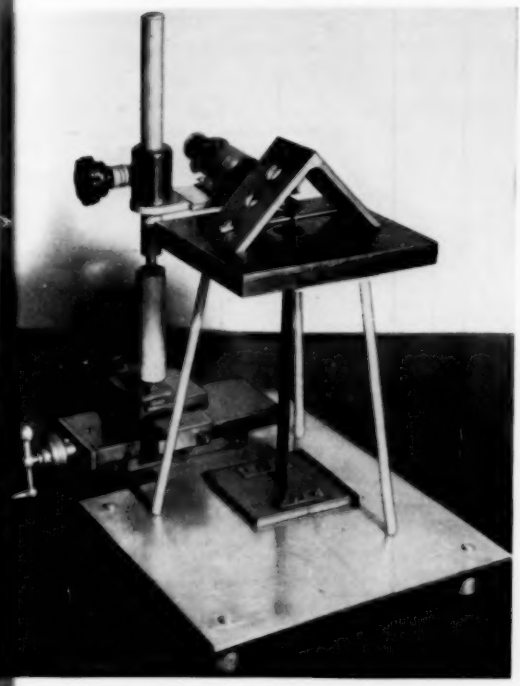

FIGURE 15. *Apparatus used for the determination of Young's modulus of elasticity.*

flection. The apparatus is shown in figure 15. The measurements that are required for the determination of the modulus are: Weight of load, deflection of center of tube, length of tube between the supports, and the inner and outer diameters of the tube. A deflection sufficiently large to be read easily with the Brinell microscope could be obtained with a tube 5 mm (3/16 in.) in diameter, having a wall thickness of not over 0.25 mm (0.01 in.), and a length of 13 cm (5 in.) between supports. The maximum loads used were about 2,500 g (5 lb.).

Young's modulus, E, is defined as the ratio of stress to strain when a material is subjected to tension within its elastic limit:

$$E=\frac{\text{stress}}{\text{strain}}=\frac{\text{tensile pull per unit area of cross section.}}{\text{extension per unit length}}$$

The modulus is calculated from the measurements of the flexure of a tube by the following formula:

$$E=\frac{4PL^3}{3\pi\delta(d_1^4-d_2^4)},$$

where

E=Young's modulus in lb/in.^{2},
δ=deflection in inches,
P=load in pounds,
L=length of specimen in inches,
d_1=outer diameter of tube,
d_2=inner diameter of tube.

For this formula to hold the strain must be less than 0.2 percent.

The measurement of the inner and outer diameters of the tube have the largest effect on the accuracy of the modulus, as these quantities enter into the equation to the fourth power, and any error is correspondingly magnified. High uniformity of wall thickness was difficult to obtain. For this reason the reported values can be considered accurate to within only about 5 percent, which is sufficient to compare the moduli of different types of chromium deposits. Before being used on chromium deposits, this method was checked by measurements on a steel tube of known modulus.

With the assistance of A. E. McPherson, of the Engineering Mechanics Section of this Bureau, a check was made on a few chromium deposits, using a wire strain gage, which operates on the principle that the electrical resistance of a wire changes when it is subjected to tension. Two wire strain gages were cemented to opposite sides of a chromium tube that had been prepared as for a tensile test. The tube was then subjected to tension in an Amsler machine, and the two gage readings were taken. Observed differences in the two gage readings indicated that the stress was not equal throughout the specimen, probably because of imperfect alinement, but the average of the two readings was a valid measure of the extension of the tube. The first gage tried was a Baldwin wire-gauze, type A–7. The results were erratic, varying by ±10 percent from the average, because of the curvature of the gage when wrapped around the tube. A single-wire gage, type A–12–4 was found satisfactory and gave results that agreed within a few percent with those obtained by flexure. A specimen carrying two of these strain gages is shown in figure 14.

3. Results of Measurements

The data (table 7) show that the tensile strength and modulus of chromium, as deposited, vary considerably with the conditions of deposition.

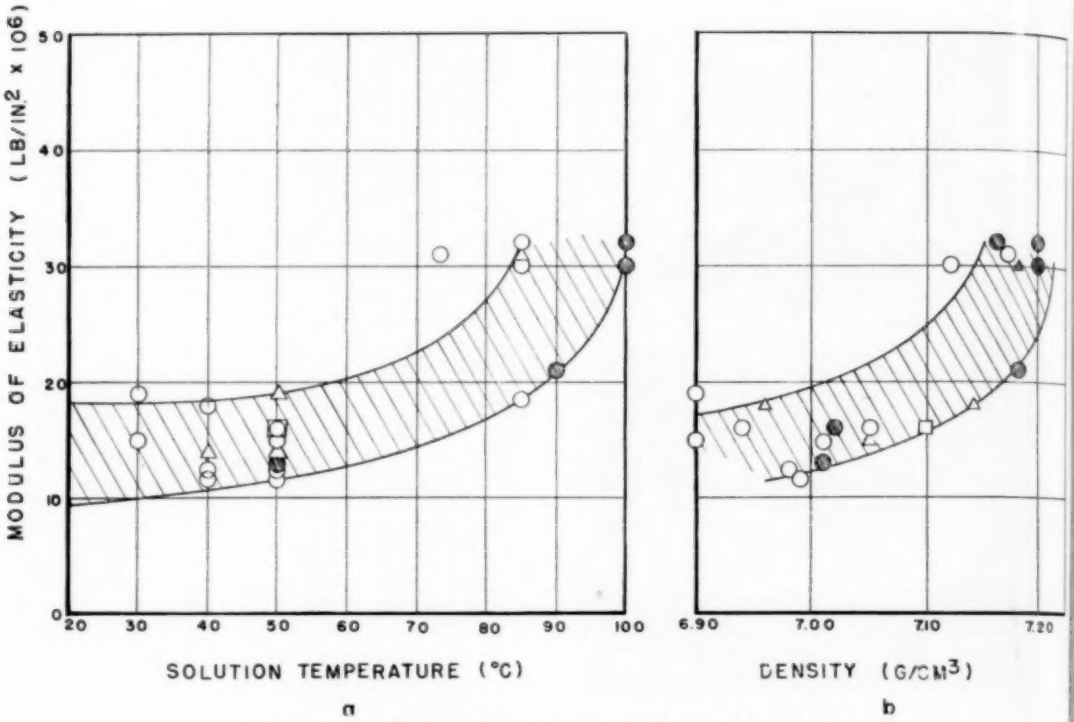

FIGURE 16. *Modulus of elasticity of electrodeposited chromium.*

a, Effect of temperature of deposition on Young's modulus of elasticity of chromium deposits—standard, ○; dilute, ●; fluoride, △. *b*, relation between modulus and density of chromium deposits.

TABLE 7. *Young's modulus and tensile strength of electrodeposited chromium*

Deposit No.	Bath	Temperature	Current density	Modulus		Tensile strength	
		°C	amp/dm²	lb/in.²	kg/mm²	lb/in.²	kg/mm²
1	Standard	30	5	19 x 10⁶	13 x 10³	19 x 10³	1
2	do	30	10	15	10	16	1
3	do	40	15	16	11	17	12
8	do	50	20	16	11	15	10
9	do	50	30	15	10		
10	do	50	40			17	12
11	do	50	60	12	8		
12	do	50	80	12	8		
14	do	50	280			8	6
26	do	75	60	32	22		
30	do	85	40			18	13
31	do	85	60			54	38
32	do	85	80	33	23	70	49
33	do	85	120			80	56
39	High SO_4	85	80	31	22	28	20
40	Dilute	50	10	16	11		
41	do	50	20	13	9		
42	do	85	20	28	20	46	32

TABLE 7. *Young's modulus and tensile strength of electrodeposited chromium*—Continued

Deposit No.	Bath	Temperature	Current density	Modulus		Tensile strength	
		°C	amp/dm²	lb/in.²	kg/mm²	lb/in.²	kg/mm²
43	Dilute	85	80	32 x 10⁶	22 x 10³		
44	do	90	80	21	15		
45	do	100	80	32	22	35 x 10³	
46	do	100	100	30	21	27	
48	Concentrated	50	20	16	11		
50	Fluoride-1	50	20	19	13		
51	do	50	30	20	14	30	
52	do	50	40	15	10		
53	do	85	20	30	21	31	
55	do	85	80	20	14	12	
57	Fluoride-3	85	20	31	22	48	
58	Fluoride-4	85	20	25	17		
59	Fluoride-4	85	80	26	18		
63	Fluoride-5	85	60	21	15		

TABLE 8. *Effect of heat treatment on modulus and tensile strength of electrodeposited chromium*

Deposit No.	Bath	Temperature	Current density	Modulus				Tensile strength			
				As deposited	Heated 1 hour at—			As deposited	Heated 1 hour at—		
					600° C	800° C	1200° C		600° C	800° C	1200° C
		° C	amp/dm²		lb/in.²	lb/in.²	lb/in.²	lb/in.²	lb/in.²	lb/in.²	lb/in.²
8	Standard	50	20	16	.....	22×10^6	33×10^6	15×10^3	19×10^3	31×10^3	57×10^3
32	do	85	80	33	.....	.....	35	70	.....	.....	.....
42	Dilute	85	20	28	.....	.....	.....	44	49	52	.....
43	do	85	80	32	.....	33	36	.....	.....	.....	46
45	do	100	80	32	.....	.....	.....	35	.....	.....	43
51	Fluoride-1	50	30	20	29×10^6	.....	37	30	50	.....	62
53	do	85	20	30	.....	.....	.....	31	.....	.....	70
55	do	85	80	20	.....	.....	29	12	.....	.....	25
57	Fluoride-3	85	20	31	.....	.....	.....	48	.....	.....	70

The tensile strength varies from about 15,000 to 80,000 lb/in.² and Young's modulus from 12×10^6 to 33×10^6 lb/in.² The values are somewhat erratic and do not show any well defined trend, except that the higher values of both were obtained on deposits made at 85° C or above (fig. 16).

The data in table 8 show that the modulus and tensile strength of chromium deposits increase on heating. The increase in tensile strength of deposits produced at 50° C is about fourfold, but the increase in modulus is not as large.

These results on modulus and tensile strength can best be interpreted on the assumption that they do not represent the true values of these properties, but that they are, "effective" values, which are dependent on, and hence a measure of, the soundness of the deposits. The presence of cracks and inclusions in the deposits, or pits and nodules on the surface, causes low results and the lack of consistency in the measurements. The deposits produced at elevated temperatures are sounder and hence give higher values of mechanical properties. The values of tensile strength are more erratic than those of modulus, which is to be expected, as in stressing a material to the breaking point, a single defect can result in a concentration of stress sufficient to prematurely fracture the deposit. The situation is very similar to that encountered in measuring the properties of a brittle substance, such as glass [29; p. 320]; no reliable measurements of tensile strength can be obtained, because the values are so dependent on the presence of flaws on the surface, although the modulus can be measured readily [29; p. 300].

The increase in tensile strength and modulus on heating is further evidence that the values obtained on chromium as deposited cannot be considered characteristic of the metal. In general when the metals are soft annealed, the tensile strength decreases [10; p. 134]; which is opposite to the effect observed here. The increase in Young's modulus was much greater than generally obtained in metals. Higher values of these mechanical properties of chromium on heat-treated specimens may be attributed to the increase in soundness of the metal.

In figure 16b, the modulus is plotted against the density. The reason for selecting the density as the dependent variable is that it can be considered a measure of the soundness of the deposit. A further correlation between the tensile strength of chromium and its soundness will be discussed in connection with the stress in the deposit.

It is believed that the most reliable value of Young's modulus for chromium is about 36×10^6 lb/in.², as this seems to be the common value approached by the modulus of several different types of deposits that have been annealed at 1,200° C. The true tensile strength is probably greater than the highest observed value of about 80,000 lb/in.².

IX. Ductility of Chromium

Although, as mentioned in the introduction, the desire to produce a ductile chromium deposit was the original motive for undertaking this study of properties, ductile chromium was not obtained. For the purposes of this investigation, a metal is considered ductile, if it acquires a permanent

deformation while being loaded to rupture. In the measurements of modulus of chromium by the method of loading a beam, indications were obtained that chromium lacked ductility. The plot of load against deflection showed no change in slope for specimens loaded to the breaking point. Plastic deformation would have been revealed by a change in the slope of the curve.

Elongation is commonly measured by the percent increase of a 2-in. gage length on a specimen that has been broken in tension. A measurement of this type was made on a few specimens of chromium prepared in the manner described under tensile strength. The measurements of length were made to 0.001 in. with a traveling microscope. No elongation was found for either bright chromium or a specimen of annealed chromium (at 1,200° C). Therefore, if chromium deforms plastically, the elongation at fracture must be less than one tenth of a percent.

The possibility is not excluded that ductile chromium can be obtained by a metallurgical process that would yield an oxide-free material, inasmuch as normally brittle metals such as titanium and zirconium have been obtained in a ductile condition. Kroll reports [21] that at high temperatures chromium can be hot worked, which is some indication that it is ductile under certain conditions.

As it appears that chromium breaks within the elastic limit, the maximum extension that can be expected when chromium is stressed in tension can be calculated. If the tensile strength of a deposit were 36,000 lb/in.^{2}, a modulus of 36×10^6 lb/in.^{2} would correspond to an extension of 0.1 percent at the breaking point. This demonstrates that a plated metal cannot undergo more than a slight flexing without cracking the deposit.

X. Stress in Chromium Deposits

Metals produced by electrodeposition are frequently highly stressed, and there is evidence that this is particularly true of chromium deposits. The stress within a metal deposit is not a physical property, but an understanding of it may help to explain the behavior of some of the deposits.

The formation of cracks in bright chromium plate is usually attributed to rupture of the deposit as a result of a high contractile stress. Some of the specimens plated from the standard bath at elevated temperatures manifested the presence of stress in other ways. For example, deposits plated at 65° C were relatively free from cracks; but when the copper base was dissolved away, some of these developed a network of cracks and fell into fragments. Deposits obtained at 85° C and 80 amp/dm^2 (from the standard solution) appeared quite sound, but developed one or more large, coarse cracks (fig. 6) when the copper was dissolved away. (It may be mentioned at this point that this troublesome cracking of the high temperature deposits can be largely eliminated by using either the dilute plating solution, 40, or one of the solutions containing fluoride instead of sulfate.)

The stress in chromium deposits was measured by a modification of that well-known method that depends on the bending of a metal strip when only one side is plated. The modification consisted in using a spiral, instead of a flat strip. The measurements were made by S. Senderoff of the Electrodeposition Section of this Bureau. The details of the method will be discussed in a forthcoming publication. The results obtained are illustrated by the curves in figure 17, in which stress is plotted against thickness.

Because the stress characteristics of the deposits are not alike, it will be necessary to discuss

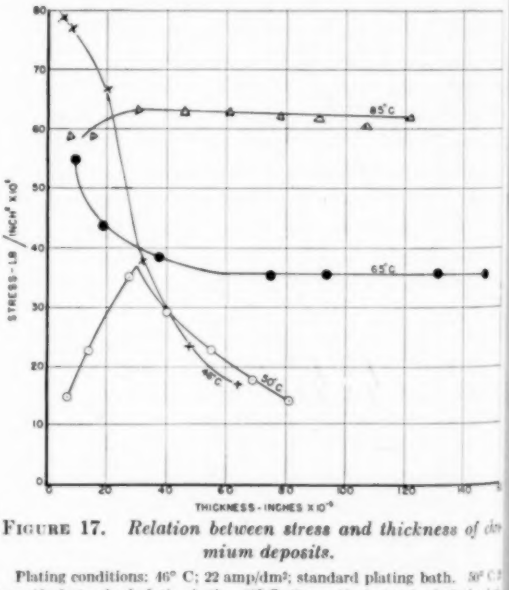

FIGURE 17. *Relation between stress and thickness of chromium deposits.*

Plating conditions: 46° C; 22 amp/dm^2; standard plating bath. 50° C; 22 amp/dm^2; standard plating bath. 65° C, 40 amp/dm^2; standard plating bath. 85° C; 20 amp/dm^2; dilute plating bath.

each curve individually. The curves for the 46° and 50° C deposits show that a high stress exists in thin deposits, and that the stress rapidly decreases as the deposit becomes thicker. One explanation of this behavior is that the thin initial deposit is sound, but, at a certain critical thickness, cracking occurs and relieves the stress. This explanation fits in with the observations of Blum, Barrows, and Brenner [4] that bright chromium deposits obtained at 46° C and thinner than 0.00002 in., do not contain cracks (immediately after removal from the bath), but that deposits above 0.00005 in. in thickness have cracks. The high stress of 80,000 lb/in.^{2}, attained with the thin deposits, correlates well with the maximum tensile strength that has been measured for chromium, and indicated that bright chromium would have as high a strength as the dull deposits, were it not for the effect of the cracks. As the deposits become thicker, the stress approaches a constant value of about 17,000 lb/in.^{2}, which is approximately equal to the tensile strength that has been measured for deposits of this type.

The 65° C deposit shows a smaller decrease in stress with thickness than the bright deposits. This result fits in with the observation, that fewer cracks are present in such deposits. The presence of a higher residual stress, than in the bright deposits, accounts for the tendency to fall apart when the support afforded by the base metal is removed. The 85° C deposit from the dilute bath (deposit 42) was usually sound and did not show much tendency to crack. This behavior is paralleled by its curve in figure 17, which shows that the stress becomes constant at a high value, indicating no relief through cracking. The stress of 64,000 lb/in.^{2} would indicate that the tensile 46,000 lb/in.^{2}, measured as described above, is too low. As the stress in the high temperature deposits is close to their tensile strength, it is not surprising that the deposits exhibited cracking occasionally.

Hume-Rothery has measured the stress in chromium deposits, but as the deposition was done at a current density of about 200 amp/dm^2, it is difficult to compare his results with ours. He found that the stress varied from about zero for bright deposits to 56,000 lb/in.^{2} for dull deposits. He attributed the low stress of the bright deposits to their preferred crystal orientation. The maxima and minima in stress that he observed in deposits obtained at certain temperatures are difficult to explain.

XI. Electrical Resistivity

The electrical resistivity of chromium is not of much practical importance in itself, but, like the density, it may be an index of the character of the deposits. Once the apparatus is set up, it can be measured quickly. The three physical properties—hardness, density, and electrical resistivity, are valuable in any study of the nature of electrodeposits, because they afford a rapid and sensitive means of following subtle changes that occur in deposits with changes in plating conditions.

Only a few papers in the literature contain data on the resistivity of chromium. Grube and Knabe [19] give a value of 14 microhm-cm at 20° C for the resistivity of powdered chromium that had been sintered in hydrogen. They have also determined the resistivities at temperatures up to 1,800° C, at which temperature the resistivity has increased to 145 microhm-cm. McLennan and Niven [24] reported a value of 44 microhm-cm, for the resistivity of chromium as deposited and 17 microhm-cm for chromium after heating, but they did not give the conditions either of deposition or of heating. Adcock [1] gives 13.1 microhm-cm for chromium annealed in hydrogen. The International Critical Tables give a value of 2.6 microhm-cm, which is incorrectly quoted from Jukov [18]. He actually reported a resistivity of 0.026 ohm-cm for compressed chromium powder, and his value is not comparable with those for electrolytic chromium.

The resistivity was determined by measuring the potential drop between two knife edges that were placed in contact with a tube of chromium. A current of about 1 ampere was passed through the tube from a separate set of leads. The resistance of the tube was computed from the ratio between the potential drop across the knife edges and the voltage drop across a standard 0.001-ohm resistance. Essentially, the method involves the comparison of the voltage drop across an unknown reistance with that across a known resistance. Because separate connections to the tube were used for the current, their contact resistance did not affect the measurement of the potential difference between the knife

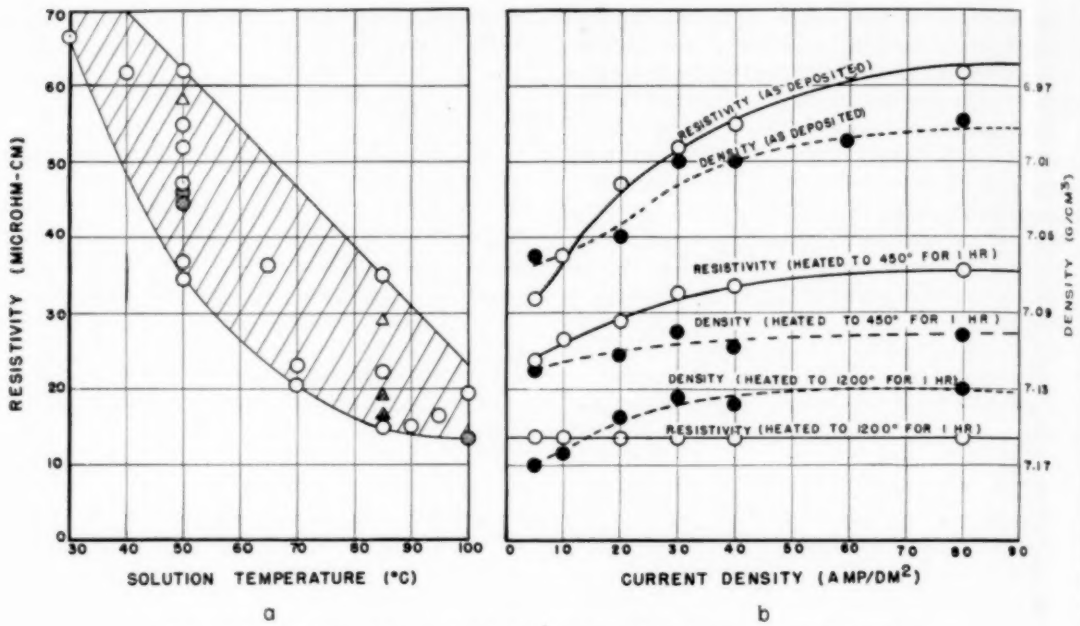

FIGURE 18. *Relation between electrical resistivity and plating conditions of chromium.*

a, Effect of temperature of deposition on the electrical resistivity of chromium deposits—standard, ○; dilute, ⊖; fluoride, △. *b*, Solid lines, effect of current density and the temperature of annealing on the resistivity of chromium. Dotted lines, effect of current density and the temperature of annealing on the density of chromium. Deposits plated at 50° C and 20 amp/dm² in the standard bath.

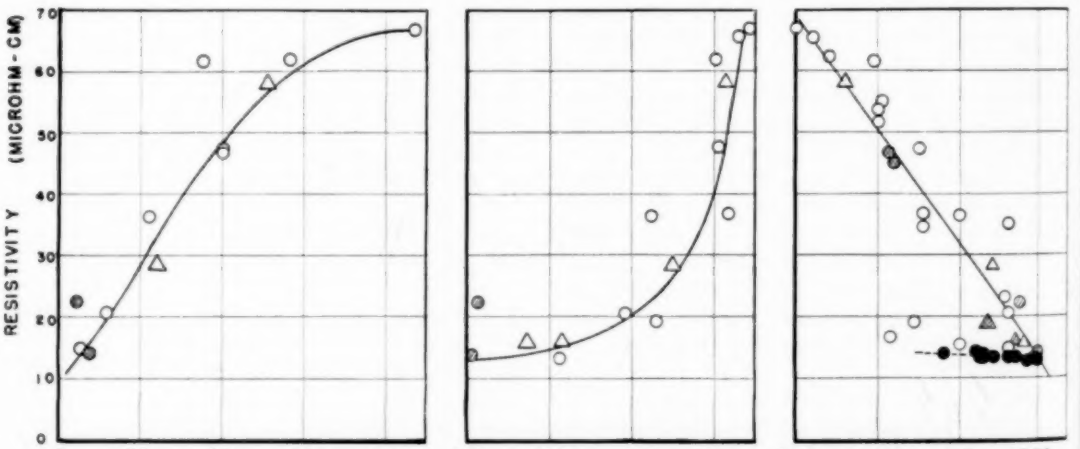

FIGURE 19. *Relation between electrical resistivity and properties of chromium.*

a, Relation between electrical resistivity and the oxygen content of chromium deposits; *b*, relation between electrical resistivity and hardness of chromium deposits; *c*, relation between electrical resistivity and density of chromium deposits—standard, ○; dilute, ⊖; fluoride, △; heat treated, ●.

edges. A Rubicon potentiometer, sensitive to 1 microvolt, was used along with a sensitive galvanometer. The chromium tubes were about 5 cm (2 in.) long and the voltage drop across them was of the order of several millivolts. The resistivity setup was designed by R. F. Kotter, of the Electricity and Optics Division of this Bureau.

The data in table 9 show that the resistivity of chromium, as deposited, varies considerably with the conditions of deposition and ranges from 14 to 65 microhm-cm. Figure 18, a, indicates that although a considerable range of resistivities can be obtained at a given temperature (for different plating conditions) the deposits of lowest resistivity are obtained at the elevated temperatures. When plotted against plating variables, such as temperature or current density (fig. 18), or against other properties of the deposits, such as hardness (fig. 19, b), density (fig. 19, c), or oxygen content (fig. 19, a), the resistivity shows a more uniform trend than do other properties similarly plotted.

TABLE 9. *Electrical resistivity of electrodeposited chromium*

Deposit No.	Bath	Temperature	Current density	Restivity		
				As deposited	Heat treatment, 1 hour, at—	
					450° C	1,200° C
		°C	amp/dm²	Microhm-cm	Microhm-cm	Microhm-cm
1	Standard	30	5	66.5	34.2	14.3
2	do	30	10	66.5		
3	do	40	15	61.8	33.1	13.8
6	do	50	5	34.5	23.8	13.8
7	do	50	10	36.6	26.5	13.6
8	do	50	20	47.5	28.9	13.5
9	do	50	30	51.8	32.6	13.6
10	do	50	40	54.8	33.6	13.6
11	do	50	60	61.6		
12	do	50	80	61.6	35.5	13.6
15	do	65	40	36.2	28.4	16.1
26	do	75	60	20.5	15.9	13.2
27	do	75	80	23.1		
32	do	85	80	14.9	13.6	13.0
34	do	85	160	35		
35	do	90	80	15.4	13.8	13.0
36	do	95	80	16.5	15.6	13.5
37	do	100	80	19.3		14.7
40	Dilute	50	10	44.8		
41	do	50	20	46.5		
42	do	85	20	22		13
45	do	100	80	13.8	13.6	12.9
51	Fluoride-1	50	30	58.2	16.8	14.1
53	do	85	20	15.8		
55	do	85	80	29		15.0
59	Fluoride-4	85	80	19.2		
63	Fluoride-5	85	60	16.0		

The resistivity of chromium deposits is lowered by annealing (table 9). The resistivity of specimens annealed at 1,200° C tends to approach a common value of 13 microhm-cm (at 28° C), which may be considered as the resistivity of pure chromium. This resistivity is attained by those specimens which had the lowest oxide content—26, 32, 35, 42, and 45. Figure 18, b, shows the effect of different temperatures of annealing on the resistivity of deposits plated at 50° C.

The high resistivity of chromium, as deposited, is to be attributed more to the oxide content than to any other factor. This is indicated by the trend of resistivity with oxygen content in figure 19, a. The effect of small quantities of impurities in greatly reducing the conductivity of metals is well known. Although the oxide is still present in the chromium after annealing, it is in an agglomerated form (fig. 5), in which condition, apparently it has little effect on the resistivity or on other physical properties.

The soundness of deposits may also be a factor in determining the resistivity. This is shown by the trend of resistivity with density (fig. 19, c), and by the fact that the deposits with the lowest tensile strength [1, 2, 3, 8, 10, and 55] are among those having the highest resistivities. The presence of internal stress in the deposit cannot be responsible for much of the high resistivity, as it has been shown for copper and iron [10; p. 138] that a high stress increases resistivity by only about 2 percent.

XII. Melting Point of Chromium

The melting point of chromium was not determined in this study. In the literature, values are given ranging from 1,500° to 1,900° C. The most reliable measurement is probably that of Grube and Knabe [14], who obtained the value of 1,890° ±10° C for chromium melted in a hydrogen atmosphere. They showed that the presence of 1 percent of chromic oxide would lower the melting point to about 1,770° C. Apparently the presence of oxide is responsible for the low and nonconcordant melting points reported by other investigators.

XIII. Heat Treatment of Chromium Deposited on a Base Metal

It would be helpful to be able to take advantage of the enhanced properties possessed by chromium that has been annealed at a high temperature. Some experiments were made to determine the effect of heating thick chromium deposits plated on steel, and on steel first plated with nickel, cobalt or iron. In all cases, after heating to 1,200° C the deposits were badly cracked, and their adhesion to the base metal was so poor that the deposit could be flaked off by bending the specimen. On the other hand, chromium from which the base metal has been stripped remains sound when annealed. The cracking of the chromium is probably a result of the difference between the coefficients of expansion of steel and chromium. The cause of the subsequent poor adhesion seems to be the formation of a brittle alloy layer between the chromium deposit and the base metal (see fig. 20). The chromium that flaked off of the base metal does not contain any of the intermediate metal upon which it was plated, whereas the material remaining on the base metal contains chromium. Hence, the break seems to come between the chromium deposit and the layer of chromium alloy. These difficulties with adhesion and cracking warrant the conclusion that a high-temperature heat-treatment will not improve the properties of chromium in contact with a base metal.

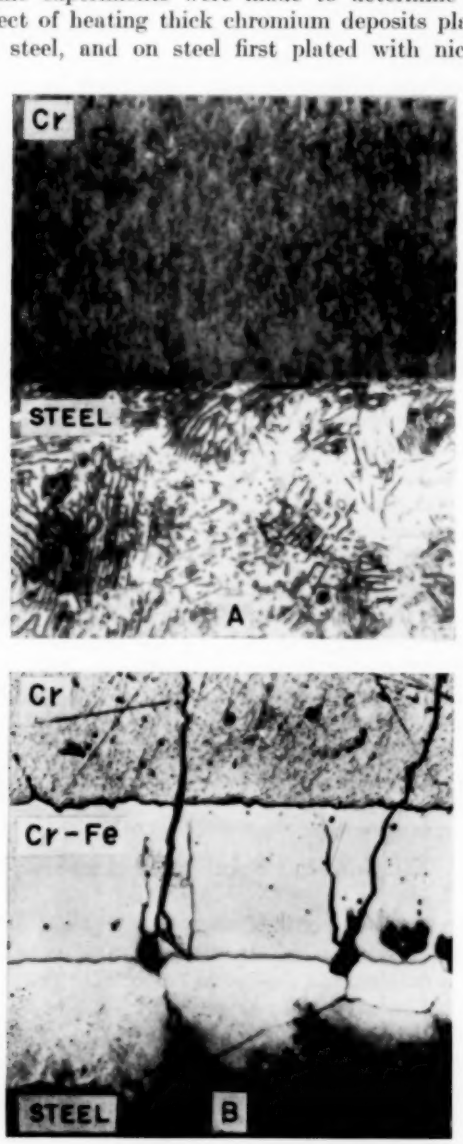

FIGURE 20. *Effect of heat treatment at 1,200° C of a thick chromium deposit on steel.*

Etched with hydrochloric acid. *a*, Before heating (×1,000); *b*, after heating (×500).

XIV. Electrodeposition and Properties of Chromium-Iron Alloys

Kroll [20] showed that a metallurgical alloy containing mainly chromium and a small amount of iron could be worked while hot. This suggested the possibility of obtaining deposits of chromium alloys that might have more ductility than pure chromium. A study was made of the deposition of alloys of chromium from chromic acid solutions, but as the results of this investigation were mainly negative, they will be described only briefly.

The literature contains a few references to attempts to deposit alloys of chromium from a chromic acid solution. Kasper [19] cites several references to the effect that other metals and chromium do not codeposit. Gardam [12] makes no mention of alloy formation in connection with the introduction of iron in the plating solution used for producing machinable chromium. Watts [34] also was unable to obtain alloys from a chromic acid solution. On the other hand, Skalozubov and Goncharova [32] reported that alloys with nickel and with iron had been obtained from chromic acid solutions.

The following metals were introduced into chromic acid solutions in the attempt to obtain alloys—iron, nickel, cobalt, tungsten, and molyb-

denum. The metals of the iron group were introduced into the solution mainly in the form of the metal dichromates, but a limited number of experiments were made by adding the metals in the form of other salts. Tungsten and molybdenum were added in the form of complexes with phosphoric, hydrofluoric, or boric acid. No alloys containing more than a few tenths of a percent of the added metal were obtained from any of the solutions except the ones containing iron, and, qualitatively at least, the deposits were usually inferior in physical properties to pure chromium deposits.

The deposits obtained from the solutions recommended by Gardam (table 10) are very similar to those obtained from the standard chromium solution [29 to 32], except that they are somewhat softer, although containing more oxide. These deposits contain only several hundredths of a percent of iron. The solution, iron-1 (see table 10) is similar to Gardam's, except that it contains twice as much iron and corresponds essentially to a 2.5-molar solution of iron dichromate $Fe_2(Cr_2O_7)_3$. The deposits contain several tenths of a percent of iron, but are not essentially different from ordinary chromium deposits. The deposits from solutions iron-3 to iron-5 are weak, brittle, and unsound.

TABLE 10. *Electrodeposited chromium-iron alloys*

Bath	Bath composition				Temperature	Current density	Cathode efficiency	Hardness, Vickers	Iron	Oxygen	Hydrogen	Ratio: oxygen to hydrogen	pH
	CrO_3	Fe	SO_4	Mg									
	Moles/liter	*Moles/liter*	*Moles/liter*	*Moles/liter*	*° C*	*amp/dm²*	*Percent*		*Percent*	*Percent*	*Percent*		
Gardam	2.5	0.4	0.025	.....	85	20 to 80	8 to 12	320 to 470	0.1	0.1 to 0.35	.....	.....	0.2
Iron-1	2.5	.8	.025 to .12	.....	85	20 to 80	7 to 12	360 to 500	.1 to .5	.1 to .35	.....	.....	.3
Iron-2	2.5	.8	.04	.....	45	20	.....	1020	.0	.4	.....	.....	.3
Iron-3	1.0	.32	.17	0.16	30	10	47	360	5.2	1.69	0.091	19	1.2
Do	1.0	.32	.17	.16	50	20	65	340	9.0	2.85	.071	40	1.2
Iron-4	1.0	.64	.96	.96	25	2.5	30	.....	6.0	2.14	.112	19	1.6
Do	1.0	.64	.96	.96	25	5	43	350	6.3	1.58	.093	17	1.6
Iron-5	1.0	.32	.33	*.32	30	10	53	350	.....	1.91	.067	28	1.4

* Potassium instead of magnesium.

Although these solutions for plating chromium-iron alloys are not of practical value, they have some points of academic interest, particularly the solutions iron-3 to iron-5. They have an unusually high cathode current efficiency, ranging from 30 to 65 percent, and contain considerably more sulfate than an ordinary chromium plating solution. Solution iron-4 contains almost as much sulfate as chromate, or a ratio of sulfate to chromic acid of about a hundred times greater than is normally present in a chromium plating bath. The high current efficiency of these solutions may be partially a result of the high pH, but this is not the whole story, as solutions with a similar pH, made up by substituting trivalent chromium for the iron, neither plated very satisfactorily, nor yielded high current efficiencies.

The deposits from iron-3 to iron-5 contain a high amount of oxygen, but are not very hard. This shows that the mere presence of oxide inclusions in a deposit is not sufficient to produce hardness, but that the state and dispersion of the basic material is equally important. Because the oxygen to hydrogen ratio of these deposits is 16 or above, the deposits apparently have no free hydrogen (on the basis of our assumption). It is possible, however, that because of the relatively high pH of the solution, the basic material has separated in the form of a basic iron or chromium dichromate, $Cr(OH)_3.Cr(OH)CrO_4$, in which the ratio of oxygen to hydrogen by weight, is 32.

XV. Summary

As the properties of various types of electrodeposited chromium approach a common value after the chromium has been heated to 1,200° C, the properties of this annealed chromium may be considered to be those of pure chromium. Support for this view is gained from the fact that the density of annealed chromium is 7.20 g/cm³, the value calculated for pure chromium from X-ray data. The following is a summary of the properties of annealed chromium.

Hardness	200 (Knoop).
Density	7.20 g/cm³.
Young's Modulus	36×10^6 lb/in².
Tensile Strength	70,000 lb/in².
Resistivity	13.0 microhms-cm.

It will be noted that some of the deposits obtained at temperatures between 85° and 100° C have physical properties very close to those of the annealed deposits. The inference is that these deposits are the purest and soundest ones and are most likely to be satisfactory for any purpose other than those requiring high hardness. In table 11, the properties of some of the best high-temperature deposits are compared with the commonly used bright chromium, deposited at 50° C and 20 amp/dm².

TABLE 11. *Comparison of properties of low temperature (50° C), high temperature (85° to 100° C), and annealed chromium*

Deposit No.	Bath	Plating conditions			Density	Hardness Knoop	Tensile strength	Young's modulus	Resistivity	Oxygen content
		Temperature	Current density	Cathode efficiency						
		° C	amp/dm²	Percent	g/cm³		lb/in².	lb/in².	Microhm-cm	Percent
8	Standard	50	20	15	7.05	920	15×10^3	15×10^6	47	0.4
42	Dilute	85	20	15	7.18	325	47	30	22	.3
53	Fluoride	85	20	15	7.18	470	31	30	16	
32	Standard	85	80	11	7.17	550	70	33	15	.1
45	Dilute	100	80	8	7.20	310	35	32	14	.0
	Annealed, 1,200° C				7.20	200	70	36	13	

The authors express their appreciation to W. Blum for his interest and guidance, and acknowledge the assistance of E. F. Osborn, formerly of the Geophysical Laboratory, in the earlier part of this study.

XVI. References

[1] F. Adcock, J. Iron Steel Inst. (London) **124,** 99 (1931).

[2] F. Adcock, J. Iron Steel Inst. (London) **115,** 369 (1927).

[3] W. Arkharow, J. Tech. Phys. (USSR) **3,** 1072 (1936).

[4] W. Blum, W. P. Barrows, and A. Brenner, BS J. Research **7,** 697 (1931) RP368.

[5] G. Chaudron and L. Moreau, Korrosion & Metallschutz **18,** 134 (1942).

[6] J. B. Cohen, Trans. Electrochem. Soc. **86,** 441 (1944).

[7] M. Cymboliste, Trans. Electrochem. Soc. **73,** 353 (1938).

[8] C. H. Desch, Trans. Faraday Soc. [2] **31,** 1045 (1935).

[9] G. Dubpernell, Trans. Electrochem. Soc. **80,** 589 (1941).

[10] C. F. Elam, Distortion of metal crystals, p. 137, (Clarendon Press, Oxford, 1935).

[11] J. A. Fellows, E. Cook, and H. S. Avery, Trans. Am. Inst. Mining Met. Engrs. **150,** 358 (1942).

[12] G. E. Gardam, J. Electrodepositors' Tech. Soc. **20,** 69 (1945).

[13] H. Gernet, J. Applied Chem. (USSR) **4,** 429 (1931).

[14] G. Grube, B. Knabe, Z. Elektrochem. **42,** 793 (1936).

[15] P. Hidnert, Phys. Rev. **39,** 186 (1932).

[16] Guichard, Clausmann, Billon, and Lanthony, Bull. Soc. Chim. **1,** [5] 679 (1934).

[17] M. Jenicek, Ladislaw, Rev. mét. **33,** 371 (1936).

[18] I. I. Jukov, J. Russ. Phys. Chem. Soc. **42,** 40 (1910).

[19] C. Kasper, J. Research NBS **14,** 693 (1935) RP795.

[20] W. Kroll, Z. Metallkunde **28,** 317 (1936).

[21] W. Kroll, Z. anorg. Chem. **226,** 23 (1936).

[22] R. R. Lloyd, W. T. Rawles, and R. G. Feeney, Trans. Electrochem. Soc. **89,** (1946).

[23] D. J. Macnaughtan, G. E. Gardam, R. A. F. Hammond, Trans. Faraday Soc. **29,** 729 (1933).

[24] J. C. McLennan and C. D. Niven, Phil. Mag. [7] **4,** 397 (July 1927).

[25] E. Martin, Metals & Alloys, **1,** 831 (1930).

[26] S. P. Markariewa, and N. D. Biriikoff, Z. Elektrochem. **41,** 838 (1935).

[27] S. P. Makariewa, and N. Dirukoff, Z. Elektrochem. **41,** 623 (1935).

[28] D. P. Smith, and G. A. Moore, Trans. Electrochem. Soc. **71,** 545 (1937).

[29] G. W. Morey, The properties of glass, Am. Chem. Soc. Monograph No. **77** (Reinhold Publishing Corp., New York, N. Y., 1938).

[30] E. R. Parker, Trans. Am. Soc. Metals **28,** 797 (1940).

[31] K. Sasaki and S. Sekito, Trans. Electrochem. Soc. **59,** 437 (1931).

[32] M. F. Skalozubov, and Goncharova, Izvest. Novocherkass-kogo Ind. Inst. im. S. Ordzhonekidze **6,** Ser. Khim. 24 (1940).

[33] H. C. Vacher and L. Jordan, BS J. Research **7,** 375 (1931) RP346.

[34] O. P. Watts, Trans. Electrochem. Soc. **84,** 350 (1943)

[35] H. B. Weiser, Inorganic Colloid Chemistry, p. 2 (John Wiley & Sons, Inc., New York, N. Y., 1935).

[36] R. M. Wick, Chromium plating, U. S. Patent 2,392,871 (January 15, 1946).

[37] W. A. Wood, Trans. Faraday Soc. **31,** [2] 1248 (1935).

[38] W. A. Wood, Phil. Mag. [7] **23,** 984 (1937).

[39] L. Wright, H. Hirst, and J. Riley, Trans. Faraday Soc. [2] **31,** 1253 (1935).

[40] W. Hume-Rothery, and M. R. J. Wyllie, Proc. Roy. Soc. (Lonon) [A] **181,** 331 (1943). Washington, July 18, 1947.

WASHINGTON, July 18, 1947.

U. S. Department of Commerce
National Bureau of Standards

Research Paper RP1855
Volume 40, January 1948

Part of the Journal of Research of the National Bureau of Standards

Surface Tension of Compositions in the Systems PbO-B_2O_3 and PbO-SiO_2

By Leo Shartsis, Sam Spinner, and Alden W. Smock

The surface tension of a series of compositions ranging from 0 to 100 percent of PbO in the system PbO-B_2O_3 and of compositions ranging from 0 to 35 percent of SiO_2 in the system PbO-SiO_2 was measured by a modification of the anchor ring method. The volatility and changes in composition of members of each system upon heating were found to be related to the surface tension and its change with composition. Some correlation between the temperature coefficient of surface tension and expansivity was noted.

I. Introduction

Commercial glasses in general are quite complex as they are formed from several oxides. The effect of varying the percentage of any one of these oxides relative to the percentage of the others is quite complicated. By systematically studying glasses formed from simpler systems of oxides, simpler relations between changes in composition and their effect on the properties of the glasses can be expected and, from such results, we can hope to reach a better understanding of the condition of matter called glass.

The oxides PbO, B_2O_3, and SiO_2 are of such great importance in the manufacture of many glasses, glazes, and enamels, that studies of systems of these components are of real interest in several fields of ceramics. For this reason, this study was made on the two-component systems, PbO-B_2O_3 and PbO-SiO_2. The study consisted of measuring the surface tensions of melts at different temperatures and with different compositions. Some tests were also made on volatilization and expansion.

II. Preparation of Melts and Methods of Test

The compositions investigated were prepared by melting, in platinum crucibles, the requisite amounts of H_3BO_3, PbO, and SiO_2 of the purity used for optical glasses. The weight of the melts ranged between 300 and 500 g. They were stirred with a platinum rod and, when they seemed homogeneous, were poured into iron molds. About half of the PbO-B_2O_3 glasses were analyzed by a triple evaporation with HF and H_2SO_4 for PbO both before and after the surface tension determinations. It was found that if the time for making the surface tension determination was kept relatively short, say 3 or 4 hours, the change in composition was negligible. As the time seldom exceeded 4 hours, the remaining compositions were not reanalyzed after test.

The method [1] [1] of measuring surface tension was that of finding the maximum pull exerted on a small thin-walled platinum cylinder when its lower edge was in contact with the molten glass. In this method, a correction factor is necessary because of the finite thickness of the walls of the platinum cylinder.

The following equation was deduced by Verschaffelt [2] for this case:

$$\sigma=\frac{F}{4\pi R}\left[1-\left(2.8284+0.6095\sqrt{\frac{h}{R}}\right)\frac{\delta}{\sqrt{hR}}+\left(3+2.585\sqrt{\frac{h}{R}}+0.371\frac{h}{R}\right)\frac{\delta^2}{hR}\right], \quad (1)$$

where

σ = surface tension in dynes/cm
$h=F/\pi R^2\rho g=W_{max}/\pi R^2\rho$
F = maximum force exerted on the cylinder = gW_{max}
2δ = thickness of cylinder
ρ = density of glass

[1] Figures in brackets indicate the literature references at the end of this paper.

R = mean radius of the cylinder

W_{max} = maximum pull (in grams) exerted on the cylinder.

The correction factor V is the expression within the brackets. To simplify the cumbersome calculations involved, the following expansion of V was made. Thus

$$V=1-\frac{2.8284\delta}{\sqrt{hR}}=\frac{0.6095\delta}{R}+\frac{3\delta^2}{hR}+\frac{2.585\delta^2}{R\sqrt{hR}}+\frac{0.371\delta^2}{R^2}. \quad (2)$$

For a given size ring, R, δ, and π are known constants, and V, containing in addition to these constants terms $1/h$ and $1/\sqrt{h}$, is a quadratic in $1/\sqrt{h}$. As $1/\sqrt{h}$ is equal to known constants times $(\rho/W_{max})^{1/2}$, V is a quadratic in $(\rho/W_{max})^{1/2}$.

A series of ρ/W_{max} values was selected and the corresponding V's were calculated. Figure 1 shows the curve obtained using $R=1.26$ cm and $\delta=0.0076$ cm. The required V can be read directly from the curve when ρ and W_{max} are known. The surface tension can now be computed from the relation $\sigma=FV/4\pi R$.

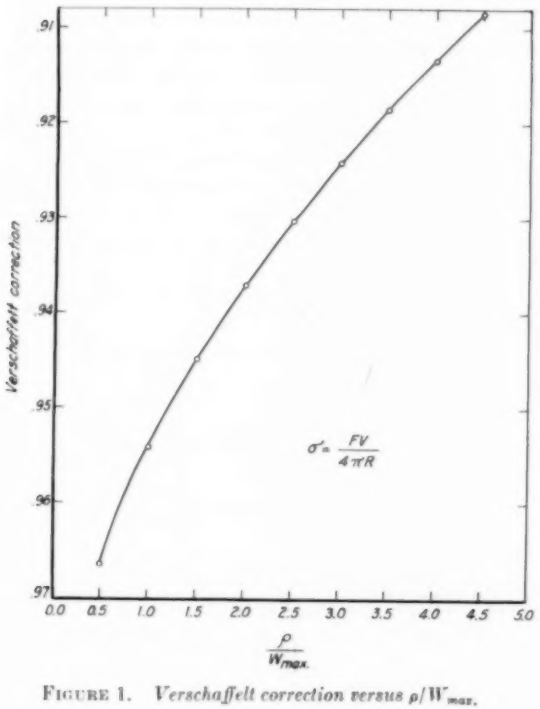

FIGURE 1. *Verschaffelt correction versus* $\rho/W_{max.}$

These corrections were computed for a cylinder of mean radius 1.26 cm and of wall thickness 0.0162 cm. Correction V is used in the surface tension equation $\sigma=FV/4\pi R$.

It was considered sufficiently accurate to calculate a V factor for each glass at one temperature only, usually 1,000° C, and to apply it to the proper $F/4\pi R$ value. The value of $F(1-V)/4\pi R$ was then subtracted from each of the $F/4\pi R$ values obtained at other temperatures.

The densities of the PbO-B_2O_3 glasses at room temperature were computed from the formula [3]

$$D=\frac{(PbO)^2}{1{,}600}+2,$$

where

D = density

PbO = weight percentage of PbO in the glass.

These densities were corrected to the desired temperature by use of available expansion data [3]. Above the interferometer softening point, the expansivity was assumed to be three times that at lower temperatures. The densities, expansivities, and interferometric softening points of some PbO-SiO_2 glasses are available in the literature [4, 5, 6].

III. Results and Discussion

1. The System PbO-B_2O_3

(a) Phase Equilibrium Relations

Figure 2 shows the phase equilibrium diagram [3] of the system PbO-B_2O_3. The broad features that may be noted are 1, the two-liquid area extending from about 9 to 43 percent of PbO; 2, the flat maximum at about 61 percent, the

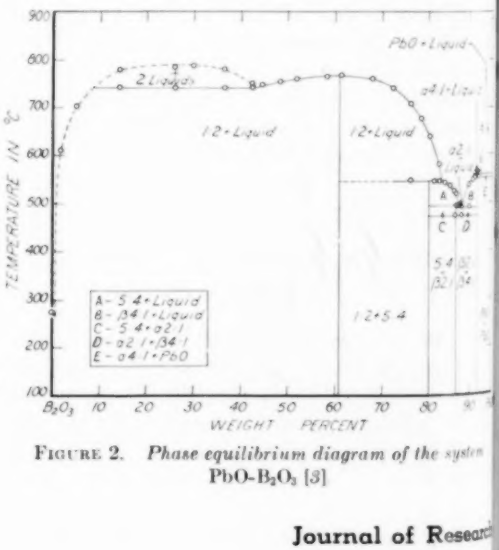

FIGURE 2. *Phase equilibrium diagram of the system* PbO-B_2O_3 [3]

tetraborate composition; 3, the steep slope of the liquidus curve at about 83 percent; and 4, the liquidus temperature being below 800° C for all compositions containing less than 95 percent of PbO.

(b) Surface Tension Data

Table 1 gives the values obtained for surface tension. Figure 3 shows a plot of the surface tension at 900° C versus percentage of PbO. In the composition region from 0 to about 40 percent

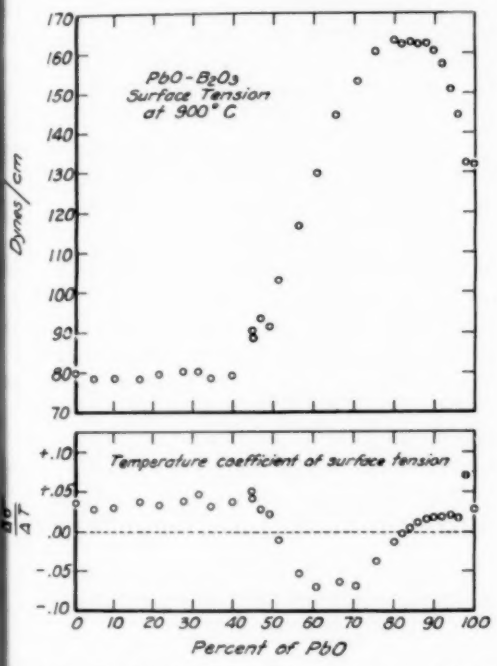

FIGURE 3. *Surface tension and temperature coefficient of surface tension of the compositions in the system* PbO-B_2O_3 *at 900° C.*

of PbO, the surface tension is almost constant. This is the region, at lower temperatures, of two immiscible liquids. However, 900° C is far above the critical solution temperature and only one liquid should exist. It is interesting to note that a large change in composition causes such a small change in surface tension. This condition may indicate that the composition of the surface layer is quite different from that of the interior of the liquid and, as the surface tension differs but little from that of pure B_2O_3, that this layer consists almost wholly of that oxide.

TABLE 1. *Surface tension of compositions in the system* PbO-B_2O_3

PbO	Number of tests	Surface tension (in dyn/cm) at—				
		600° C	700° C	800° C	900° C	1,000° C
Percent						
0 (100 B_2O_3)	2	.....	.....	75.9	79.5	83.0
4.9	1	.....	.....	75.5	78.2	.....
10.1	1	.....	.....	75.5	78.4	.....
16.6	2	.....	.....	74.5	78.2	82.1
21.6	2	.....	.....	76.1	79.4	.....
27.8	2	.....	.....	76.3	80.1	.....
31.4	2	.....	.....	75.5	80.1	.....
34.4	2	.....	.....	75.4	78.5	.....
39.9	2	.....	.....	75.4	79.1	.....
44.9	4	.....	.....	84.8	89.3	.....
47.0	1	.....	.....	90.6	93.3	.....
49.1	2	.....	.....	89.4	91.6	.....
51.3	2	.....	.....	104.0	103.0	.....
56.3	1	.....	.....	121.8	116.4	.....
60.9	1	.....	.....	136.8	129.8	.....
66.4	2	.....	159.8	150.6	144.2	.....
70.7	2	172.3	165.2	157.7	152.9	.....
75.5	2	.....	166.0	162.6	160.3	.....
80.0	2	167.6	165.7	164.3	163.0	.....
82.0	2	163.6	163.0	162.3	162.0	.....
84.1	2	161.6	162.2	162.4	162.8	.....
86.0	2	159.0	160.0	161.6	162.2	.....
88.1	2	156.8	159.1	160.6	162.2	.....
89.8	2	156.5	155.7	158.4	160.4	.....
91.1	1	151.5	152.7	155.4	157.4	.....
94.0	1	.....	.....	.....	151.0	153.1
96.0	1	.....	.....	.....	144.5	146.2
97.9	1	.....	.....	.....	132.3	139.3
100.0	1	.....	.....	.....	132.0	134.8

From about 40 to 80 percent of PbO, the surface tension rises rapidly to a flat maximum near 84 percent of PbO. Above this percentage it drops to the value for pure PbO.

The lower part of figure 3 shows a plot of the temperature coefficient of surface tension at 900° C versus composition. From 0 percent of PbO through the two-liquid region, the coefficient is positive and probably constant within the limits of experimental error. Increasing PbO beyond the two-liquid region causes the coefficient to drop and become negative. The maximum negative value occurs between 60 and 70 percent of PbO. Further increase in PbO causes the coefficient to increase to zero at about 82 percent, and from this percentage to pure PbO it is positive. The positive coefficients of pure PbO and B_2O_3 indicate that they are molecularly complex [7]. It is interesting to note that a region of negative temperature coefficients of surface tension exists in a sys-

708101—48——5

tem whose end members have positive coefficients of surface tension.

(c) Some Effects of Heating Various Compositions

Table 2 presents data on the effect of heating various compositions. The first column gives the percentage of PbO calculated from the batch components. The second column gives the composition of the resulting glasses as found by chemical analysis. Note that the percentage of PbO found is higher than that in the first column until 80 percent is reached. Beyond this the agreement is fairly good. These results seemed interesting enough to warrant checking by prolonged heating of some of the glasses. The results are shown in the third column. Below 80 percent, heating resulted in an increase in the percentage of PbO, and above 80 percent a decrease resulted. These results can be interpreted in the light of the surface tension curve previously shown (fig. 3). From 50 to 80 percent of PbO, the surface tension increases as the percentage of PbO increases. According to the Gibbs adsorption isotherm, a substance that raises the surface tension is negatively adsorbed; its concentration is less in the surface than it is in the body of the liquid. If the intrinsic volatilities of the two end members are approximately equal, relatively less PbO than B_2O_3 will be lost and the liquid will become richer in PbO. The reverse behavior is to be expected in that region where increasing PbO causes the surface tension to fall. From 84 percent upward there is more PbO in the surface than in the body of the liquid. Therefore, relatively more PbO is lost and the liquid becomes poorer in that oxide.

The last column of table 2 is a record of some volatilization experiments. Although the results are somewhat scattered, there is evidence of minimum volatility at about 82 percent of PbO. If the surface tension is considered as arising from an internal attraction of the molecules, it is obvious why a composition having a high surface tension should also have a low volatility. However, caution must be exercised in applying these conclusions to other liquids, because the relation between the surface and the interior of such liquids may vary greatly from that of the compositions under consideration.

(d) Temperature Coefficient of Surface Tension and Expansivity

The temperature coefficient of surface tension is related to the mean coefficient of cubical expansion [7]. It has been deduced from theoretical considerations that the ratio of the coefficient of surface tension to the coefficient of cubical expansion should be equal to 2.33. For many substances, the ratio is approximately constant, and the average is about 2.3. Data on the volume expansion of lead borates at 900° C were not available and, therefore, the expansion coefficients

TABLE 2. *Change in composition and volatility on heating* $PbO\text{-}B_2O_3$ *melts*

PbO			Volatilization loss
Calculated from batch	Found	After heating	
%	%	%	mg [1]
50.0	51.33	52.91	
55.0	[2] 56.23	-----	[2] 44
60.0	60.98	-----	67
65.0	66.50	67.01	[2] 60
70.0	70.70	-----	[2] 50
75.0	75.54	76.48	[2] 64
80.0	79.94	80.40	[2] 28
82.0	82.08	81.21	[2] 16
84.0	[2] 84.12	83.64	[2] 13
86.0	[2] 85.97	-----	[2] 13
88.0	[2] 88.04	87.92	----
90.0	[2] 89.84	-----	[2] 33
92.0	[2] 91.91	91.63	[2] 126

[1] Glass sufficient to yield 0.3 ml was placed in standard 25 ml platinum crucibles and heated at approximately 900° C for 16 hr.

[2] Average of 2 determinations.

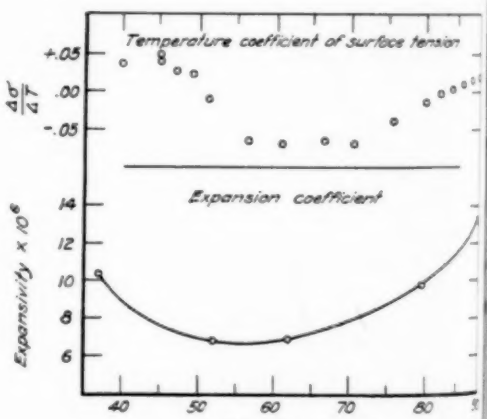

FIGURE 4. *Comparison of the temperature coefficient of surface tension with expansitivity [3].*

Surface tensions of compositions in the system $PbO\text{-}B_2O_3$ at 900° C. Expansivity determined between room temperature and 250° C.

from room temperature to 250° C [3] have been plotted in figure 4. One sees that the two curves are similar.

2. The System PbO-SiO_2

(a) Surface Tension Data

Table 3 presents the data obtained on compositions ranging from 0 to 35 percent of SiO_2. Melts containing more than 35 percent of SiO_2 were difficult to obtain with the apparatus available. Figure 5 shows a plot of the surface tension at 1,000° C versus percentage of SiO_2. The upper

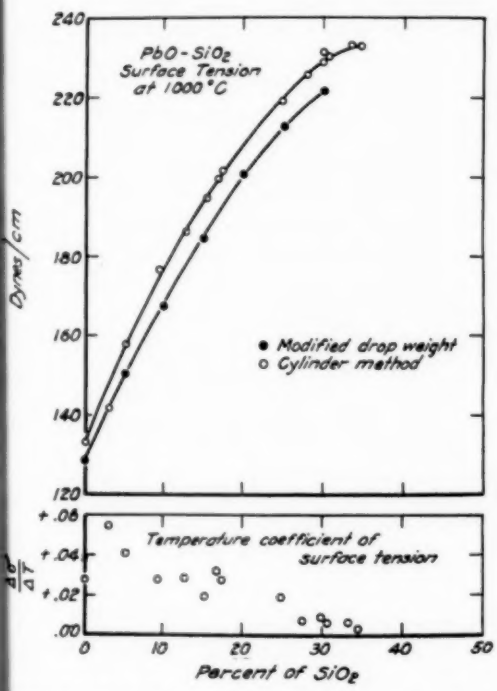

FIGURE 5. *Surface tension and temperature coefficient of surface tension of compositions in the system* PbO-SiO_2 *at 1,000° C.*

curve shows the data obtained by using the maximum-pull method, and the lower curve shows the data obtained by Appen [8], who used a modified drop-weight method. Although Appen's results are distinctly lower, the difference being ascribed to the different methods, both curves show a rapid increase in surface tension with increasing amounts of silica.

TABLE 3. *Surface tension of compositions in the system* PbO-SiO_2

SiO_2	Number of tests	Surface tension (in dynes/cm) at—							
		700° C	800° C	900° C	1,000° C	1,100° C	1,200° C	1,300° C	1,400° C
Percent									
3.20	1	.....	.....	134.4	142.0	145.4	154.2	158.0	161.3
5.17	1	.....	.....	147.8	157.7	152.1	158.0	164.1	162.7
9.36	1	.....	.....	173.6	176.5	179.2	182.0	183.3	.....
13.18	2	.....	.....	183.7	186.5	189.6	193.9	197.3	.....
15.30	2	.....	187.3	192.4	194.6	196.1	.....	.....	.....
16.76	3	.....	.....	.....	199.4	202.2	205.7	210.2	.....
17.50	2	193.2	196.8	199.1	201.6	204.4	208.2	209.4	.....
24.30	3	.....	.....	217.1	219.1	221.0	222.6	223.4	.....
27.12	3	.....	.....	224.5	225.6	225.7	226.5	227.2	.....
28.31	3	.....	.....	.....	227.8	228.4	227.5	228.5	.....
30.08	3	.....	.....	.....	231.3	232.0	232.7	230.5	229.1
30.16	2	.....	.....	.....	230.0	230.8	230.8	231.7	232.2
32.74	3	.....	.....	.....	233.7	235.0	235.6	234.5	235.1
34.91	2	.....	.....	.....	233.0	233.7	234.0	235.0	235.7

(b) Surface Tension and Volatility

Inasmuch as the surface tension rises as the percentage of silica is increased, it is to be expected that the volatility will decrease. This was found to be the case by Preston and Turner [9] in their important work on the volatility of various systems.

(c) Temperature Coefficient of Surface Tension and Expansivity

The lower part of figure 5 is a plot of the temperature coefficient of surface tension versus composition. The temperature coefficients are all positive, become smaller as the percentage of silica increases, and approach zero at about 35 percent of SiO_2. From the parallelism that was shown to exist between the expansion coefficient and the temperature coefficient of surface tension, the expansion coefficient should decrease with increasing silica. Expansion values were available only in the range from room temperature to a few hundred degrees. As the following data [6] show, these values decrease as the silica increases.

SiO_2	Coefficient of expansion from 200° 300° C
Percent	
12	13.1×10^{-6}
21	10.4
34	7.9

IV. Summary

The surface tensions of a series of molten lead borates and lead silicates have been measured; the changes in composition on heating and the volatility of the compositions have been related to their surface tensions; and the similarity of the composition-expansivity curve to the composition-temperature coefficient of surface tension curve has been pointed out.

V. References

[1] Leo Shartsis and Alden W. Smock, J. Research NBS **38,** 241 (1947) RP1771.

[2] F. C. Champion and N. Davy, Properties of matter, p. 126 (Prentice-Hall, Inc., New York, N. Y., 1937).

[3] R. F. Geller and E. N. Bunting, J. Research NBS **18,** 585 (1937) RP995.

[4] G. J. Bair, J. Am. Ceram. Soc. **19,** 347 (1936).

[5] G. W. Morey, Properties of glass, pp. 239, 374, A.C.S. Monograph No. 77 (Reinhold Pub. Corp., New York, N. Y., 1938).

[6] R. F. Geller, A. S. Creamer, and E. N. Bunting, J. Research NBS **13,** 237 (1934) RP705.

[7] H. Freundlich, Colloid and capillary chemistry, pp. 29 to 31, 76 to 77 (E. P. Dutton & Co., Inc., New York, N. Y., 1922).

[8] A. A. Appen, Optiko-Mekh. Prom. **6,** 7 to 12 (March 1936); Ceram. Abst. **16,** 242 (August 1937).

[9] E. Preston and W. E. S. Turner, J. Soc. Glass Tech. **19,** 296 to 311 (1935).

WASHINGTON, September 9, 1947.

U. S. Department of Commerce
National Bureau of Standards

Research Paper RP1856
Volume 40, January 1948

Part of the Journal of Research of the National Bureau of Standards

Expansion Effects Shown by Some Pyrex Glasses

By Arthur Q. Tool and James B. Saunders

Thermal expansion data are presented, which apparently confirm a previously expressed belief that some of the borosilicate glasses containing a high percentage of silica are essentially two-component glasses. One of these components is presumably composed almost entirely of silica and forms into a comparatively rigid and continuous spatial network that pervades the whole glass. This formation develops before the glass is cooled into the annealing range of the other component that is composed of a portion of the silica and most of the other constituents. On being cooled into its annealing range and particularly on reaching temperatures below this range, the low-temperature component also forms a fairly rigid network that is interlaced with that of the high-temperature component. The latter, being composed mainly of silica, possesses a considerably lower expansivity than the other. Consequently, the low-temperature component, whenever it behaves as a rigid network, elastically compresses the other component on cooling and is, in turn, elastically distended. Annealing the glass at suitable temperatures relaxes the compressions and distensions. Such relaxations cause expansions and contractions that are unlike those found in a normal single-component glass. As a result, thermal expansion cycles obtained on glasses containing a high percentage of silica show certain peculiarities. Several cases in which these peculiarities appear are presented and discussed.

I. Introduction

1. Possibility of Two-Component Glasses

In previous papers [1, 2, 3] [1] attention has been called to certain peculiarities possessed by borosilicate glasses with a rather high silica content, such as is found in some Pyrex glasses. In one of these papers [1], it was pointed out that such glasses behave, while within their annealing ranges, as if they consist of a comparatively rigid framework or cellular structure of large and possibly complex molecules that is surrounded or filled by a component that is still fluid. Thus, the glass at this stage appears to consist of two components or glasses, one that has practically reached the vitreous solid state and another that is still in the highly viscous liquid state. Possibly, most glasses possess this characteristic to a limited extent.

The possibility that borosilicate glasses with high-silica content are in effect composed of two-component glasses was first suggested by the double endothermic effect that is observed in some samples of this type of glass when they are heated. This view concerning the nature of these glasses was considerably strengthened when it was found that it could be used to anticipate the consequences that variations in annealing or other heat-treating schedules have in changing the temperature range and magnitude of the endothermic effects of heat-treated samples. By properly regulating the treating schedule, the endothermic effect can be reduced to practically a single effect (as it normally appears in ordinary glasses), or its apparent duality can be accentuated.

2. Softening Ranges and Probable Compositions of Components

From a study of the endothermic effects, as exhibited by heating curves obtained on a number of samples that had received different heat treatments, it appears that the more fluid component of some of the glasses tested became a vitreous solid at a temperature that was approximately 100° C below that at which the less fluid compo-

[1] Figures in brackets indicate the literature references at the end of this paper.

nent reached a stage of comparative rigidity. Roughly speaking, the softening range of the first of these components in ordinary Pyrex glasses extended from somewhat below 500° to 600° C, and the other extended from approximately 600° to 700° C.

In speaking of glass as consisting of two or more component glasses, there is no intention of suggesting that the constituent molecules are sharply divided among them according to definite categories. More probably, the division of the molecules between the components is somewhat indefinite and subject to some change whenever the glass is treated differently at temperatures within or just above its annealing range. Moreover, some individual molecules or complexes of all categories may form a part of both components. Whenever one constituent is in excess and is also capable of forming a glass of itself, it is likely to predominate in one of the components. In view of the composition, it seems that the predominant constituent of the high-temperature component in ordinary Pyrex glasses is silica. In other words, this component consists, for the most part, of associated complexes of silica molecules and chains, and the other consists of almost all the remaining constituents with an appreciable portion of the silica. Heating curves that exhibit endothermic effects supporting this surmise concerning the constituency of the high-temperature component were shown in another publication [4].

In the investigation reported in reference [4], samples of a Pyrex glass were held for considerable periods at temperatures above 650° C to devitrify them. At such temperatures, the low-temperature component is sufficiently mobile to act as an efficient flux that aids in the disintegration of the partially softened high-temperature component and in the formation of cristobalite from it. After the crystallization of the silica is carried as far as possible, the remaining glass no longer shows an endothermic effect corresponding to the high-temperature component. In other words, this component, as a glass, has apparently vanished. Moreover, the remaining endothermic effect is not unlike that of an ordinary borosilicate glass, and it actually occurs in a slightly lower-temperature range than that of the low-temperature component before the other component was removed. This result indicates that the low-temperature component may also have lost some silica as a result of the devitrification. Thus, there is little doubt that silica is also an important constituent of the low-temperature component.

3. Density and Expansivity of a Two-Component Glass

Besides causing uncommon variations in the endothermic effects of a glass, the presence of two components with widely different softening ranges affects other phenomena associated with the annealing and disannealing of glasses. Two of these phenomena are the density changes caused by annealing and the extraordinary expansion of glasses in their annealing ranges. Some of the density changes observed as a result of heat treating these supposedly two-component glasses have already been presented [2, 3]. Also, preliminary results on the peculiarities of the extraordinary expansions of these glasses were included in a paper [5] read at the Toronto meeting of the American Ceramic Society in 1930.

A more extended set of observations on the extraordinary expansions is the subject of the present paper; but before they are taken up, it should be pointed out that the general nature of the results of the experiments can be anticipated from the implied concepts involved in the hypothesis of a two-component glass, especially if there is sufficient knowledge of the nature of the components. In the case of an ordinary Pyrex glass it has been presumed that the high-temperature component is predominently silica. Consequently this component, as compared to ordinary glasses of lower silica content, has a low expansivity and a high annealing range in which the extraordinary expansion is probably not outstanding and the density changes resulting from variations in annealing are small. The other component presumably contains most of the remaining constituents of the glass. As a result, the composition of the latter is not unlike that of some ordinary glasses that are normal both in respect to expansivities and annealing ranges and that, after being well annealed, show a considerable increase in density and also a moderately large extraordinary expansion if reheated through the annealing range.

When measured at some standard temperature well below the annealing range, the expansivity of any ordinary glass so far tested always decreases as the equilibrium temperature is decreased, and the maximum change attainable appears to be

about 10 percent. The same result should also be obtained on a two-component glass, such as that described above, because changes in the effective annealing temperature of the low-temperature component should dominate any expansivity changes of this nature, although the expansivity of the glass as a whole naturally lies between the expansivities of the two components. In other words, it is impossible to produce by annealing treatments any change in the expansivity of the high-temperature component that is not overshadowed by changes of similar origin in the other component. Moreover, because of the dominance of the low-temperature component in this effect, the range of annealing temperatures within which such a decrease in expansivity is producible will approximately coincide with the annealing range of that component (that is, from 450° to 600°C, approximately, for an ordinary Pyrex glass). These conclusions are seemingly corroborated by the results obtained in the investigation [3] of the effect of heat treatment on the expansivity of a pyrex glass.

II. Probable Results of Certain Heat Treatments of Two-Component Glasses

1. First Type of Glass

With regard to the extraordinary expansions of two-component glasses, a great variety of results can be obtained by varying the heat treatments. These effects develop not only as the glass is being heated or cooled through the annealing range, but also while it is being held at a constant temperature in that range. Because these effects are closely associated with the endothermic and exothermic effects, which may be observed by heating a glass through its annealing range, and are also related to density changes, the effects of which persist even after a glass is cooled to ordinary temperatures, it is obvious that any peculiarities in the extraordinary expansions will be associated with corresponding peculiarities in the heat effects and density changes. With this picture of the particular two-component glass under consideration, the following conclusions can be reached as to its probable behavior and properties after it is subjected to certain specific heat treatments.

Treatment (a).—The first treatment to be considered is that in which the glass is cooled rapidly to atmospheric temperatures from temperatures that are above the annealing range of the high-temperature component. This treatment corresponds to that received by glass tubing and small or thin articles that, after being drawn, molded, or blown, are cooled in air at atmospheric temperatures and receive no intermediate or later annealing. At high temperatures suitable for drawing and molding, thermal agitation holds the components in a comparatively high degree of disorganization and the rapid cooling allows very little of the organization [2] that slow cooling and annealing encourage. After being so treated, the glass, on being reheated at a normal rate for testing, will show extraordinary expansions that differ little if any from those shown by a single-component glass treated similarly and having the approximate composition of the low-temperature component. That is, the expansion curve will indicate a small or possibly negative expansion as the annealing range of the low-temperature component is entered, and this effect will be followed by a very large expansion in the upper part of this same annealing range. At higher temperatures, the low-temperature component having fully assumed the characteristics of a liquid glass [6] expands much more rapidly than at temperatures below its annealing range. This increased expansion obliterates any peculiarities that the high-temperature component contributes, in its annealing range, to the expansion curve. Moreover, it is impossible to obtain satisfactory linear-expansion curves in that range because the softening of the low-temperature component has too greatly increased the inelastic deformability of the glass.

Fortunately, the exothermic and endothermic effects that are shown by differential-heating curves, obtained in the usual manner [1], can be observed throughout the annealing ranges of both components. A study of the genesis of these heat

[2] "Organization" as used here and in the following discussion refers to the development of molecular relationships that may or may not be the same as any of those more-or-less hypothetical relationships that have been proposed by various investigators in discussions of vitreous materials. Examples of the hypothetical molecular structures that have been discussed are the silica, threadlike structure considered by R. B. Sosman in his monograph on "The properties of silica" (Chemical Catalog Co., New York, N. Y., 1927) and the chain or ring-like structures considered by E. Preston (J. Soc. Glass Tech. **26**, 82, 1942). Seemingly, such structures should be conducive to the building up of extended networks especially in silica-rich glasses. Other (although not always wholly different) hypotheses concerning extended molecular structures have been advanced in discussions on the constitution of glasses. Some of these hypotheses are mentioned by G. W. Morey in his monograph on "The properties of glass" (Reinhold Publishing Corp., New York, N. Y., 1938). As some of the proposed structures or networks concern silica glasses containing other constituents, they must be considered as possibilities especially in connection with the low-temperature component.

effects [6, 7], and of the conditions probably developed by the heat treatment under consideration, leads to the conclusion that the general appearance of the heating curves obtained in this case will differ little from those that would be obtained on any chilled ordinary single-component glass if it had an unusually broad annealing range. In other words, the curves will indicate that an exothermic effect developed near the lower limit of the annealing range of the low-temperature component, and that the following endothermic effect extended without apparent break over the annealing ranges of both components. Curve 5 in figure 1 presents such indications. Excepting

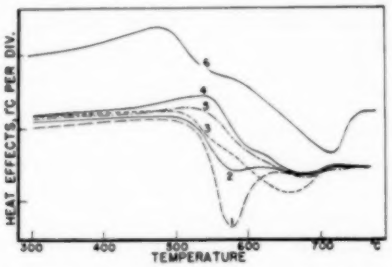

FIGURE 1. *Differential heating curves showing exothermic and endothermic effects.*

Ordinary Pyrex glass, such as used in chemical ware: Curve 1, after treatment for 21 days at 450° C; curve 2, untreated glass; curve 3, after treatment for 30 hours at 550° C; curve 4, after treatment for 1 hour at 700° C; curve 5, after treatment of 1 hour at 850° C. G702P glass; curve 6, untreated.

a slight change in curvature just above 600° C, there is no indication in this curve of an exothermic effect near the beginning of the annealing range of the high-temperature component. As this component was chilled by the treatment imposed on the glass, it should produce an exothermic effect as it anneals near 600° C during the heating required by the test. However, such an effect will be comparatively small if the component is constituted mainly of silica. Moreover, such an effect may be practically obliterated because it is overlapped by the endothermic effect of the low-temperature component.

After this type of cooling treatment, which usually follows the production of any small glass article and which in this case allows neither component opportunity to develop molecular reorganization and compaction to the degree normally induced by annealing, the density will be definitely lower than after any annealing treatment that is capable of increasing the general compaction and which thereby appreciably reduces the "unoccupied" or intermolecular space. However, when a glass is composed of two major components with appreciably different properties, it must be expected that the interaction between these components during various heat treatments and especially during rapid coolings or heatings will cause extraordinary variations in the unoccupied space. Hence, this interaction must be taken into account when considering the effects that heat treatments have on density.

During a rapid cooling the behavior of both components, even before they reach their respective annealing ranges, is very much like that of vitreous solids. This likeness increases very rapidly as the temperature decreases and the viscosity increases. In other words, there is comparatively little shifting of the relative positions of the molecules except through the development of elastic molecular strains. Such strains are doubtless compressions of the component with a low expansivity (the high-temperature component in the glasses now under consideration) and distensions of the component with a high expansivity. Release of these strains by annealing in the annealing range of the low-temperature component will modify the compaction (increase in density) normally developed by annealing. The normal density change caused by annealing a chilled glass is an appreciable increase that develops at a decreasing rate as equilibrium is approached at the annealing temperature. In the beginning of an annealing of a chilled two-component glass in the annealing range of the low-temperature component, the same sort of compaction develops and increases the elastic strains. As these strains increase, their rate of relaxation increases if the viscosity is not too greatly increased by the compaction. As the strains relax, the compressed and comparatively rigid high-temperature component expands the glass. This expansion continues long after the previously ascendant contraction of the low-temperature component is practically ended. That is, a two component glass after being subjected to treatment (a) should first contract and then expand under certain conditions of annealing. Experimental results showing such a reversal are discussed later.

Treatment (*b*).—When the rapid cooling begins after the glass has been held for a short time at a

temperature that is near the upper limit of the annealing range of the high-temperature component, and which is too low for working the glass, the organization of this component into a sort of framework that extends throughout the body of the glass will be somewhat more definite than it was after treatment (a). Nevertheless, it, as well as the low-temperature component, will be chilled. Consequently, both components will show exothermic effects when reheated for test and these effects may be more distinct than before if, as suspected, the organization of the high-temperature component has withdrawn some silica from the other component. Curve 4, figure 1, is an example of the heating curves obtained on samples heat treated in this manner. However, this treatment does not differ sufficiently from that discussed under treatment (a) to produce a materially different density or expansion curve.

Treatment (*c*).—If the rapid cooling from high temperatures is stopped at some temperature in but above the midpoint of the annealing range of the low-temperature component, the other component, despite its very high viscosity, will become almost completely organized and annealed if a reasonable time is allowed before the rapid cooling is resumed. Annealing of the high-temperature component at such a comparatively low temperature is possible because of the fluxing action of the more mobile low-tempearture component which, with comparative rapidity, reaches an equilibrium condition corresponding to the holding temperature. During this rapid adjustment, the low-temperature component shrinks and there is, in the initial stages of this shrinkage, a negative expansion of the glass. However, as this adjustment nears completion and consequently slows up, a slower developing positive expansion effect gains ascendency as the high-temperature component frees itself from compression as described under treatment (a).

When this treatment of the glass is completed by a rapid cooling to atmospheric temperatures, the low-temperature component is only partially annealed in the sense of being brought to equilibrium at low annealing temperatures. However, the other component should be rather thoroughly annealed. Consequently, a heating curve test will show an indication of only one exothermic effect and that will be comparatively small and near the lower limit of the annealing range of the low-temperature component. On the other hand, the indication of an endothermic effect in this curve will be especially marked in the annealing range of the high-temperature component. Curve 3, figure 1, is such a heating curve.[3]

Because of the expansion of the high-temperature component as it is released by heat treatment (c) from much of the compression imposed upon it by the other component, the density of the glass on reaching atmospheric temperatures is appreciably lower than when the cooling is rapid and continuous from high to atmospheric temperatures as in treatments (a) and (b). Thus, this release from compression accounts for the apparent minimum density obtained by certain treatments in previous investigations [2, 3].

An expansion curve obtained after treatment (c) will resemble, in many respects, that of a slightly annealed ordinary glass because the low-temperature component, which mainly determines the form of the curve below its softening range, has received such an annealing. Consequently, the curve will show no reduction in the expansion rate at temperatures near the beginning (lower end) of the annealing range of this component, but it will show a very rapid expansion in the range of the first endothermic effect. However, if the heating for the test is stopped sharply and held at a temperature near the upper limit of the annealing range of this component, the glass will contract somewhat at the constant temperature instead of expanding slightly for a time as a normal glass does in continuing to equilibrium. This contraction develops because the glass has been heated beyond the holding point of the previous treatment by which the high-temperature component was to a great extent freed of compression and by which a sort of equilibrium condition was established between the two components. In heating beyond this point, the more rapidly expanding low-temperature component elastically distends the comparatively rigid spatial network of the high-temperature component. In other words, the mole-

[3] All of the heating curves, such as curves 1 to 5 in figure 1, which were obtained on an ordinary Pyrex glass, indicate that the endothermic effect of the high-temperature component occurs between 600° and 700° C, approximately. For a pure silica glass it occurs near 1,100° C and is small and not particularly definite. Presumably, this effect of the high-temperature component occurs at considerably lower temperatures and is comparatively large and definite under some conditions because the component is not composed of silica alone and also because of the solvent action of the other component at temperatures well above its annealing range.

cules of the highly viscous low-temperature component being hampered by the almost rigid network of the other component cannot flow immediately into all of the excessive intermolecular spaces as they develop. Consequently, a slight overexpansion of the glass has developed when it reaches the top temperature of the expansion test described. At this temperature, the overexpansion soon disappears as the elastic network frees itself of distension and the excessive intermolecular spaces are filled through flow of the low-temperature component. This contraction effect is an exception to Marchis' [8] rule that the expansion cycle of glasses is counterclockwise.

Treatment (*d*).—The molded object, from which the samples corresponding to curves 1 to 5 in figure 1 were taken, was large and thick compared to ordinary tubing, although it was doubtless cooled rather rapidly through the annealing range of the high-temperature component. However, because of the size of the object, the cooling rate on reaching the annealing range of the low-temperature component must have been appreciably slower than the rates to which smaller objects, such as ordinary tubing, are subjected in their production. Consequently, such a treatment should give the low-temperature component an intermediate annealing, but should leave the other component in a highly compressed condition.

The density of the glass on reaching atmospheric temperatures in a condition such as this will appreciably exceed that found after treatments (a) and (b). Density determinations made on a similar glass that had received a treatment not unlike that being discussed were presented in a previous publication [2].

The expansion curve following treatment (d) resembles that described under treatment (c), but the rapid expansion is somewhat greater. The endothermic effect of the low-temperature component is relatively definite, although decreased somewhat by the following exothermic effect of the other component. This decrease appears because the two effects tend, as usual, toward mutual obliteration. Having been chilled, the high-temperature component contributes only a small endothermic effect. Curve 2 of figure 1 represents a heating curve of this kind.

Treatment (*e*).—If a sample of either of the glasses yielding curves 2, 4, and 5 is retreated for a very long period at a temperature near the lowest possible effective annealing temperature for a low-temperature component, this component will receive a very thorough annealing and will shrink considerably. The other component will remain in a chilled state and will be subjected to a very severe compression. As a result, the density at room temperature after the glass receives such a treatment will approximate the highest that the glass can attain. However, if the treatment at the low-annealing temperature is extended to a duration of some months, the density will begin to decrease very slowly. This decrease develops because the compressed high-temperature component, even at such low-annealing temperatures, is still capable of freeing itself slowly from the compression despite the extremely high viscosity of the other component.

The expansion curve of the glass after being treated as suggested under treatment (e) will be similar to those described for treatments (c) and (d), except that the rapid expansion in the temperature range of the endothermic effect of the low-temperature component will be still more pronounced. (Expansion curves of the various types mentioned are shown in later figures.) The heating curve of this glass will show a very pronounced endothermic effect for the highly annealed low-temperature component, but the endothermic effect for the high-temperature component will be small as in the case of treatment (d). Curve 1, figure 1, is the type of differential heating curve obtained after treatment (e).

2. Second Type of Glass

Curve 6 of figure 1 is a heating curve obtained on glass tubing marketed under the designation G702P. As this glass had presumably received no heat treatment except that of a rapid cooling after drawing, its treatment probably approximated treatment (a), but the curve more nearly resembles curve 4 obtained after treatment (b). The indications of exothermic and endothermic effects in this glass are more pronounced than in ordinary Pyrex glasses. Also, there appears to be a more definite separation between the annealing ranges of the two components. In other words, the indicated annealing range of the low-temperature component is somewhat lower, and that of the other is somewhat higher in curve 6 than in curves 1 to 5. The very distinct indication of an endothermic effect for the high-temperature com-

ponent suggests that this component is unusually well organized in this glass even after a rapid cooling from high temperatures. The comparatively large effect may also mean that the composition of the high-temperature component in this glass differs materially from the composition of the corresponding component in ordinary Pyrex glasses.

The comparatively marked indications of all heat effects in curve 6 suggest that the variations in the rapid-expansion effects and in the density changes resulting from differences in treatment will also be comparatively large in G702P. As the composition of this glass was doubtless designed to produce a somewhat higher expansivity than that of ordinary Pyrex, such results are to be expected. That is, an increased expansivity in the vitreous-solid condition is usually accompanied by an increased expansivity for the glass after it definitely becomes a viscous liquid on being heated to the annealing range or higher.

III. Expansion Effects

1. Typical Expansion Curves of Chilled Glasses

Having arrived at specific conclusions relative to the expansion effects to be observed as a result of tests made after a two-component glass is heat treated according to different schedules, these conclusions will now be used as aids in interpreting a great variety of results obtained by a somewhat wider range of treatments and tests. These expansion tests were all made on tubing having an outside diameter of about 12 mm. The approximate composition of this ordinary Pyrex tubing has been given in a previous publication [3], and this composition is not markedly different from that of the glass used in procuring the previously discussed heat effects. The method of measuring the expansions was also described in that publication. The heating rate used in the expansion tests approximated 3° C/min and, above 450° C, the cooling rate was not appreciably different from that of heating.

Figure 2 presents the expansion curves (both heating and cooling branches) to 600° C for samples from two pieces of ordinary Pyrex tubing. These samples had received no additional treatment before the tests. Consequently, their condition presumably approximated that produced by treatment (a). Curves for two samples

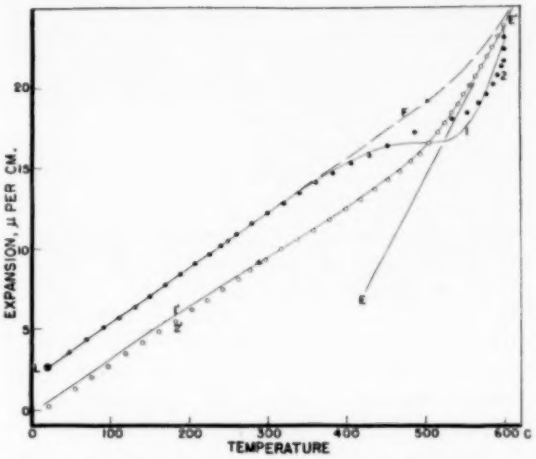

FIGURE 2. *Thermal-expansion cycles of two samples of ordinary Pyrex tubing.*

Curves 1 and 1′, unbroken lines, heating and cooling branches for sample from the glass used in tests represented by figures 3 to 8, and 10. Curves 2 and 2′, dots and circles, similar branches for sample from glass used in tests represented by figure 9. Curve *F*, representation of contraction probably followed as tube was cooling after being drawn. *L*, The point reached by curve *F* at 20° C. (If the length of the sample at the end of cooling branch 2′ is considered to have been 1 cm, it follows that $L = 1.00025$ cm, approximately, was the initial length of the specimen). Line *EE*′ is tangent to cooling branches at 600° C. (For a one-component glass, this tangent usually indicates approximately the trend of the equilibrium curve.)

are presented in order to show the maximum variation observed in the heating branches of expansion curves obtained on original specimens that have been chilled in their production. Special chilling treatments of considerable severity cause a much more pronounced reduction in the rate of expansion than is exhibited by curve 1 between 375° and 535° C. Less severe chilling treatments result in curves that resemble curve 2, which is indicated by dots. In comparing curves of this nature, care must be taken to insure that the heating rates within the annealing range have been the same in the two or more tests. For instance, a somewhat higher rate of heating in procuring curve 2 could have been the cause of an appreciable part of the difference between curves 1 and 2.

In these tests, the samples were held 1 hour at the top temperature. During this period of constant temperature, there was a small expansion as the low-temperature component approached its equilibrium condition at that temperature more closely, and also as the high-temperature component completed the freeing of itself from the compression previously imposed upon it. The

magnitude of this compression when 600° C is reached in a heating test depends to a great extent on the rate of heating.

The maximum compression of the high-temperature component developed at some time before the top temperature, 600° C, was reached in the test. This maximum compression derived from two sources. Part of it developed during the initial cooling from the drawing temperature, and it developed because of the comparatively low expansivity of the high-temperature component. Obviously, most of this part is automatically relieved by reheating to 600° C, if no complicating conditions develop. The other part of the compression developed during the reheating, and it developed because the low-temperature component shrunk in the range of its exothermic effect; but most of this compression was also relieved before 600° C was reached. This relief results from the extraordinary expansion of the low-temperature component in the range of its endothermic effect. Consequently, on reaching 600° C in expansion tests on chilled samples of these two-component glasses, very little of the compression of the high-temperature component remains except the portion that developed before 600° C was reached during the cooling that caused the chilled conditions. Furthermore, much of this portion will also have been dissipated before reaching such temperatures if a low heating rate is employed in the expansion test.

The decrease in length from point L to approximately zero (about 2 μ/cm) resulting from the expansion cycle was caused by the partial annealing of the low-temperature component. Most of this annealing (decrease in equilibrium temperature) took place during the cooling from 600° to 500° C while procuring the cooling branch. The shrinkage accompanying this annealing again compressed the high-temperature component, but to a lesser degree than that which existed prior to the test. A lower cooling rate would possibly have resulted in a smaller compression, but to what extent is uncertain because a lower rate develops more shrinkage of the low-temperature component as well as allowing more time for the other component to free itself from compression.

Curve 1, figure 3, represents the expansion cycle obtained on a sample of the G702P tubing before it received additional treatment. Consequently, the discussions presented under treatment (a) and in section II, 2 apply. As expected, the expansion effects are much more pronounced in this glass than in ordinary Pyrex. After the first expansion cycle, the resultant decrease in length per centimeter approximated that shown by Pyrex (curve 2) under the same conditions. Considering the greater expansions of G702P this result may seem strange, but a second cycle on the same sample yielded an explanation. In this test, the heating branch coincided with the cooling branch of the first cycle until the annealing range of the low-temperature component was reached. From this point to 600° C, the heating branch was steeper than the cooling branch of the previous cycle. Therefore, the length of the sample was about 1.75 μ greater than before at the top temperature. As a result, the sample has practically regained its initial length at the end of the second cycle. This indicates that the shrinkage caused by the partial annealing of the low-temperature component was offset completely by relieving the high-temperature component of the compression imposed on it before the glass had reached 600° C during its initial cooling. Enough of this offset developed during the first cycle to prevent an exceptional shrinkage as compared to that obtained on ordinary Pyrex.

During the 1-hour holding period at 600°C in the second test, there was a slight shrinkage of

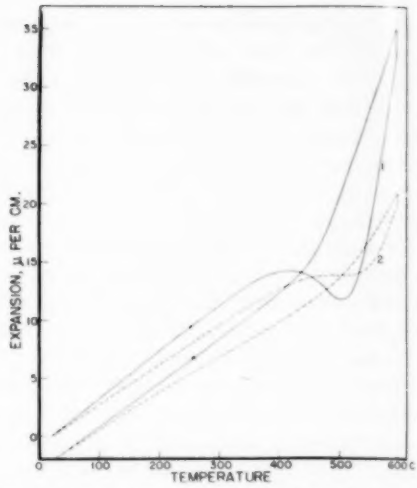

FIGURE 3. *Comparison of the thermal-expansion cycles for G702P and an ordinary Pyrex glass.*

Curve 1, cycle for G702P; Curve 2, reproduction of branches 1 and 2 figure 2.

stead of an expansion as in the equal holding period of the previous test. This shrinkage cannot be ascribed to deformation, because the softening point of both this glass and ordinary Pyrex is about 670° C—if that point is defined as the temperature at which the rate of collapse of the fine points supporting the sample and the top plate of the interferometer equals the rate of expansion while heating at a rate of 3° C/min. This shrinkage, resulting from a slight over-expansion developed in heating to 600° C for the second time, corresponds to the possible effect that was mentioned in the last paragraph under treatment (c).

Doubtless, the high-temperature component, in freeing itself from the compression that developed above 600° C during the cooling after the drawing of the tubing, contributed appreciably to the rapid expansion between 500° and 600° C in the heating branch of curve 1. However, most of this very large expansion is the result of the comparatively high expansivity of the low-temperature component in its liquid state and of the superheating imposed on this component after it passes through an equilibrium condition at a temperature near that of the minimum of the curve. This expansion developed at the rate of about 0.31μ/(cm, deg. C), whereas the corresponding rate for ordinary Pyrex is about 0.14. These rates depend on the rate of heating and are even larger for most ordinary glasses.

The rate of contraction between 600° and 500° C, as indicated by the cooling branch of curve 1, approximates 0.15 μ/(cm, deg C). This rate is lower than the expansivity of the low-temperature component as a liquid because there is some undercooling (departure from the equilibrium curve), even when cooling at a rate of 3 deg. C/min, and also because of the lower expansivity of the high-temperature component. For ordinary Pyrex, the contraction rate of the cooling branch under similar conditions is about 0.08 μ/(cm, deg. C). After considering both the apparent rates of expansion and contraction and the general appearances of the curves above 500° C, it is estimated that the expansivities of the low-temperature components in the liquid phase are (in the above units) about 0.24 for the G702P and 0.09 for the ordinary Pyrex, provided the effect of the high-temperature component is ignored.

Compared to the above expansivities for the liquid phases of the low-temperature components, the expansivities for the glasses in the vitreous solid conditions at 100° C are (when expressed in the same units) about 0.039 and 0.034 for G702P and ordinary Pyrex, respectively, before the glasses receive any heat treatment. Long periods of treatment at 450° C reduce these expansivities at 100° C to about 0.035 and 0.031, respectively.

2. Reversal from Contraction to Expansion by Chilled Glass at Constant Annealing Temperatures

In figure 4, curves *A* and *B* represent the first, and curves *C* and *D* the second, expansion cycle on a previously untreated sample of ordinary

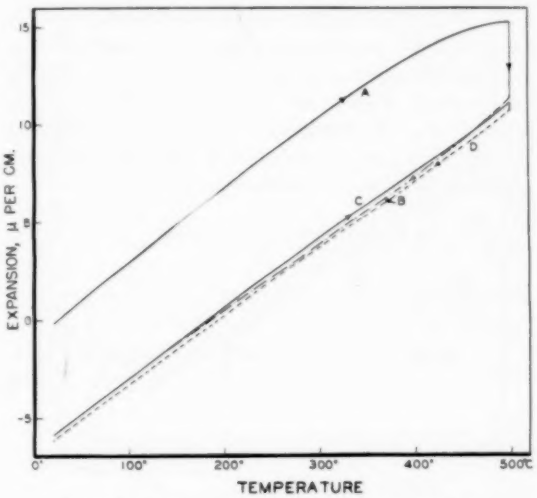

FIGURE 4. *Thermal-expansion cycles to 500° C.*

Curves *A* and *B*, heating and cooling branches of first cycle. Curves *C* and *D*, same for second cycle. Holding periods for contraction at constant temperatures were 2 hours for each cycle. A reversal from contraction requires a much longer total holding period.

Pyrex tubing. In these cycles, the top temperature was 500° C, and the holding period was 2 hours in each case. Throughout the 4 hours of treatment at this temperature, the contraction of the low-temperature component completely overshadowed any expansion caused by the other component as it freed itself from compression. According to experience gained in procuring data for the previously mentioned [2, 3] curve showing the change in density with change in treating temperature, a treating period of not less than 1 day would be required before these opposed effects became balanced so that the contraction ceased.

The two cycles shown in figure 5 were obtained under conditions like those mentioned in connection with the previous figure, except that the holding temperature was 525° C. In this case, the 2-hour holding period of the first cycle was more than sufficient to reach a balance between the contraction and expansion of the low- and high-temperature components, respectively. Consequently, the glass began to expand at a slow rate before the end of the holding period of the first cycle. This expansion continued during the second cycle, and the cooling branch *D* would have been brought closer to branch *A* than to branch *B* in the range of atmospheric temperatures if, in procuring branch *D*, the cooling rate had been increased greatly and the holding period at 525° C had been made as long as those required to establish an equilibrium condition at this temperature in the previously mentioned density experiments. The possibility of this change from contraction to expansion during an annealing treatment (as shown in figs. 5 and 6) was discussed under treatment (a), section II.

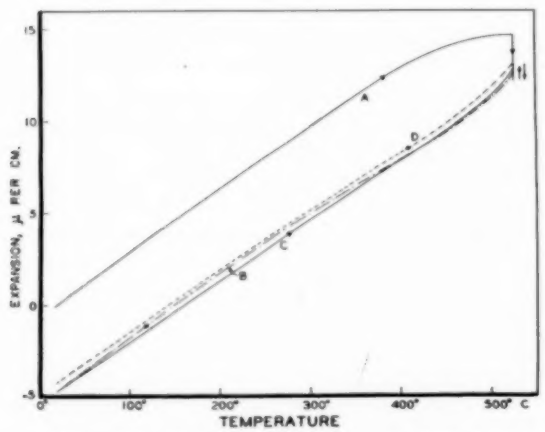

FIGURE 5. *Thermal-expansion curves to 525° C.*

Curve designations have same significance as in figure 4. Holding periods, 2 hours for each cycle. Reversal takes place during first cycle.

When the holding temperature was raised to 550° C without other change in the test conditions, the results shown in figure 6 were obtained. In this case, there was a change from contraction to expansion before the first holding period of 2 hours was half over. Moreover, branch *C* of the second cycle shows that the freeing of the high-temperature component from compression was renewed as

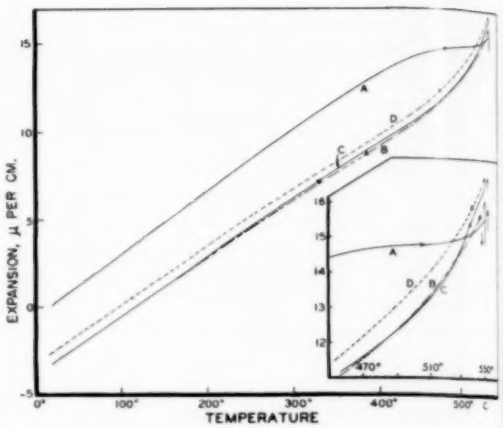

FIGURE 6. *Thermal-expansion cycles to 550° C.*

Curve designations same as in figure 4. Holding periods, 2 hours for each cycle. Inset is an enlargement to show reversal more clearly.

the glass was heated from 530° to 550° C and was continued throughout the second holding period at the latter temperature. In normal glasses in which there is practically no indication of this freeing effect, branch *C* remains below branch *B*. Had the holding period of the second cycle been increased to 3 or 4 days, as in the previously mentioned density experiments, and had the cooling rate been made high enough to chill the low-temperature component severely and thereby to prevent that part of its contraction which an approach to equilibrium at temperatures below 550° C causes, branch *D* would have been above branch *A*. That is, the treatments provided by the two tests would have lengthened rather than shortened the sample tested.

The initial contraction during the first holding period at 550° C shows that the low-temperature component was still approaching equilibrium from a condition corresponding to a higher temperature. This contraction effect in a normal glass does not cease until branch *A* cuts the equilibrium curve. It is estimated that an extension of branch *A* (fig 6) to approximately 560° C would have been required before such an intersection was reached. Curves 4 and 5 of figure 1 indicate about the same temperature because the exothermic effects, attributed to the low-temperature component, end in that neighborhood. This estimate places the intersection almost 30 deg C above the intersection of curve 1 with curve *EE'* in figure 2. However, *EE'* is merely the approximate slope of the expan-

ion and contraction curves in the neighborhood of 600° C, which was found to be the lowest temperature at which heating and cooling curves obtained by using rates of 3 deg C/min still coincided approximately. For a normal glass, this tangent usually approximates the equilibrium curve as determined by dimensional measurements. Apparently, a two-component glass has no such fairly definite equilibrium curve.

3. Overexpansion Effects

Raising the holding temperature to 575° C without any other change in the test conditions yielded the curves shown in figure 7. In this test, the low-temperature component on the first heating (branch *A*) crossed its equilibrium curve near

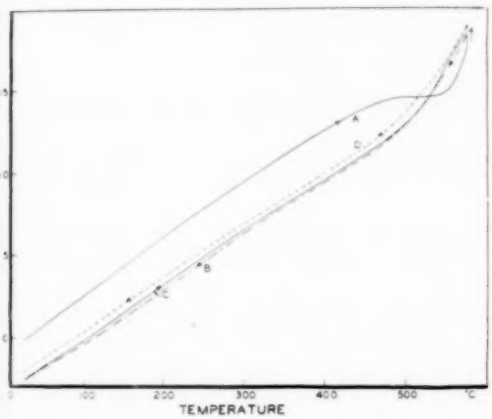

FIGURE 7. *Thermal-expansion cycles to 575° C.*

Curve designations same as in figure 4. Holding periods, 45 minutes for each cycle. No contraction at this temperature. The practical completion of the expansion would require less than 1 day.

560° C and became superheated to an undetermined degree. The degree of superheating is uncertain because, as indicated above, the location of this equilibrium curve is undetermined. On becoming superheated, the low-temperature component no longer contracts, but instead, begins to expand rapidly before 575° C is reached. At the same time, the increased deformability allows the high-temperature component to free itself more rapidly from compression and, thereby, to add materially to the rate of expansion. On reaching 575° C, some superheating and compression still remained to contribute an expansion during the holding period. This delayed expansion continued even during the second holding period and had not been completed after a total holding time of 1 and ½ hours. Had it been completed and had the cooling rate of the second cycle been very rapid, branch *D* would have remained well above branch *A* throughout its whole course. Completion of this expansion during the holding period of the first cycle would have caused an over expansion to take place during the second heating, and a small contraction would have resulted during the second holding period at 575° C. As mentioned under treatment (c), a sufficiently long holding (or annealing) period at temperatures in the upper part of the annealing range of the low-temperature component results in such contraction effects on the second heating to the holding temperature.

This overexpansion effect appears in the second cycle of figure 8, which shows the curves obtained by tests in which the holding temperature was 600° C. The relatively high deformability of the low-temperature component at this holding temperature allowed the delayed expansion to be practically completed during the first holding period. This completion sets the conditions for an overexpansion during the succeeding cycle. As long as devitrification does not develop, the point approached by the expansion and contraction of the first and second holding periods, respectively, is a point on the equilibrium curve of the glass as a whole.

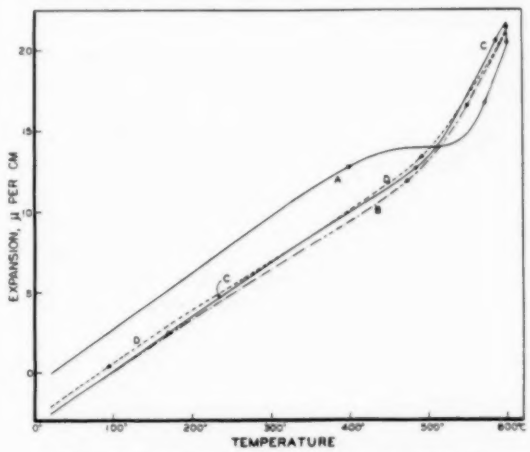

FIGURE 8. *Thermal-expansion cycles to 600° C.*

Curve designations same as in figure 4. The delayed expansion was practically completed during the holding period of 45 minutes in the first cycle. The overexpansion developed during the second heating caused a contraction during an equal holding period of second cycle.

It is only at holding temperatures in the range from about 575° to 650° C that overexpansion effects are observed, and they do not appear at such temperatures unless the high-temperature component has first been freed from compression at temperatures well below the proposed holding temperature. Also, these effects are never very marked unless the low-temperature component has first been brought to equilibrium at temperatures below 575° C. However, reducing the equilibrium temperature below 500° C will seldom result in such an effect unless the high-temperature component has been freed from compression by treatment at a higher temperature. The overexpansion effect is not observed at holding temperatures below 575° C in this glass, because the rapid expansion effect does not begin, even in a well annealed sample (see curve *A*, fig. 11), until temperatures near 550° C are reached. It is not observed above 650° C because the deformability has become so great in that range that all delayed expansions and contractions are practically completed before that temperature is reached.

The samples used in the expansion tests so far discussed were not in the condition required to develop an overexpansion on the first heating because none of them had received any treatment except the rapid cooling following the drawing of the tubing. Moreover, the holding temperatures were in the range of possible overexpansion in only three cases (figs. 2, 7, and 8). The expansion curves presented in figure 9 show some of the treatments (all followed by rapid cooling) that result in delayed expansions, on the one hand, and in overexpansions, on the other, when the samples receiving these treatments are subjected to a first expansion cycle with 600° C as the holding temperature. From the curves and the data presented in the legend it will be noted that the treatments resulting in delayed expansions (curves 0, 1, 2, 8, 9, and 10) at the holding temperature fall into two categories: (1) those that allowed neither the freeing of the high-temperature nor the annealing of the low-temperature component (because the treating temperatures were too high), and (2) those that allowed a rather thorough annealing of the low-temperature component but no freeing of the other from compression (because the treating temperatures were too low). The treatments resulting in overexpansions (curves 3 to 7) were all

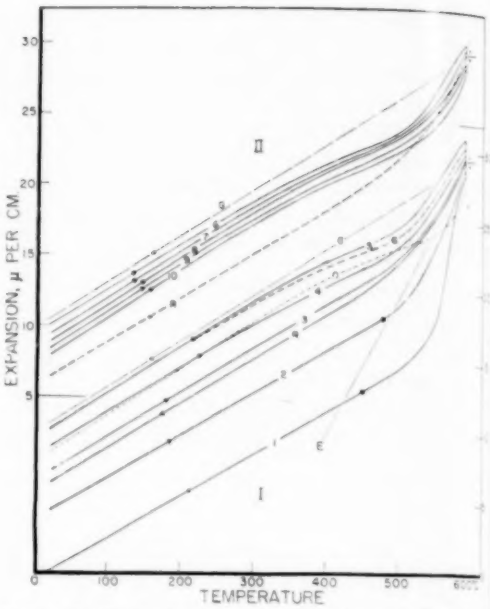

FIGURE 9. *Expansion or contractions shown at 600° C by number or differently treated samples.*

Curves divided into two assemblages (I and II) to avoid interference. Numbered curves are heating branches. Curve *R*, cooling branch common to all cycles in both assemblages. Curve *G*, (both assemblages) estimated course of common cooling branch from 600° C if cooling rate had been very high and equilibrium had been established at that temperature. Curve *EE* reproduced from figure 2. Holding periods, 45 minutes. According to the results the samples tested fall into two fairly distinct groups. Group 1, samples showing delayed expansions on reaching 600° C, curves 0, 1, 2, 8, 9, and 10. Treatments of corresponding samples: 0, untreated (see curve 2, fig. 2.); 1, treated 2 months at 450° C; 2, 2 months at 475° C; 8, 2 hours at 700° C; 9, 1 hour at 725° C; and 10, 1 hour at 750° C. Not included in figure: Sample treated 6 hours at 675° C, curve between 7 and 8. Group 2, samples showing overexpansion and resultant contraction on reaching 600° C, curves 3 to 7, inclusive. Treatments of corresponding samples: 3, 2 months at 500° C; 4, 1 month at 525° C; 5, 9 days at 550° C; 6, 7 days at 575° C; 7, 3 days at 625° C. Not included in figure: Sample treated 28 hours at 650° C, curve between 7 and 8; also one treated 3 days at 600° C; curve between 6 and 7. All above treatments followed by rapid cooling.

intermediate, as the treating temperatures ranged from 500° to 625° C. The maximum effects resulted from the treatments at 550° and 575° C (curves 5 and 6) as should be expected from the previous discussion. In all of these tests, the annealing caused by the heating required to obtain an expansion curve has an appreciable effect. Had this not been true, it is improbable that the treatment at 625° C (curve 7) would have resulted in an overexpansion effect.

Figure 10 presents examples of the clockwise cycles mentioned under treatment (c) in section II. As in the regular tests, the heating and cooling rates for these short or secondary cycles were about

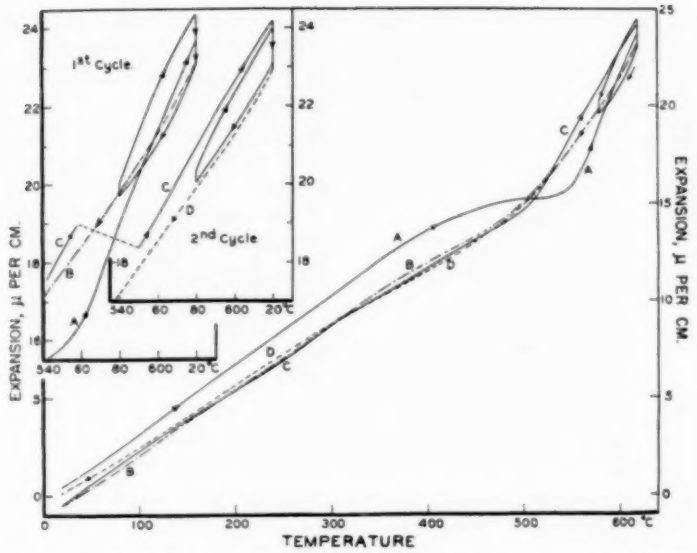

FIGURE 10. *Clockwise expansion and contraction effects between 580° and 620° C.*

As insets indicate, one minor cycle was interposed between branches *A* and *B* of the first major cycle and another between branches *C* and *D* of the second major cycle, although the second minor cycle is omitted from the primary graph. In normal glasses, minor cycles within the annealing range are always counterclockwise.

3° C/min, although control of the rates is rather difficult when the cycles are so short. The holding periods at the end temperatures (580° and 620° C) of these cycles were about 45 min, although both longer and shorter periods were sometimes used. At the lower end of the cycle this period is too short to complete all of the molecular readjustments and attendant expansion required to establish equilibrium at that temperature. However, at the upper temperature the period of 45 min appeared to be long enough to establish equilibrium. Apparently, these clockwise cycles can be repeated any number of times without any significant change in their form except some changes that can be ascribed to a lack of perfect control of the heating and cooling rates. Also, repeating the cycles causes no appreciable change in the length of the sample if its length is always measured at some temperature near 600° C where equilibrium can be easily established before the measurement is made.

4. Expansion of Annealed Glass at Constant Annealing Temperatures

As shown in previous publications [2, 3], the highest density obtained for an ordinary Pyrex glass was reached when it was treated several weeks at 450° C after it had been chilled from a high temperature. However, a slight decrease from the maximum density was noted when the treatment was increased to several months at 450° C. This decrease suggests that the reversal from contraction to expansion (as shown in figs. 5 and 6) also takes place at this low annealing temperature whenever the treatments are extended sufficiently. Any normal glass, after it has been brought to a high density by being reduced to equilibrium at a very low annealing temperature, expands whenever it is retreated at a higher temperature. This expansion continues until the equilibrium curve is again reached, and the rate of expansion depends on the mobility of the glass and the extent of the departure from equilibrium. Two-component glasses also expand under such conditions, except in those cases in which an overexpansion has been developed.

Figure 11 is presented to show this expansion and the change in rate of expansion when an annealed ordinary Pyrex glass is held at different temperatures. The samples used in this test were treated at 450° C until the maximum density for that temperature was approximated. However the preceding chilling treatment of these samples was not that which followed the drawing of the

768101—48——6

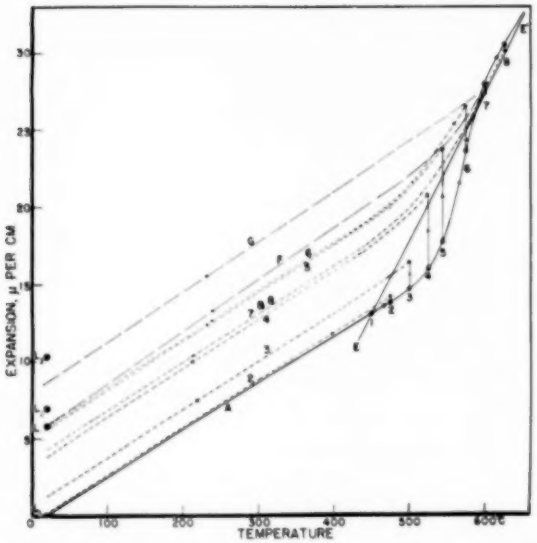

FIGURE 11. *Expansions of an ordinary Pyrex tubing at various temperatures after pretreatment described below.*

The pretreatment consisted of a very rapid cooling from 675° C followed by an annealing of 74 days at 450° C. Curve *A* represents the heating branches of the expansion cycles for all samples. The vertical lines at the holding temperatures, as designated by the sample numbers, represent the delayed expansions (or contractions) during the holding periods. The holding temperatures were 450°, 475°, 500°, 525°, 544°, 575°, 600°, and 625° C, and the holding periods were 6 hours at temperatures 1 to 6, 5 hours at temperature 7, and 15 minutes at temperature 8. The broken curves numbered for the samples are the cooling branches. Curve *G* is the probable trend of the cooling branch for samples 4, 5, and 6 if they had been annealed until the completion of their delayed expansion and cooled very rapidly. Curves *F* and *EE'* reproduced from figure 2 after an arbitrary and immaterial shift in their ordinates. Significance of points *L*, L_1, and L_2, and L_3 discussed in text.

tubing, as they had all been used in some of the tests previously described. To bring them to a uniform chilled condition prior to the final prolonged annealing treatment at 450° C, they were heated for 6 hours at 675° C. This temperature is near the upper limit of the range of intermediate treating temperatures from which chilling treatments were found to set up conditions that are conducive to overexpansion effects even if such treatments are followed by no other annealing than that imposed by the heating necessary to the expansion test. In view of the treatments received during the previous tests and the long annealing treatment which followed the chilling treatment from 675° C, the slight over-expansion effects shown at the holding temperatures 600° and 625° C in figure 11 do not seem unreasonable. (See fig. 9 also.) Curve *A*, from the beginning to point 1, is the common heating branch for all of the tests from 1 to 8. From point 1 to point 2, it is the same for all tests above number 1, and so on as each treating temperature is reached. The vertical lines represent the expansions (or contractions) at the corresponding treating temperatures. The cooling branches are represented by the broken curves 2 to 8.

The expansions that developed during a holding period of 6 hours at the various holding temperatures from 450° to 575° C show graphically how the rates of expansion vary. Had the holding periods been extended sufficiently, the expansions at all of these temperatures would have risen above the curve *EE'*. In fact, experience has shown that a holding period of 6 hours is sufficient to cause the completion of only about two-thirds of the possible expansion even at 575° C. Curve *G* and the point L_3 also indicate that the expansion at this temperature was not completed. Curve *G* is not experimental but was drawn on the assumption that the slope of a cooling curve resulting from a very rapid cooling would have been throughout the length of the curve, practically the same as the slope of the actual cooling branch in the neighborhood of 200° C. According to the previously mentioned investigations [2, 3] on density changes, $L_3 - L_1$ is the increase in length that should occur if the expansion at 575° C had been completed. Apparently, completion of the expansion in test 6 would have caused curve *G* to pass very close to L_3.

From the same results [3] on density changes $L_2 - L_1$ represents the expansion that should occur at 500° C when the holding period is made sufficiently long. Apparently, the expansion at this temperature (curve 3) was about one-fourth completed in 6 hours. Excepting an immaterial shift in their ordinates, point *L* and curves *F* and *EE'* were introduced into figure 11 directly from figure 2. Consequently, $L - L_1$ should represent the contraction in length caused by the preparatory annealing at 450° C after the chilling from 675° C. However, this change in length was also computed from the previously mentioned results on density changes. It is obvious that L_1 was arbitrarily made to coincide with the origin of curve *A*. Consequently, when considered as representing a length, L_1 must be assigned the magnitude of 1 cm because the data for the expansion curves were reduced to expansions per centimeter of the initial

length of the samples. The ordinates of figure 2 represent the expansions per centimeter of the sample following the test. These differences, in the method of computation and in the conditions of the samples assumed to have unit length, account for the difference in the ordinates of point f and of the curves F and EE' as shown in figures 2 and 11.

5. Expansion Effects in Second Type of Glass

Figures 12, 13, and 14 represent some of the expansion data procured on samples of the glass G702P. These results were obtained under the

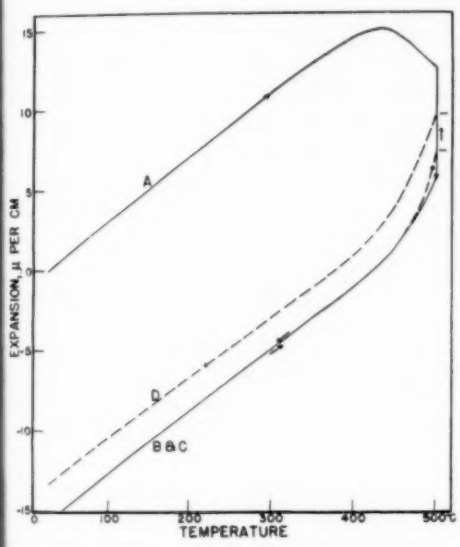

FIGURE 12. *Thermal-expansion cycles of G702P glass to 500° C.*

Curve designations same as in figure 4. No pretreatment. Holding periods 2 hours for each cycle. Compare these curves with those in figure 5 for an ordinary Pyrex glass.

conditions that applied when the expansions shown in figures 4, 5, and 6 were procured on samples of ordinary Pyrex. However, it will be noted that these curves for G702P correspond more closely to those shown in figures 5 to 7. Consequently, it appears that the annealing range of the low-temperature component of the G702P glass is about 25 deg. C lower than that of the same component in ordinary Pyrex glass. That this difference would be found was evident from the curves in figures 1 and 3.

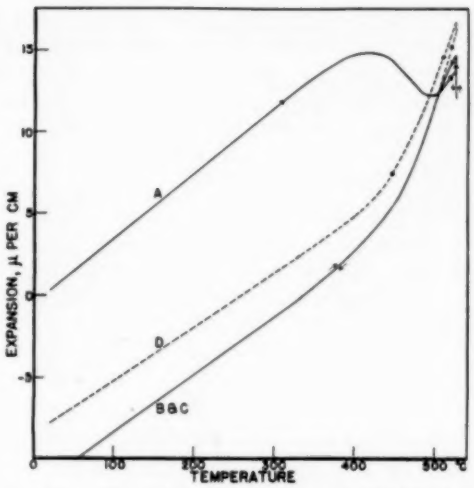

FIGURE 13. *Thermal-expansion cycles of G702P glass to 525° C.*

Curve designations, pretreatment, and holding periods same as in figure 12. Compare these curves with those for an ordinary Pyrex glass in figure 6.

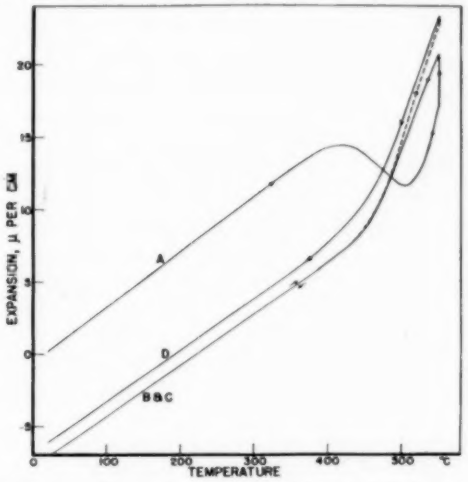

FIGURE 14. *Thermal-expansion cycles of G702P glass to 550° C.*

Curve designations, pretreatment, and holding periods same as in figure 12. Compare these curves with those for an ordinary Pyrex glass in figure 7.

IV. Discussion

1. Precision of the Data and the Adequacy of Their Representation by the Curves Presented

In procuring the data for the curves showing heat effects and for those showing expansions, observations were taken at intervals seldom

greater than 10 deg. C change in temperature. In the critical ranges, the intervals were often as small as 2 deg. C. In the case of figure 1, trebling the thickness of the curves would have covered practically all of the observed points. Repetition of the tests always showed some variation in the results, but most of this variation was directly attributable to the difficulty of exactly duplicating the rate of heating.

The same difficulty was encountered in determining expansions (or contractions) in the critical ranges where any variation in elapse of time affects the results. However, the uncertainties caused by inadvertent failure to duplicate the heating and cooling rates are generally insignificant in those cases where no more than two cycles are considered. When only two cycles, such as those in figures 4 to 8, were procured, the two tests were made without removing the sample from the furnace and the approximate duplication of test procedure was accomplished with the least difficulty. Furthermore, the matching of several curves procured on a number of different samples and by a series of tests that required several weeks for its completion was not required as in figures 9 and 11. The change caused by a small and unsuspected variation in heating rate within the critical range could cause a change in the order of some of the curves shown in figure 9. Excepting the lower half of the cooling branches, the expansion curves as drawn usually represent the observed points almost as well as the curves in figure 1. Even in the cooling branches, the worst deviations from the curves as drawn were roughly $\pm 0.5\mu$. Although about one-half of the observed points are omitted, curves 2 and 2′ present a fair sample of the usual set of observations.

2. Significance of the Results

It is believed that the expansion data presented here fully support the idea that the glasses in question are two-component glasses. Originally, this idea was based almost entirely on the peculiarities of the exothermic and endothermic heat effects that they showed when heated. As a result of this attempt to coordinate the peculiarities of the expansion effects of these glasses, it now appears that the expansion data present a rather clear picture of the manner in which the components of these glasses react upon each other during heating, cooling, and annealing procedures. There seems to be no indication that the components are immiscible. It seems, rather, that they are mutually bound in a rather close association, and that the glasses behave as if made up of two components because one constituent is present in such an excess that some, but not all of it, is sufficient to form a continuous spatial network that extends throughout the whole body of the glass. If the abundant constituent, with some aid from the other constituents, forms a sufficiently dense network, it appears that this network alone takes on the character of an overdistended vitreous solid, if the presence of the other component that is made up of that part of the constituents not included in the network, is ignored.

However, the unincluded part of the constituents also forms a network that has the properties of a distended vitreous solid. Such a picture of the constitution of two-component glasses does not require the concept of immiscibility, even though the chief constituent of the high-temperature component can be reduced to the crystalline phase by suitable heat treatments [4, 9].

V. Summary

The thermal expansion data presented above appear to confirm the previously expressed belief that some borosilicate glasses that contain a high percentage of silica are essentially two-component glasses.

One of these components becomes a practically rigid and continuous framework that extends throughout the body of the glass before 600° C is reached on cooling.

This high-temperature component is interlaced by the other component that is still so inelastically deformable at 450° C that its state above 500° C is definitely that of a liquid glass.

The expansivity of the low-temperature component is so much higher than that of the other that the latter suffers appreciable elastic compression whenever the glass is cooled and, under rapid cooling, this compression begins at rather high temperatures because even the low-temperature component acts as a solid when cooled rapidly.

Because of the additional contraction of the low-temperature component whenever it is annealed, the extraordinary compression of the high-temperature component is greatly accentuated by

annealing treatments at temperatures below 400° C.

Annealing treatments at temperatures between 500° and 600° C ultimately allow the high-temperature component to free itself from the extraordinary compression because such temperatures do reduce the viscosity of the low-temperature component that this component flows under the pressure exerted by the compressed component.

Normalizing the compression of the high-temperature component causes the glass as a whole to expand to such a degree that its specific volume after a thorough annealing at 550° C is greater than after a long annealing treatment at 450° C and is also greater than after a thorough annealing at 600° C if the latter treatment is followed by a rapid cooling to the standard temperature for density determination.

The mechanical processes (the building up of, and the relaxation of, elastic molecular strains) between the two components also cause a number of more-or-less minor effects that are discussed in some detail.

VI. References

[1] A. Q. Tool and C. G. Eichlin, J. Am. Ceramic Soc. **8,** 1 (1925).

[2] A. Q. Tool and E. E. Hill, Trans. Soc. Glass Tech. **9,** 185 (1925).

[3] A. Q. Tool and J. B. Saunders, BS J. Research **11,** 799 (1933) RP626.

[4] A. Q. Tool and H. Insley, J. Research NBS **21,** 743 (1938) RP1152.

[5] A. Q. Tool, E. L. Peffer, and J. B. Saunders, Toronto Meeting of Am. Ceramic Soc. (Feb. 19, 1930).

[6] A. Q. Tool, J. Research NBS **37,** 73 (1946) RP1730.

[7] A. Q. Tool and C. G. Eichlin, Am. Ceramic Soc. **14,** 276 (1931).

[8] L. Marchis, Les modifitions permanents du verre et les deplacement du Zero des thermometres (A. Hermann, Paris, 1898).

[9] A. Q. Tool and J. B. Saunders, J. Research NBS **21,** 773 (1938) RP1153.

Washington, June 13, 1947.

U. S. Department of Commerce
National Bureau of Standards

Research Paper RP1857
Volume 40, January 1948

Part of the Journal of Research of the National Bureau of Standards

Cavity Pressure Method for Measuring the Gain of Hearing Aids

By E. L. R. Corliss and G. S. Cook

A cavity pressure method for measuring the gain of hearing aids has been developed. It has the advantage of requiring no "dead" room, allowing a compact setup. The method has been investigated as to its validity and the degree to which diffraction effects are avoided. Comparisons with free-field data are made. The applicability of results obtained by this method to the specification of gain characteristics for hearing aids is discussed.

I. Introduction

The gain of a hearing aid is a numerical quantity expressing the degree of amplification that the aid will provide. Knowledge of the gain of a hearing aid is of importance to both manufacturers and users, as the gain largely determines the degree of hearing loss that can be compensated. Although the performance of a hearing aid depends on other factors, such as the presence or absence of harmonic distortion, and its suitability involves such considerations as durability, battery economy, and even size, a hearing aid is fundamentally a device for amplifying sound waves. Hence the degree of amplification, or gain, of a hearing aid is a quantity that is always taken into account whenever the performance of the instrument is evaluated.

The procedure of measurement in general use at present [1] involves exposing the hearing aid to a sound field set up in a free-field, or "dead" room. This is a room that must be sensibly free of echoes or standing sound waves. To that end, a room of large volume is constructed, the walls of which are covered with a material having a high sound-absorption coefficient. The room must also be free of extraneous sound disturbances, necessitating a sound- and vibration-isolating type of structure. The construction and maintenance of such a room is expensive.

The technique to be described in this paper was devised in an effort to avoid the use of a dead room. It is an easily standardized procedure by means of which the sound pressure applied to the hearing aid may be determined. No specially treated room is required, although the location should be reasonably quiet. The measuring equipment can be set up on an ordinary laboratory table. The only special construction involved is the source cavity, which may be built in the average shop. The method has the additional advantage of being readily adaptable to a recorder technique. By the use of two matched amplifier systems, the sound pressure that is applied to the hearing-aid microphone and the sound pressure generated by the receiver can be recorded simultaneously. The relative freedom from diffraction effects is of great assistance in permitting the evaluation of the combined microphone, amplifier, and receiver performance, as distinct from the characteristics of the hearing aid when it is worn under various conditions.

II. Measurement of Gain

The actual gain of a hearing aid may be defined as the ratio of the sound pressure produced by the receiver in the ear canal of the user to the sound pressure incident at the face of the microphone. The gain varies with the frequency of the incident sound, and depends not only on the intrinsic properties of the aid, but is also affected by the acoustic impedance of the user's ear.

If results found at various times for different hearing aids are to be comparable, the measurements must be made in a standardized way. The use of a coupler to represent the ear canal and to

[1] Tentative code for measurement of performance of hearing aids, by American Hearing Aid Association, J. Acous. Soc. Am. 17, 144 (1945).

measure the acoustic output of a hearing-aid receiver has been generally accepted. The pressure gain of a hearing aid may be defined as the ratio of the sound pressure in whatever receiver coupler is used to represent the ear canal to the sound pressure at the diaphragm of the microphone. The pressure gain approximates the actual gain only to the extent that the receiver coupler represents, in volume, shape, and impedance, the average ear canal. However, there appears to be significant agreement between the pressure gain and the gain as it appears to the user of the aid.

III. Comparison of Free-Field and Pressure Techniques

In the gain measurements to be described in this paper, the sound pressure generated by the hearing-aid receiver is measured by placing it on an "artificial-ear" coupler of 2-cm^3 volume. This coupler is employed in both free-field and cavity methods. The coupler is similar to the 2-cm^3 receiver coupler designed by Romanow,[2] except for the addition of a small capillary leak, which prevents a building up of pressure in the coupler when the receiver of the hearing aid is sealed on to it. The sound pressure at frequencies used in testing hearing aids is not affected appreciably by the leak.

The technique commonly used for applying the input sound level is to expose the hearing-aid microphone to sound pressures in a free field. The sound field is arranged to approximate a plane wave incident upon the microphone in a direction perpendicular to the plane of the microphone diaphragm. The free-field sound pressure is measured (with the hearing aid removed) at the point in the field in which the hearing-aid microphone is to be placed, and is taken to be the input sound level.

In the cavity procedure the hearing-aid microphone is placed on a source cavity in which sound pressures are produced by a dynamic speaker and measured by means of a calibrated condenser microphone. As in the free-field method, the output of the hearing-aid receiver is measured on the 2-cm^3 coupler. The cavity method must be used under conditions such that the pressure indicated by the measuring microphone is substantially the same as the sound pressure applied to the hearing-aid microphone.

The free-field gain of the hearing aid is the ratio of the sound pressure produced in the receiver coupler to the sound pressure in the free field at the locus of the hearing aid, with the hearing aid removed. Expressed in decibels, it is the difference between the sound-pressure level produced in the receiver coupler and the sound-pressure level incident at the location of the hearing aid in the free field. In the cavity method, the pressure gain is the ratio of the sound pressure developed in the receiver coupler to that in the source cavity, and is expressed as the difference in decibels between the sound-pressure level in the receiver coupler and the sound-pressure level measured in the source cavity.

Neither of these methods yields an accurate representation of the actual gain of the hearing aid. In actual use, the sound is incident on a hearing aid worn on the user's body; it may be worn out in the open, or under one or more layers of clothing. Furthermore, the impedance of the receiver coupler is only a rough approximation to the impedance of an actual human ear, and the sound pressure developed in the ear of the user depends on his ear mold and the volume of his ear canal. However, both free-field and cavity methods do serve to indicate the general gain characteristics of the hearing aid being measured.

IV. Experimental Results and Discussion

The design of the source cavity is shown in figure 1. Because it is impractical to measure the sound pressure with the measuring microphone directly at the face of the hearing aid microphone, a symmetrical arrangement is used to achieve this condition in effect. The face of the measuring microphone is placed opposite the face of the hearing-aid microphone at an equal distance from the axis of the source tube. The transverse dimensions of the cavity have been kept to a minimum in order to keep the first transverse mode of the cavity outside the range of frequencies for which the gain of the aid is to be determined. The first transverse resonance of this cavity when terminated at the hearing-aid opening with a flat plate is at about 6,800 cycles per second. The diameter of the hearing-aid opening of the cavity

[2] F. F. Romanow, J. Acous. Soc. Am. **13**, 294 (1942). Methods for measuring the performance of hearing aids.

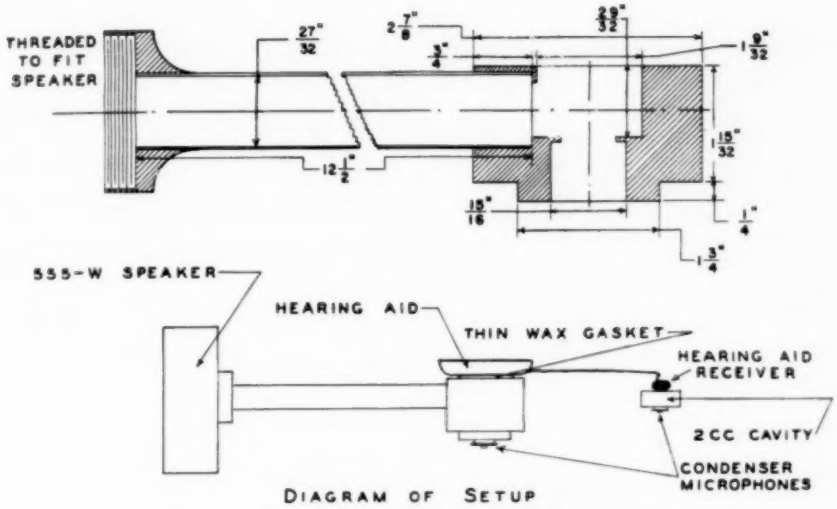

FIGURE 1. *Cross section of cavity.*

is about the same as that of the usual hearing-aid microphone.

The computation of gain from data obtained by the cavity technique involves the assumption that the sound pressure indicated by the measuring microphone is the same as that applied to the microphone of the hearing aid. The extent to which this assumption is valid under various conditions can be inferred from the data in figure 2.

The results plotted in figure 2 were obtained by substituting another condenser microphone for the hearing aid. This microphone was mounted in brass fittings by means of which the plane of the diaphragm could be set at various fixed distances from the plane of the cavity opening. These distances from the plane of the cavity opening will be referred to in the succeeding discussion as "offsets". The brass fittings provided a series of offsets ranging from a nearly flush closure of the cavity to an offset greater than the total thickness of most hearing aids. The diameter of the offset fittings was the same as that of the cavity.

It is evident that if care is taken to set the instrument on the cavity so that the face of the hearing-aid microphone is as close as possible to the cavity opening, no significant error will be introduced. The error may be kept to less than 5 db at the high-frequency end of the range. The effects of cavity sound pattern will not be serious unless a hearing aid with a deeply set microphone is being measured or unless the sealing gasket is made too thick. Variations in gain definitely traceable to cavity pattern are not usually encountered, even where they might be expected. This may be due to the damping of the cavity resonance by the resistance and leak produced by the grill-work of the aid.

As the cavity method involves only the face of the microphone, the pressure gain may be expected to show less dependence upon the shape of the hearing-aid case than would the free-field gain. This inference is confirmed by the results shown in figure 3. For these data, cavity pressure and free-field responses of a commercial hearing-aid microphone were measured. Measurements of response were made on the unmounted microphone, and also on the microphone when it was mounted in two hearing-aid cases differing considerably in size. All other components of the hearing aids were left in place, and the microphone leads were brought out through the receiver plug. This was intended to simulate the actual mounting of a microphone in a hearing aid. The data presented in figure 3 were obtained for a microphone cartridge of the type that is provided with an integral pinhole-and-cloth grillwork. This type was chosen for graphical presentation because its generally flat response and the protected mounting of its diaphragm make it possible to show directly the diffraction introduced by the cases and grillworks. The same measurements were also made on an ordinary crystal microphone with

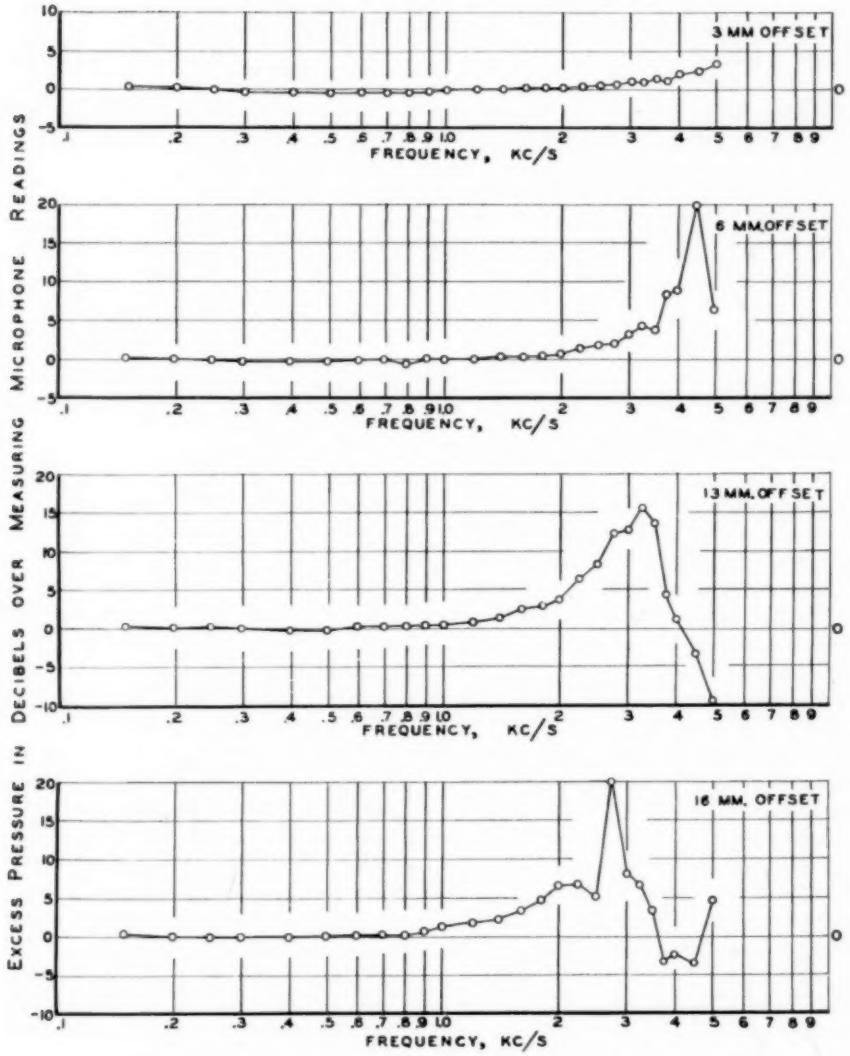

FIGURE 2. *Sound pattern in source cavity.*

Effects of off-setting microphone from flush closure.

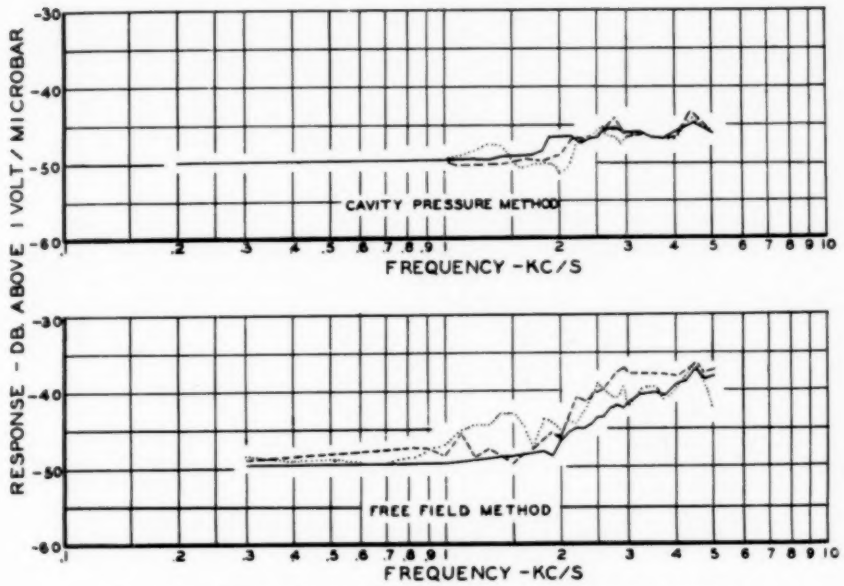
RESPONSE - DB. ABOVE 1 VOLT/ MICROBAR
-30
-40
-50
-60
CAVITY PRESSURE METHOD
.2 .3 .4 .5 .6 .7 .8 .9 1 2 3 4 5 6 7 8 9 10
FREQUENCY - KC/S
FREE FIELD METHOD
FREQUENCY - KC/S

FIGURE 3. *Effect of hearing aid case on apparent microphone response.*

Crystal microphone: ——, unmounted; — — —, in small case; . . . , in large case.

a bare foil diaphragm. Mounting this type of microphone in a case depresses and broadens its resonance peak. The results of measurements on this type of microphone agreed with results obtained on the microphone of figure 3, but the differences were not so obvious because of the larger effect of the mounting on the resonance peak of the microphone.

In free-field and cavity methods alike, changes in measured response appear when the microphone is mounted in a hearing-aid case. The changes introduced by the case are greater in the free-field measurements because the total size of the case affects the free-field diffraction pattern. The grillwork affects the measured response in both free-field and cavity techniques, but the effect is not very large. From figure 3 it can be seen that the changes introduced by the case in the cavity-pressure method are generally less than 5 db. As threshold measurements are usually made to no greater precision than 5 db—the smallest step on most audiometers—this variation does not seriously affect the usefulness of the gain data.

Figures 4, 5, and 6 show the gains of three commercial hearing aids on which both free-field and cavity data were obtained. The agreement on general characteristics is good. The differences are chiefly due to diffraction effects and are small compared to the peculiarities of the gain characteristics produced by the receiver response.

In figure 5, an extra resonance is seen to be present in the cavity measurement at about 2,400 cycles per second, which was not found in the free-field results. This was at first supposed to be due to cavity pattern or a possible coupling between the space behind the grillwork and the cavity volume, but the results of further free-field measurements seem to show that it was an instability in the hearing aid itself. Free-field measurements have been made on the same instrument subsequent to the data from which this curve was drawn that exhibit the same peak as that found in the cavity measurements.

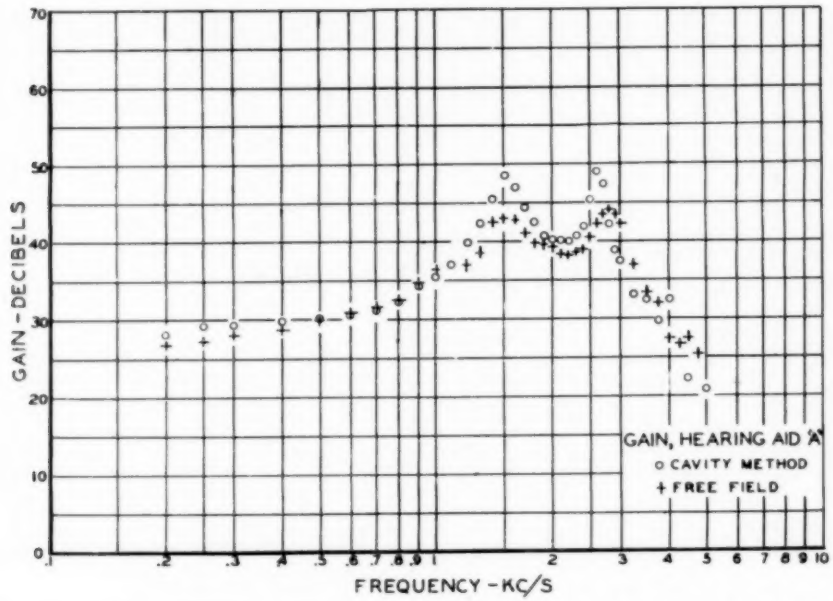

FIGURE 4. *Gains of commercial hearing aid on which both free-field and cavity data were obtained.*

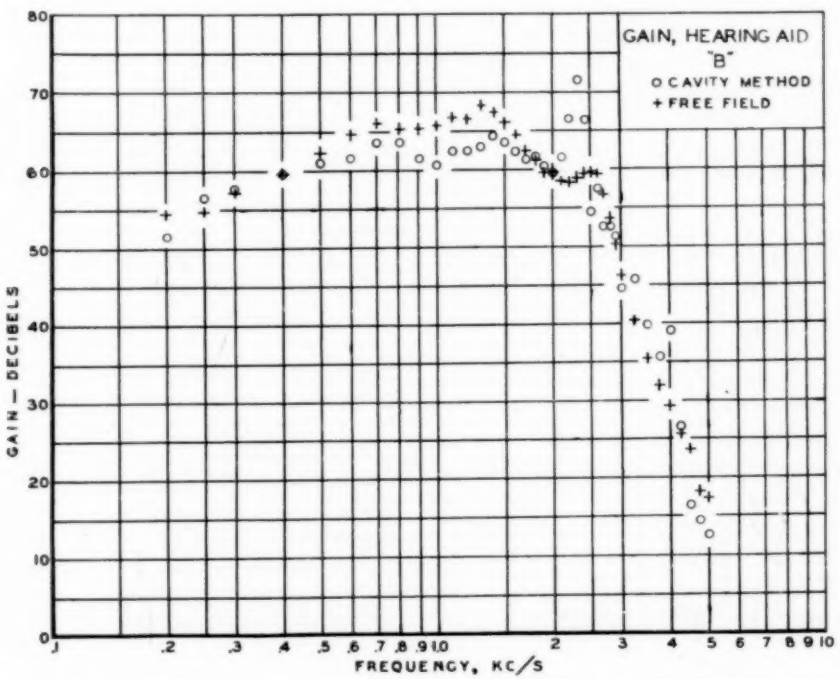

FIGURE 5. *Gains of commercial hearing aid on which both free-field and cavity data were obtained.*

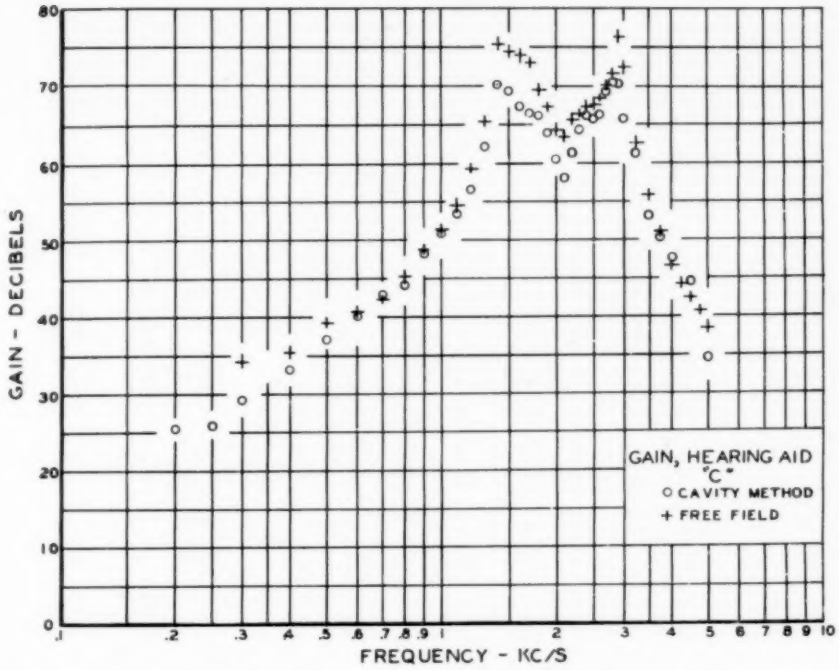

FIGURE 6. *Gains of commercial hearing aid on which both free-field and cavity data were obtained.*

V. Summary

The gain of a hearing aid can be measured by a cavity-pressure technique. The chief advantages of the method are its compactness and simplicity. Results of measurements are equal in validity to those obtained by the more familiar free-field method. A study of the properties of the method shows that a pressure gain measurement is approached (see fig. 3). This property may prove to be valuable in permitting the specification of an inherent pressure gain for a hearing aid. The effects of external conditions, such as the geometry of the case, the size of the body baffle, and filtering through clothing, may be determined by separate investigations. These generally applicable data might be incorporated in the specification for pressure gain. It should not be necessary to measure them for each instrument, as they are the same for all hearing aids. The separation of the problem of determining the actual gain of a hearing aid as worn into a pressure-gain measurement, objectively reproducible, and a study of body diffraction and ear impedance, which are independent of the intrinsic properties of the aid, appears to be desirable and useful.

WASHINGTON, September 15, 1947.